Studies on a new ultrasound contrast agent: Strategies for increasing the population of nano bubbles and for encapsulation of Paclitaxel

A Thesis

Submitted to the Faculty

of

Drexel University

by

Shweta Naidu Chitoor

in partial fulfillment of the

requirements for the degree of

Master of Science

June 2011

THIS IS MY DEDICATION TO GOD

ACKNOWLEDGEMENTS

Firstly, I would like to thank God for giving me the opportunity of doing a thesis when I really did not expect it to come my way. Thank you for giving me the strength to handle the situation in a calm way.

Secondly, I express gratitude to Professor Margaret Wheatley for having faith in me and motivating me all throughout the thesis process. Then I would like to express my sincere thanks to Boriphat Methachan for being the most wonderful mentor teaching me every single thing and having lots of patience answering my silly queries and also to my lab member Archana Nagaraja for guiding me during thesis.

Thirdly, I would like to thank Professor Andres Kriete for being in my thesis committee and giving me suggestions regarding the statistical analysis of data and designing of experiments.

Finally, I would like to thank Professor Fred.D.Allen for being in my thesis committee and motivating me during my research work.

TABLE OF CONTENTS

LIST OF TABLES

LIST OF FIGURES

LIST OF ABBREVIATIONS

SOP: Standard operating procedures

PBS: Phosphate buffer saline

PFC: Perfluorocarbon gas

SPAN 60: Sorbitan Monostearate

TPGS: D-α-tocopheryl polyethylene glycol 1000 succinate

ABSTRACT

Studies on a new ultrasound contrast agent: Strategies for increasing the population of nano bubbles and for encapsulation of Paclitaxel.

Shweta Naidu Chitoor

Paclitaxel (Taxol) is an anti-cancer drug obtained from the bark and needles of Taxus brevifolia. It is known for its unique mode of action and used for the treatment of breast and ovarian cancer. Also, paclitaxel shows very low solubility in water and is associated with a number of toxic side effects. The currently used formulation of paclitaxel with cremophor EL results in several hypersensitivity reactions. In order to tackle this problem, there is a need to develop targeted paclitaxel therapy for cancer treatment. Since, paclitaxel is highly hydrophobic, it can be incorporated in the hydrophobic core of vesicles such as SE61, a surfactant stabilized mixture of micro and nano gas bubbles.

When ultrasound is transmitted in the body and encounters a medium with different acoustic impedance, such as a gas bubble, the backscatter is greatly increased, giving contrast enhancement. Ultrasound also causes the bubble to oscillate and break releasing any entrapped drug, for example at a tumor site. This helps in controlled and target drug release, preventing the drug action on normal healthy cells. An added advantage is that ultrasound facilitates drug uptake by increasing the permeability of the cell membrane. Nanobubbles can easily pass through the capillary walls of blood vessels in the targeted tumors enabling site specific delivery of drug. The gas core of SE61 contrast agent was

made up of perfluorocarbon (PFC) and stabilized by mixture of two surfactants- span 60 (Sorbitan Monosterate) and TPGS (water soluble Vitamin E- nonionic surfactant).

In the first part of the study, acoustic characterization of standard SE61 micro and nanobubbles were performed. The average diameter of standard SE61 microbubbles was 2-2.3 μm and provided contrast enhancement between 18- 24 dB. Nanobubbles with mean diameter of 350-480 nm were separated from the primary mixture and provided contrast enhancement between 18-23 dB. The second part of the study involved studying the effects of changing salt concentration and surfactant ratios on the population of nanobubbles. Due to difficulty in counting the number of nanobubbles, the increase or decrease in the amount of nanobubbles produced were compared by means of turbidity measurement at 610 nm. From the salt study, nanobubble population was found to be highest at 387mM total sodium chloride with 80: 20 molar ratio of span 60: TPGS. In case of microbubbles, 262mM total sodium chloride concentration gave slightly higher maximum enhancement (28 ± 1.5 dB) compared to standard 650mM SE61 microbubbles (25.72 ± 0.855 dB) at dose of 60 μl/L. From the surfactant study, 1: 0.43 (for nanobubbles) and 1: 0.25 (for microbubbles) molar ratio of span 60: TPGS were chosen as the ratio in newly formulated bubbles.

The third part of the study involved encapsulating paclitaxel into the shell of the bubble by a direct loading method. The Paclitaxel encapsulation efficiency was compared between the newly formulated (from salt and surfactant study) and standard SE61 bubbles using high performance liquid chromatography. When compared with microbubbles, paclitaxel loaded in standard SE61 microbubbles was 29.4% and in paclitaxel loaded newly formulated microbubbles was 10.98%. In case of nanobubbles,

formulation change did not affect paclitaxel encapsulation efficiency. The encapsulation efficiency of paclitaxel loaded into standard SE61 nanobubbles was 14.4% and in paclitaxel loaded newly formulated nanobubbles was 13.9%.

CHAPTER 1: OBJECTIVES OF THESIS

The overall goal was to study a new ultrasound contrast agent SE61 which exhibited a mixed population of micro and nano surfactant stabilized gas bubbles and to study the effects of loading paclitaxel into it. The study was in two parts: a study of the effect of varying total salt concentration and surfactant concentration on SE61, and paclitaxel loaded SE61 contrast agents and studying of the efficiency of paclitaxel encapsulation into contrast agent by high performance liquid chromatography.

Detailed objectives of the thesis are:

1) Preparation of standard SE61 micro and nano surfactant stabilized gas bubbles. Perform size analysis and study the acoustic behavior using dose responses, and stability of bubbles.

2) Increase the nanobubble population by varying parameters used in the preparation:

- Total sodium chloride concentration
- Surfactant concentration- D-alpha tocopheryl polyethylene glycol 1000 succinate, (TPGS)

3) Study the effect of paclitaxel loading in micro and nanobubbles on the echogenecity and stability of the agent

4) Study the efficiency of paclitaxel encapsulation in contrast agent by high performance liquid chromatography.

Micro and nanobubbles where prepared using two surfactants – Span 60 and D-α-tocopheryl polyethylene glycol 1000 succinate. For the first part of study, the total sodium chloride concentration was varied keeping span 60: TPGS molar ratio same as standard SE61. This was done to analyze which concentration of total sodium chloride gave higher nanobubble population. Also, the effect of varying total sodium chloride concentration on microbubble echogenecity and stability were studied.

For the second part of study, the TPGS concentration was varied keeping span 60 and total sodium chloride concentration same as standard SE61. Also, increase or decrease in nanobubble population was studied at each TPGS concentration level.

Paclitaxel was directly loaded into the hydrophobic region of the bubble. Paclitaxel encapsulation efficiency was compared between the newly formulated (from salt and surfactant studies) and standard SE61 bubbles by high performance liquid chromatography.

CHAPTER 2: BACKGROUND

Ultrasound imaging has become a successful and well established diagnostic technique for clinical decision making [1]. This is because ultrasound imaging is non-invasive [2] , less expensive[3] and provides real time images of soft tissue structures such as heart and blood flow without the use of ionizing radiation [3].Ultrasound waves can be used for tumor imaging and controlled drug release by focusing ultrasound beam at the tumor site [4].

Over the last few decades a lot of hard work is being dedicated towards improving the image quality by modifying the transducer or by image processing technologies. But still ultrasound images lack contrast to identify metastatic lesions in soft tissues and abnormalities in body cavities and vessels [5]. To deal with this problem ultrasound contrast agents have been developed which when injected intravenously provide contrast enhancement thus improving image quality. Also, these contrast agents can be used for targeted drug delivery by encapsulating the drug in the agent.

The introduction gives brief description on physics of ultrasound and effects of ultrasound on contrast agents. Also, information about the pharmacology of paclitaxel, the drug being loaded into the bubble and its therapeutic potential is being discussed in detail. Also, the advantages of using nanobubbles containing encapsulated drug in targeted cancer treatment are mentioned in the background.

2.1 Introduction about ultrasound

Ultrasound waves are sound pressure waves with frequencies greater than 20 kHz usually generated by piezoelectric transducer [2]. The Human ear can hear in the frequency range of 20Hz to 20 kHz [3]. In Diagnostic ultrasound, frequency range from 2-12 MHz [6] is used to provide real time images of body tissues such as for abdominal and gynecological applications. Therapeutic high frequency focused ultrasound operates around 1 MHz [7] and is used for break kidney stones and heal damaged tissues in the body. Higher ultrasound frequencies provide poor penetration in deeper tissues as lose their signal strength quickly [6]. However, image resolution increases with the increase in ultrasound frequency improving the diagnostic potential by the physician. Attenuation of ultrasound waves at higher frequencies occurs due to scattering of wave or due to absorption where a portion of ultrasonic wave is absorbed by tissue and by conversion to heat [7].

2.1.1 History of ultrasound

The evolution of ultrasound as an image modality dates back in 19^{th} century when the scientists wondered about the use of ultrasound in medicine. In 1826, Jean-Daniel Colladon, Swiss physicist studied the compressibility of liquids and determined the speed of sound using underwater bell [8]. In 1880, Pierre and Jacques Curie discovered a phenomenon called “piezoelectricity” using quartz crystals which generated electric charge when pressure was applied to them [8]. Conversely, when rapidly changing electric potential was applied to the crystal, it caused crystal to vibrate and produce ultrasound waves [8]. This marked the basis for the development of modern day

ultrasound transducer although many modifications have been made over the last few decades for improving the image quality.

Later, ultrasound was used for military applications in quest for naval superiority. In 1915, Paul Langevin and Chilowsky developed a hydrophone which generated and received ultrasound waves [8] which helped in the detection of ice bergs in sea. Ludwig and Struthers, scientists at Naval medical research found that the mean velocity of ultrasound in soft tissue was 1540m/s [8]. In 1950's Ian Donald used A-mode ultrasound machine to differentiate tissues in excised fibroids and ovarian cysts[8]. Later use of ultrasound was extended to cardiac evaluation and blood flow recordings. A major transition was experienced after 1975, when real time B-mode imaging and pulse Doppler systems were introduced [9]. With the invention of Doppler color-flow mapping and Power Doppler in recent years, the scope of applications of ultrasound has widened making ultrasound imaging a successful and popular image modality among surgeons and physicians.

2.1.2 Physics behind ultrasound

Ultrasound waves are longitudinal mechanical waves requiring a physical medium for propagation [10]. The wave propagation occurs by longitudinal motion (compression and rarefaction) and not by transverse motion (side by side). Ultrasound waves travels in waves that emanate from a source [7]. The high rests and low troughs represent amplitude values of the wave which corresponds to peak compression and peak rarefaction values [7].

Frequency of the ultrasound wave is related to the time period represented by equation 2.1

$$f = 1/T \quad \text{(Eq2.1)}$$

Where f is the frequency of ultrasound wave in Hz and T is the time for one cycle to occur in seconds.

The speed of sound (c in m/s) is related with the frequency of the ultrasound wave and is represented by the equation 2.2.

$$c = \lambda * f \quad \text{(Eq2.2)}$$

where λ is the wavelength of the wave in meters [7]

For medical applications, the propagation speed c in tissues is assumed to be 1540m/s [7]. Two different modes are used are used in medical ultrasound as shown in figure 2.1. One mode is to continuously excite the ultrasonic transducer with a sine wave with constant amplitude called continuous wave ultrasound (CW ultrasound) [7]. Another mode is called the pulse wave ultrasound mode where the transducer is exited with very short electrical signals waiting for some time and again repeating the electrical shocking [7]. Pulse repetition frequency is an important parameter to be considered in pulse wave ultrasound mode.

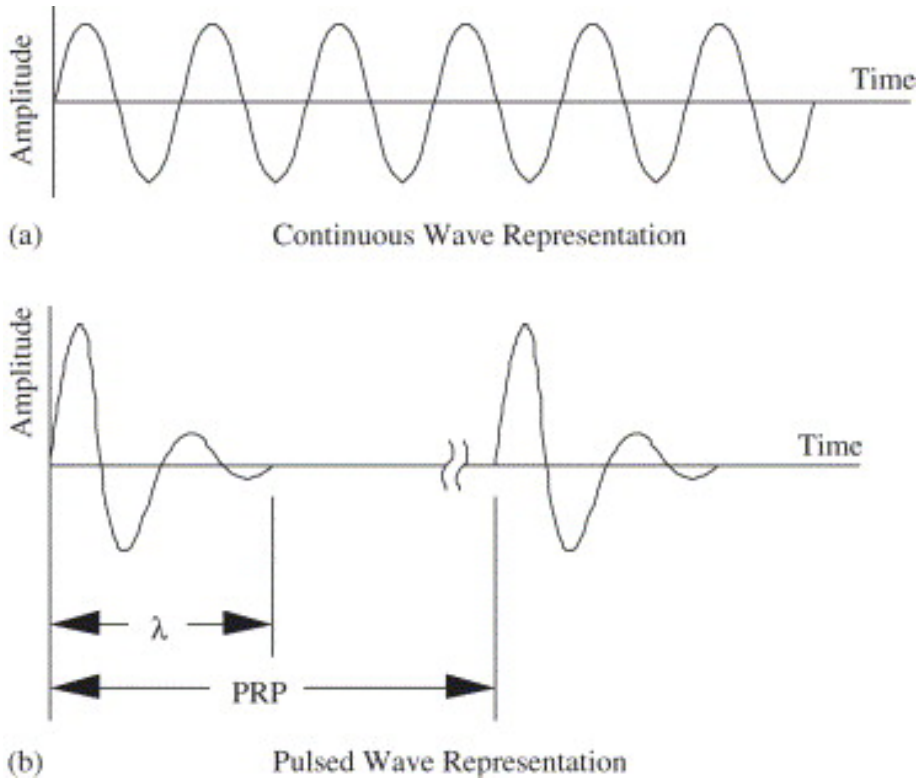

Figure 2.1: Representation of continuous and pulsed ultrasound waves [7]

The magnitude of Acoustic impedance is defined as the product of density of the material (ρ) and speed of sound in the material (c) [7] and is represented in the equation 2.3. The unit for acoustic impedance is rayl (kg/m^2s) and density of material in kg/m^3.

$$Z = \rho * c \qquad \text{(Eq. 2.3)}$$

The propagation of ultrasound is influenced by changes in the acoustic medium [10]

Pressure reflection coefficient R is described by the equation 2.4

$$R = (Z_2 - Z_1) / (Z_2 + Z_1) \text{ [10]} \qquad \text{(Eq2.4)}$$

Negative value of reflection coefficient indicates 180 degrees phase shift between the transmitted and reflected ultrasound wave.

Acoustic intensity I can be computed using the formula described in equation 2.5

$$I = P^2 / 2\rho_0 c_0 \qquad \text{(Eq2.5)}$$

where P is the pressure amplitude of the wave in Pascals and acoustic intensity is in W/m^2 [10]

As ultrasonic waves propagate through homogenous media attenuation occurs with distance due to acoustic absorption [10] and is described in equation 2.6.

$$I = I_0 e^{-2\alpha 1 Z} \qquad \text{(Eq2.6)}$$

where I_0 is the initial intensity in W/m^2 and $\alpha 1$ is the amplitude absorption coefficient of the medium [10]

For inhomogeneous medium, attenuation occurs due to acoustic scattering although for many tissues scattering is smaller than absorption [10].Tissues have higher attenuations that increase linearly with frequency [10]. When ultrasound wave propagates in tissue, a mechanical strain is induced due to stress where there is relative change in dimension or shape of the body termed as ultrasound –induced cavitation [7]. When ultrasound waves hits the bubble , it oscillates at high ultrasonic pressure levels and finally collapses due to cavitation [7].

2.2 Ultrasound contrast agents

Ultrasound imaging lacks ability to differentiate between tissues having similar acoustic properties[11]. The solution to this problem is use of ultrasound contrast agents which

when, injected intravenously improve the contrast between the two tissues by changing the reflection coefficient [11]. Ultrasound contrast agents could be in the form of solid particles in suspension, liquid droplets (emulsion), gas bubbles, encapsulated gases or liquids [12]. When ultrasound hits the gas bubbles, the wave will be reflected at the surface of the bubble because of large difference in acoustic impedance between the surrounding medium and gas inside the bubble [1]. They increase the backscattered signal giving contrast enhancement in the image thus improving the image quality [11]. They also enhance the resolution of images and enhance the diagnostic power of the physician [13].

During the initial years of contrast agent development, the main challenge most scientists faced was to produce small microbubble (< 8 μm) that could pass through the lung capillary circulation and were stable enough to reach the left heart after an intravenous injection [1]. An ideal contrast agent should be non-toxic, easily injected through intravenous route and stable for recirculation[14]. Also, it should be able to traverse the capillary and pulmonary circulations to provide view of the target tissue or deliver drug at particular site [14]. The bubbles must be less than 8μm in diameter in order to effectively pass through the lung capillaries [15].

As shown in figure 2.2, different gases can be used in preparation of gas core microbubbles such as air, perfluorocarbon and sulfur hexafluoride. Also, the shell composition of the bubble can surfactant stabilized or made of biocompatible polymers or protein like albumin. The size of the microbubbles is a very important parameter considered during characterization of contrast agents. In the figure 2.2, the size of the

microbubbles shown is less than 4 μm which can easily pass through the capillaries and ideal for medical imaging.

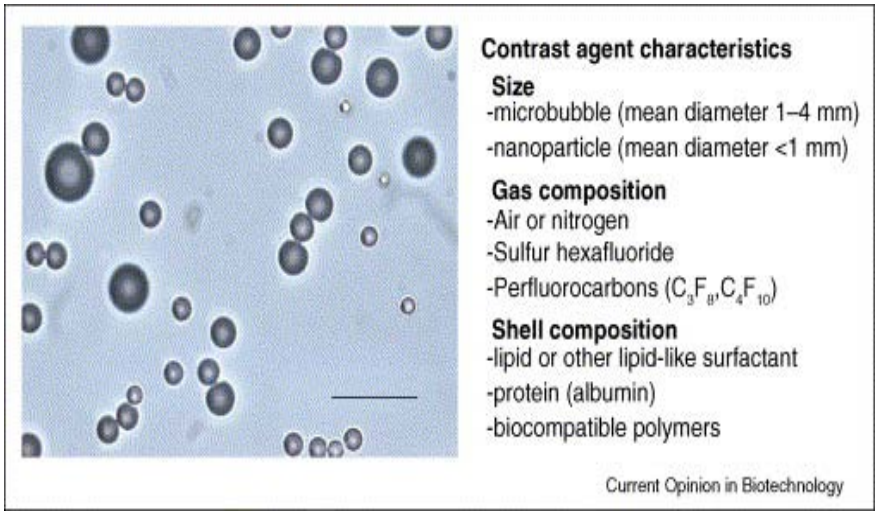

Figure 2.2: Microscopy of ultrasound contrast agent[16]

2.2.1 Targeted drug release using contrast agents

Ultrasound contrast agents can act as drug delivery vehicle to particular sites enabling targeted drug delivery. Targeted drug delivery is very important when the drug has toxic side effects such as anti-cancer drugs. Also the drug release can be controlled by the ultrasound beam reducing the toxic side effects of anti-cancer drugs used in cancer treatment.

The conventional cancer chemotherapy has several side effects associated with the procedure. Therefore targeted drug delivery is particularly essential in cancer treatment where the normal healthy cells are unaffected with the drug and the tumor site receives the drug for treatment. This will facilitate in providing drug at the tumor site where cells

may have survived surgery, thus preventing regrowth and metastasis of tumor [17]. Targeted drug delivery minimizes toxic side effects, lower the required drug dosage amounts and decrease costs for the patients [3, 18, 19]

Gas filled microbubble are more compressible than water or tissue [16] and undergo volumetric oscillation consisting of compression which occurs during pressure peaks and expansion which occur during pressure nadirs of the ultrasound wave [16]. The destruction caused due to the ultrasound beam causes collapse of microbubbles producing a high amplitude response [3, 20]. This violent microstreaming encourages diffusion of drugs into tissues and lesions when the contrast agent is encapsulated within the drug [3, 21].

Also, ultrasound increases membrane permeability by shear stress and causes entry of the drug into cells and tissues [3] shown in figure 2.3. Ultrasound improves transfection by causing transient non-lethal perforation of capillary and cell membrane by cavitation [3] shown in figure 2.3. Ultrasound can change the chemical property of the drug such as hematoporphyrins which, when activated by ultrasound causes cancer cell death [3, 22]. This is a very important use of ultrasound which is currently being exploited in cancer research. A flow chart showing different applications and mechanisms of ultrasound mediated drug / gene delivery are shown in figure 2.3.

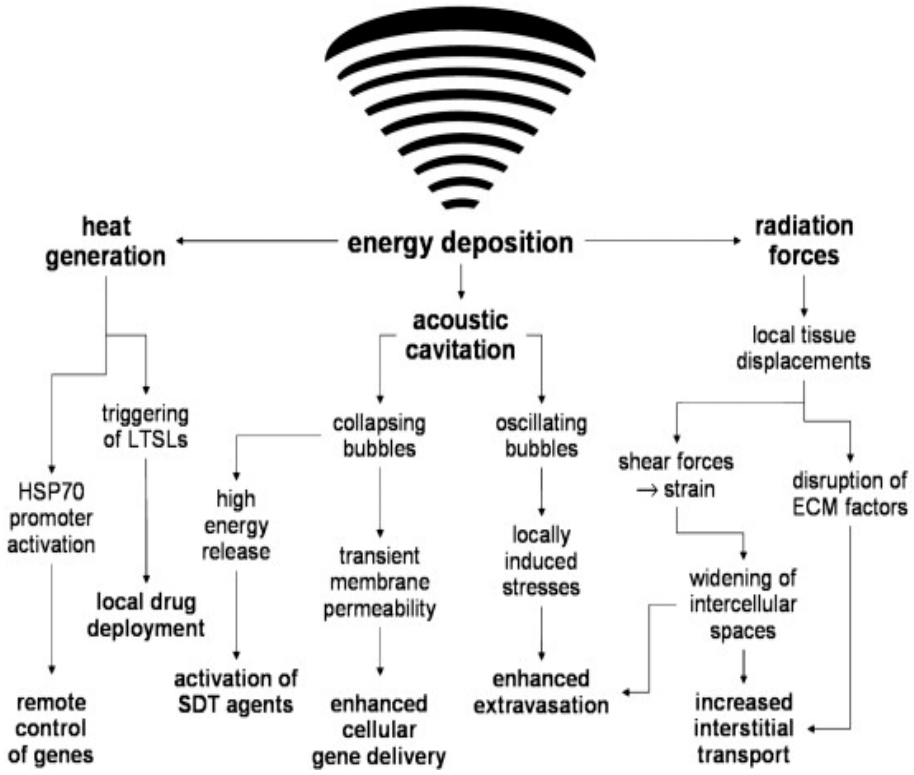

Figure 2.3: Representation of mechanisms and applications of focused ultrasound beam in drug/ gene delivery [23].

Delivery to specific target sites can be further aided by attaching ligands into the membrane of gas bubbles that interact with the target receptors on the cell membrane[3]. As shown in figure 2.4, drugs can be directly attached to the membrane surrounding the gas bubble represented as A , or can be imbedded within the membrane materials (B), can be made to bind non-covalently to the surface of bubbles (C) or loaded in the interior of the gas bubble (D) or hydrophobic drugs that can be incorporated into a layer of oily material which is later surrounded by stabilizing membrane (E) [3, 24].

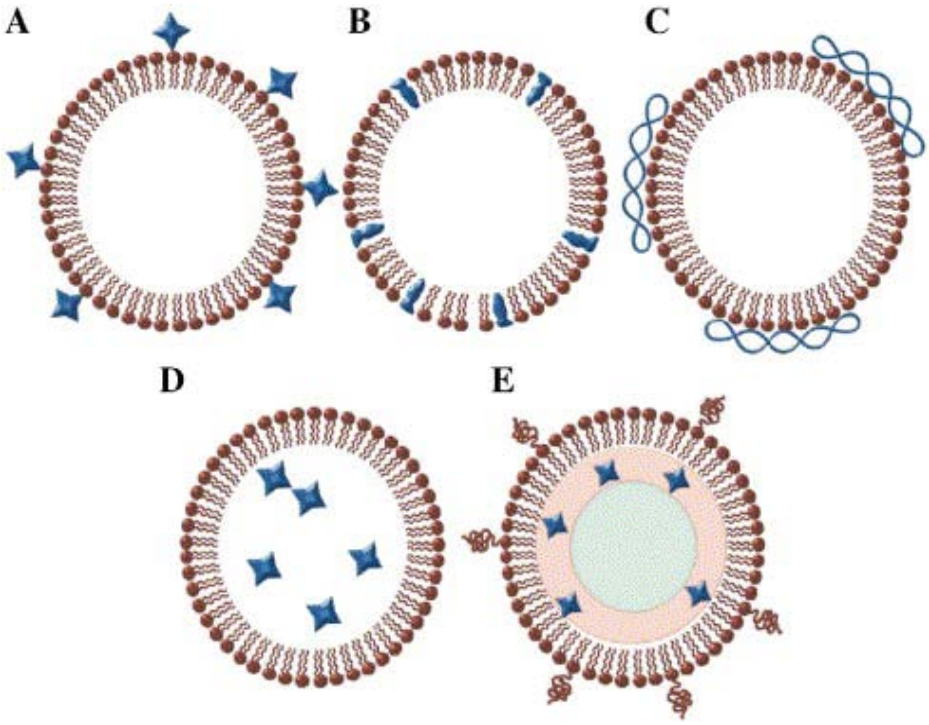

Figure 2.4: Schematic representation of different ways microbubble can carry drugs for targeted delivery [3, 24]

Ultrasound energy can help agents such as drugs to penetrate through various tissues such as skin and even blood clots [3, 25]. Gas microbubbles suspended in liquid are extremely efficient ultrasound reflectors making them useful as ultrasound contrast agents [3]. Coated microbubbles are more stable in the bloodstream because the shell protection the gases from getting diffused into the blood [3].

2.2.2 Gas core of the bubbles

The stability of microbubbles contrast agents can be improved by using gases with relatively low diffusion coefficients and low solubility in water and blood [16] The most common gases used for this purpose include perfluorocarbon (such as octafluoropropne [C_3F_8] and decafluororbutane [C_4F_{10}]) [16]. Second generation microbubbles contain perfluorocarbon as the gas core rather than air which permits a longer window of time to

image the patients[3]. Previous studies from the laboratory showed that certain mixtures of non-ionic surfactants produced stabilized micron sized bubbles, particularly a mixture of span 60 and tween 80, which is designated by us as ST68 [13]. It was also shown that perfluorocarbon filled ST68 micro bubbles produced higher vascular enhancement (26.1 dB for dose of 0.1ml/kg) than air filled ST68 microbubbles (18.3 dB for dose of 0.13ml/kg) [14]. Also, the enhancement for ST68- PFC microbubbles lasted for 8 min than ST68-Air micro bubble which showed less stability of less than 2 min [14].

2.3 Surfactants used for bubble preparation

Two non-ionic surfactants are used for preparation of SE61 microbubbles and nanobubbles. The procedure for micro and nanobubble preparation was similar to the Standard laboratory procedure mentioned in [5] for ST68 with slight modifications. The patent protecting and describing the invention in the laboratory is mentioned in reference [26]. Investigations into developing an agent with a more biocompatible mixture of surfactants, and one with a higher proportion of nanobubbles, lead us to employ TPGS in the place of Tween 80, and the resulting agent is designated SE61. This introduction gives a brief description of the chemical structure, uses and properties of the two surfactants used in the preparation of SE61 micro and nanobubbles.

2.3.1 Span 60 (Sorbitan Monostearate)

Span 60 is a synthetic non-ionic emulsifier used in small concentrations as food additive [27]. It consists of partial esters of stearic acid and mixed anhydrides of sorbitol [27]. In simpler words, Span 60 is an ester of sorbitan and stearic acid. The IUPAC name of Span 60 is [(2R)-2-[(2R,3R,4S)-3,4-dihydroxyoxolan-2-yl]-2-hydroxyethyl]octadecanoate. The chemical structure of Span 60 is shown in (Figure 2.5). Span 60 has molar mass of

430.62g/mol with molecular formula as $C_{24}H_{46}O_{6.}$ Apart from being used as an emulsifier, Span 60 is used as flavor-dispersing agent in food and beverages industry [28]. It is also used in some pharmaceutical creams for topical use [28]. Apart from that Span 60 is used in bread, cakes, whipped vegetable oil and fat-water emulsions [28]. The insolubility and waxy nature of Span 60 makes it unsuitable for parenteral administration [28].

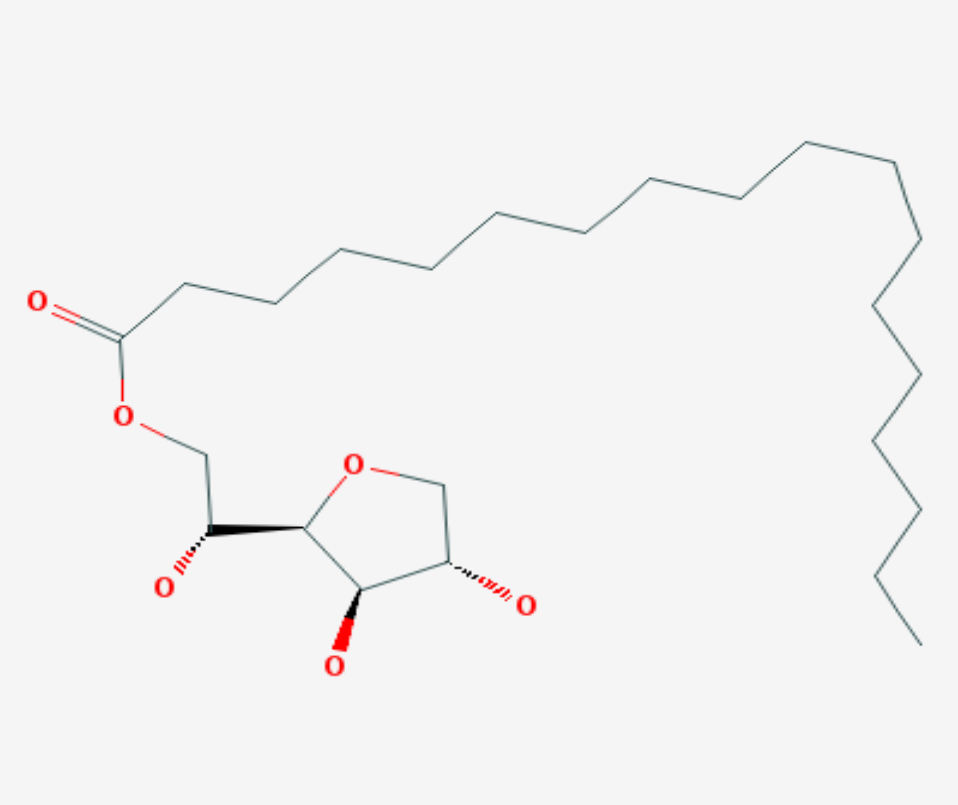

Figure 2.5: Structure of Span 60 obtained from Sigma Aldrich website(PubChem Substance Id: 24899728 and Substance summary SID 24899728)

In a mice study Span 60 was given at dose levels of 0·5, 2·0 or 4·0% of the diet for 80 weeks where no carcinogenicity was observed at any dose levels [28]. But enlargement of kidneys and higher incidence of nephrosis was observed at 4% Span 60 diet level [28].

2.3.2 TPGS

D-α-tocopheryl polyethylene glycol 1000 succinate (TPGS) is a water- soluble succinate ester of vitamin E [29]. TPGS is an amphiphilic compound having lipophilic alkyl tail and hydrophilic polar head [29, 30]. The chemical structure of Vitamin E TPGS and Vitamin E are shown in figure 2.6. It melts at 37- 41 degree Celsius and is heat stable under temperature 200 degree Celsius [31]. TPGS improves the drug encapsulation efficiency due to its bulky structure and large surface area [29, 30]. TPGS is synthesized from α-tocopherol (vitamin E) by grafting to polyethylene glycol (PEG) oligomer through succinate diester linker [32]. TPGS 1000 where 1000 denotes molecular weight of polyethylene glycol chain [32].

TPGS is approved by Food and[32] Drug Administration as a drug solubiliser in oral, parenteral, topical and nasal therapies [32-34]. It is an excellent emulsifier, solubiliser and increases the bioavailability of hydrophobic drugs [35, 36]. TPGS is a used in fabricating nano/microparticles with high drug entrapment efficiency [35, 37, 38].

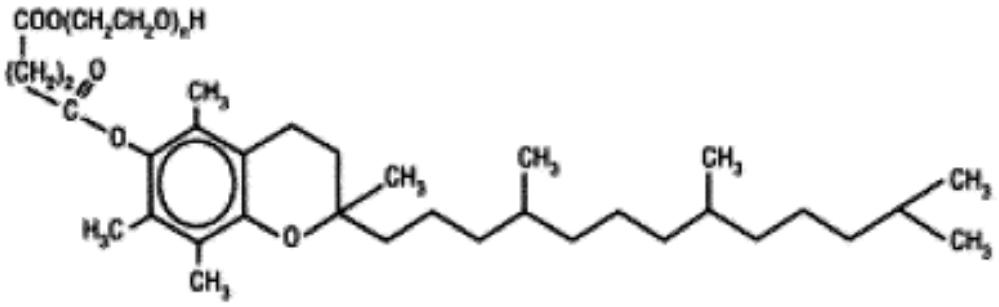

Vitamin E TPGS

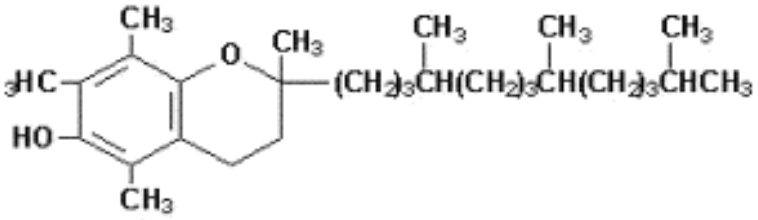

Vitamin E

Figure 2.6: Structures of Vitamin E and Vitamin E TPGS [31]

The lipophilic alkyl tail (polyethylene glycol) and hydrophilic polar head portion (tocopherol succinate) are bulky and have large surface area [31]. Vitamin E TPGS is readily absorbed in the gastrointestinal tract (GI) and enhances the cytotoxicity of paclitaxel and doxorubicin by inhibiting P-glycoprotein in the intestine [31, 39]. Non-ionic surfactants are more hydrophobic and less toxic to biological membranes, enhancing the capability to dissolve poor water solubility drugs like paclitaxel [40, 41].

2.4 Paclitaxel (drug)

Paclitaxel is an antineoplastic agent derived from bark of Pacific yew Taxus brevifolia [42]. It is an effective anticancer drug used as a single agent or in combination with other agents for the treatment of breast, ovarian and non-small-cell lung cancer [42, 43]. Paclitaxel shows very low aqueous solubility of < 0.03 mg/ml [42, 44] and does not

contain any functional groups that can be ionized by altering pH [42]. It is white to off-white crystalline power and is highly lipophilic[45]. In the blood stream, paclitaxel is extremely protein bound (95-98%) [17] [46]. Also, paclitaxel has shown dose-dependent antiangiogenic activity as per the experiments conducted using chick chorioallantoic membrane [17, 47-50]. Paclitaxel is a highly functionalized diterpenoid with molecular formula of $C_{47}H_{51}NO_{14}$ and molecular weight of 853.9 Da [45, 51].

2.4.1 History of development of paclitaxel as anti-cancer drug

Paclitaxel was discovered during a broad screening programme for natural products conducted by National Cancer Institute in 1960s [45]. The crude extract from bark of Taxus brevifolia showed antitumor activity against several cancerous cell lines which led to its popularity [45, 52]. In 1963, Wall and Wani demonstrated cytotoxic activity against L1210 and P388 leukemia's, sarcoma 180 and B16 melanoma using crude extract from Taxus brevifolia [53]. In 1971, structural identification of paclitaxel as active constituent in the crude extract was performed [52, 53]. In 1983, Phase 1 studies were initiated and 1986, hypersensitivity reactions due to paclitaxel treatment was observed in the patients [45]. Paclitaxel was proven effective against ovarian cancer in 1989, breast cancer in 1991 and for non-small cell lung cancer in 1992 [45]. United States Food and drug administration approved Paclitaxel for refractory ovarian cancer in 1992 and for metastatic breast cancer in 1994 [45]. Paclitaxel popularity was due to extraction from plant source, unique mechanism of action and being effective anti-cancer drug for a wide range of tumors.

2.4.2 Structure of Paclitaxel

Paclitaxel is a diterpene alkaloid with a complex chemical structure shown in Figure 7. The chemical name of paclitaxel is 5b, 20-epoxy-1, 2a, 4, 7b, 10b, 13a-hexahydroxytax-11-en-9-one-4, 10-diacetate-2-benzoate 13 ester with (2R, 3S)-N-benzoyl-3-phenylisoserine [45]. Paclitaxel structure consists of 14-membered taxane ring linked to an ester side chain at position 13 [53]. The detailed chemical structure of paclitaxel is shown in figure 2.7. Also, presence of hydroxyl group at 2" position of ester side chain increases cytotoxic activity of the drug [45, 54]. Also, the side chain is very important for anti-tumor activity because analogs of Paclitaxel which do not possess this side chain are not cytotoxic [55, 56]. Paclitaxel is stored at or below -20° C and has molecular weight of 853.91.

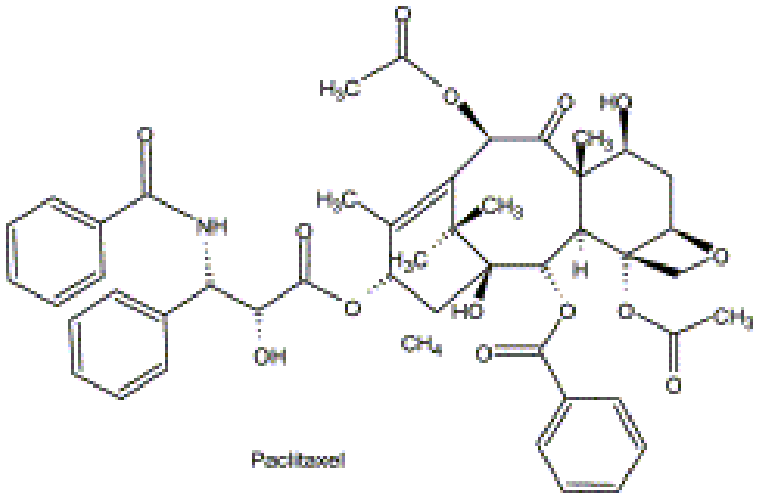

Figure 2.7: Chemical structure of Paclitaxel [51]

2.4.3 Original paclitaxel formulation vehicle

Paclitaxel (6 mg/ml) for intravenous infusion is formulated in a 1:1 v/v mixture of Cremophor EL and dehydrated alcohol [42]. Cremophor EL is polyethoxylated castor oil

used as a formulation agent for Paclitaxel drug delivery. Intravenous route for Paclitaxel administration is not a safe route because there are several risks associated with this technique such as catheter related infection, potential thrombosis and presence of particulate matter in the intravenous infusion formulation [42]. Also, severe hypersensitivity reactions, hypotension and vasodilation have been observed in patients treated with paclitaxel with cremophor EL [42, 57]. During those days, it was not known whether the observed effects were due to paclitaxel itself or the due to the formulation vehicle used during intravenous injection. In order to tackle the problem of hypersensitivity reactions, patients were pretreated with mandatory premedication with corticosteroids, diphenhydramine and H2- receptor antagonists before treating with paclitaxel [45].

Later on several studies were conducted to study biological effects of cremophor EL which revealed important results. Cremophor EL resulted in anaphylactic hypersensitivity reactions characterized by dyspnoea, flushing, rash, chest pain, tachycardia, hypotension, angio-oedema, and generalized urticarial (hives) [58]. However, it blocks P -glycoprotein drug efflux pump and helping in increasing delivery of paclitaxel to target tumor cells by reversing multi-drug resistance phenomenon [59].

Since paclitaxel is highly hydrophobic, it can be incorporated in the hydrophobic core of the SE61 surfactant stabilized micro and nanobubbles. This helps in eliminating use of cremophor EL vehicle and reduces the problems of conventional paclitaxel chemotherapy.

2.4.4 Mechanism of action

Paclitaxal inhibits cell cycle in late G_2 mitotic phase [60, 61]. Guanosine triphosphate associated proteins are required for tubulin assembly under normal conditions which are not necessary when paclitaxel is used [60]. Paclitaxel promotes polymerization of tubulin dimers to form unusually stable microtubules and prevent depolymerization [45, 61, 62]. The binding site for Paclitaxel is N-terminal 31 amino acids of β – subunit of tubulin in the microtubule [45, 63]. Paclitaxal disturbs the equilibrium between microtubule assembly and disassembly and disrupt the formation of normal spindle during metaphase stage [61, 64]. The microtubules formed are dysfunctional causing death of cancer cells [43, 45]. The mechanism of action of paclitaxel is shown in figure 2.8 showing the formation of ultra stabilized microtubules.

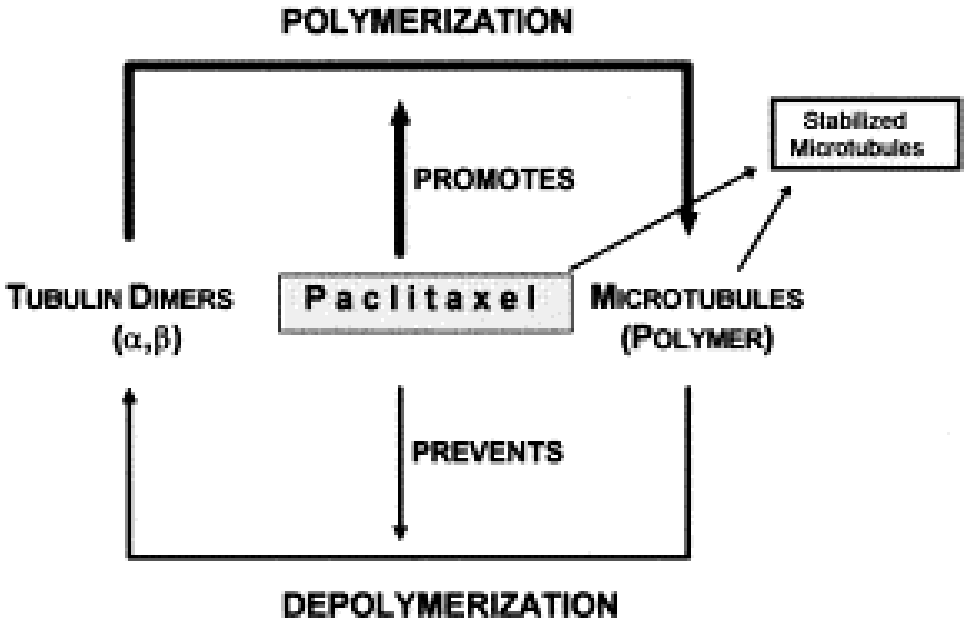

Figure 2.8: Unique mode of action of Paclitaxel [45, 61, 62]

As shown in figure 2.9, paclitaxel shows direct cytotoxicity by stimulating macrophages and killing the tumor cells. Also, indirect way of tumor cell death by paclitaxel occurs by

inducing secretion of cytokines which further activates dendritic cells, natural killer cells and cytotoxic T lymphocytes [65].

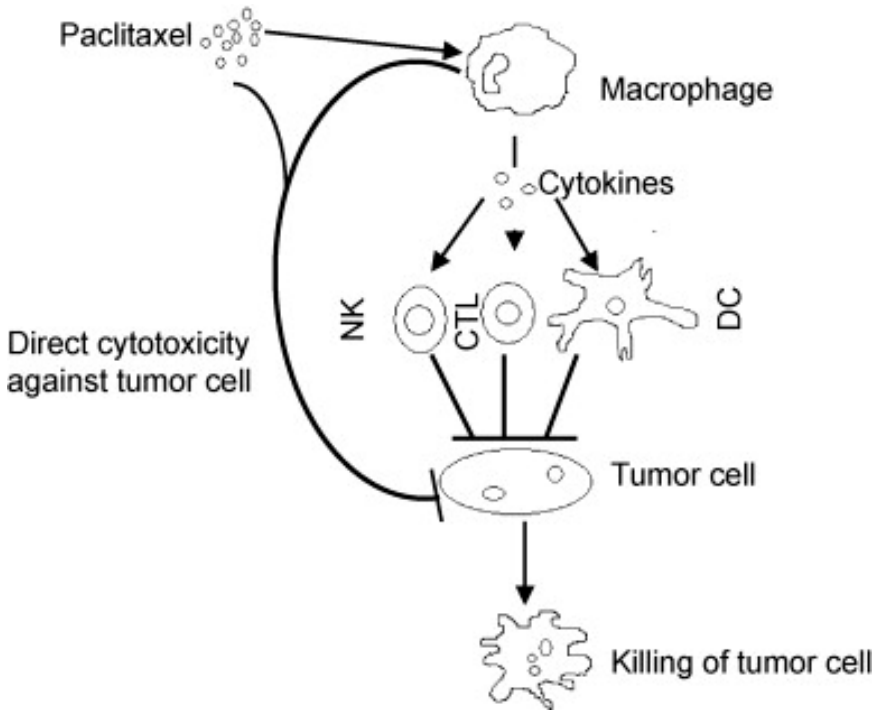

Figure 2.9 : Paclitaxel exhibiting direct and indirect cytotoxicity against tumor cell [65].

2.4.5 Pharmacology of paclitaxel

Paclitaxel binds to proteins in plasma, tissues and tubulins [66]. More than 90% of the paclitaxal rapidly binds to plasma proteins [51] [67, 68]. Paclitaxel shows affinity for distribution in specific tissue types such as kidney, lung and spleen which have the highest tissue concentrations [66, 69, 70]. Paclitaxel metabolism is due to oxidative metabolism and biliary excretion, only 5-10% is renally eliminated [66, 71]. The main hepatic metabolites detected are 6α-hydroxypaclitaxel (major metabolite), p-hydroxyphenyl-C3'-paclitaxel (minor quantities), and dihydroxypaclitaxel (barely detected) [72, 73].

2.5 Cancer

2.5.1 Multi-drug resistance and p-glycoprotein

There are several problems associated with conventional cancer chemotherapy such as drug solubility, narrow therapeutic index of drug and P-glycoprotein efflux transporter specificity [40]. Multi-drug resistance has posed serious problems in targeted cancer treatment. Multidrug resistance (MDR) is simultaneous cellular resistance to a range of drugs which are not related [74].

P-glycoprotein is a 170kDa plasma membrane glycoprotein [74] drug efflux pump responsible for multidrug resistance phenomenon occurring during cancer treatment [75]. In humans, P-glycoprotein is encoded by MDR1 and MDR3 (multi-resistance genes) out of which MDR1 is associated with multi- drug resistance phenotype [76-78]. It consists of 1276- 1280 amino acids with each half containing site for nucleotide binding and hydrophobic regions [74]. A structure of P-glycoprotein is shown in Figure 2.10 where the 2 ATP binding domains plays important role in drug efflux reducing the intracellular concentration.

P-glycoprotein is an extrusion pump specific to a broad range of substrates such as anti-cancer drugs [79, 80]. It causes efflux of anti-cancer drugs out of the cells decreasing their concentration in cells and their cytotoxic effect on the targeted tumor cells [79, 80].

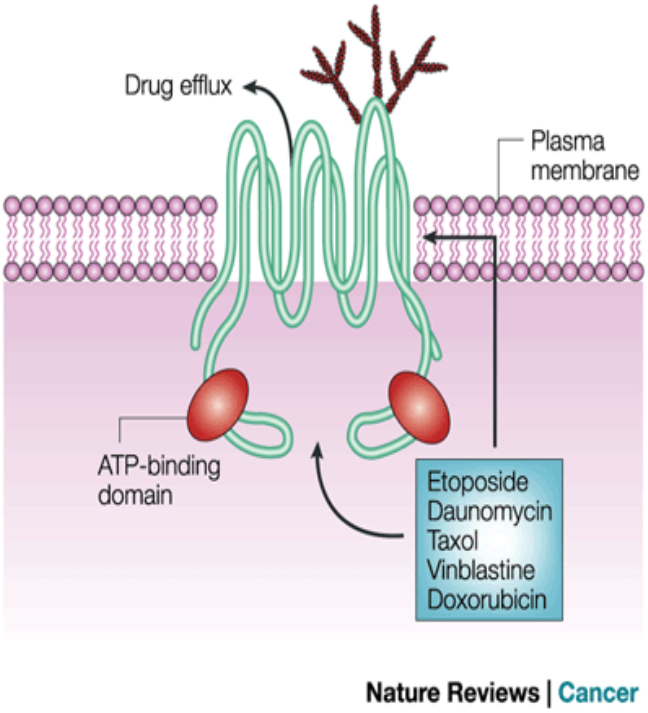

Figure 2.10 : Structure of P-glycoprotein efflux transporter with two ATP binding domains required for drug efflux [81]

P-glycoprotein inhibits the drug permeability and expels drug molecules back into gastrointestinal lumen limiting absorption of the drug [40]. Also, p-glycoprotein influences the excretion of the drug by affecting both biliary and renal tubular functions [40]. In tumor cells, expression of P-glycoprotein causes multi-drug resistance limiting the pharmacological response [40]. In the past, a lot of research work has been done towards increasing the bioavailability of anti-cancer drugs in tumor cells by inhibiting P-glycoprotein transporter directly [40]. Other approaches include development of formulations that allow drug to bypass the P-glycoprotein transporter or agents which are non-P-glycoprotein substrates [40].

Surfactants such as Tween 80, Cremophor EL, TPGS modulate efflux pump by competitive inhibition of substrate binding, alteration of membrane fluidity and inhibition

of efflux pump ATPase activity [29, 39, 82]. D-α-tocopheryl polyethylene glycol 1000 succinate (TPGS) modulates ABC-transporter P-glycoprotein activity by inhibition of efflux pump ATPase activity [39, 82, 83].

2.5.2 Tumor microenvironment

In the case of solid tumors, conventional chemotherapy alone is the seldom curative [23, 84]. The anticancer drugs are useful for killing tumor cells grown in monolayer cultures [23, 85]. However, they cannot kill all tumor cells that later develop into tumor in vivo [23, 85]. The tumor microenvironment is characterized by abnormalities in the vasculature and extracellular matrix responsible for insufficient delivery of drugs at the targeted site [23, 86]. There are abnormalities in vasculature such as blood vessels being leaky and possess large gaps between the endothelial cells [23, 87]. Leakiness of tumor blood vessels is due to open pores of sizes range from 380nm to 780nm at certain interendothelial junctions[88, 89]. The vasculature is disordered in regard to spatial distribution, random interconnections and abnormal length and diameter of microvessels [23, 86, 90].

In the blood flow in the tumor cells is further made worse by proliferating tumor cells which generate solid pressure on the vessels [23, 90]. Due to a lack of functional lymphatics, there is increase in the interstitial fluid pressures in tumor cells [23]. Apart from the poor organization of tumor vasculature, there is reduced delivery of oxygen and build up of metabolic products such as carbonic acids and lactic acid which reduce the extracellular pH [23, 85]. Nano-sized contrast agents are useful in imaging tumors as they provide higher tissue extravasation rate causing high number of agents passing through the vessels in the targeted tumor [88]. The tumor vasculature exhibits enhanced

permeability and retention effect causes retention of nanoparticles that are smaller than pore size which makes the development of nano-sized contrast agents of immediate importance [88, 91, 92]. The phenomenon of enhanced permeability and retention effect is shown in figure 2.11.

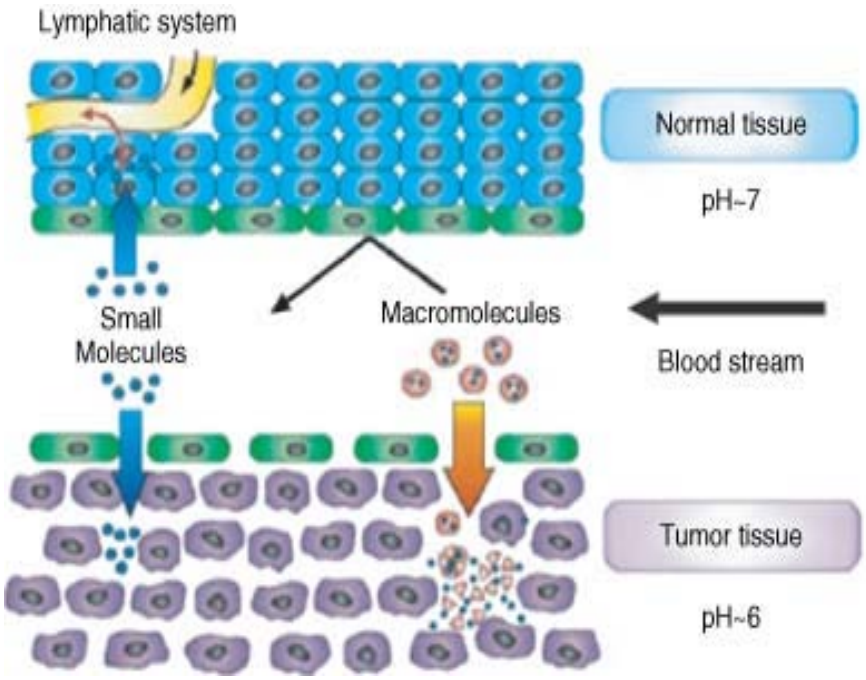

Figure 2.11 : Normal tissue and tumor vasculature being compared where tumor tissue exhibits enhanced permeability and retention effect [93].

2.5.3 Angiogenesis

Angiogenesis is a process where growth of new capillary blood vessels occurs [94] which plays a important role in development of cancer. Without angiogenesis, tumor cells do not enter into circulation and are limited to a very small size [94]. A change in the angiogenic balance between pro-angiogenic growth factors (VEGF, FGFs) and angiogenesis inhibitors (TSP-1) is responsible for angiogenesis progression [95-98]. Oxygen consumption by neoplastic cells and endothelial cells and poor oxygen delivery causes low oxygen concentration called hypoxia in tumor cells [99]. Vascular endothelial

growth factor (VEGF) is an inducer of angiogenesis and is responsible for endothelial cell proliferation [100, 101]. VEGF is produced due to hypoxia- inducible factor-1 released by tumor cell in response to decrease in oxygen concentration (hypoxia) [100, 102-105]. High VEGF expression allows tumor cells to enter blood stream and reduce the delivery of anti-cancer drugs for cancer treatment [90, 99, 106, 107]. Anti-angiogenic therapy inhibits endothelial cell proliferation or cause apoptosis of these cells in the tumor [94].

2.5.4 Paclitaxel and apoptosis

The time course for apoptosis induced by paclitaxel was conducted in vivo in murine model and in patients undergoing paclitaxel chemotherapy [108-111]. In murine model, peak of apoptosis was observed within 24 hours and in clinical studies, peak was observed within 48 hours [108, 111]. However, the continuation of apoptotic response after initial intravenous push of paclitaxel in murine model was until 72 hours and in clinical studies, it continued until 96 hours [108, 111].

CHAPTER 3: MATERIALS AND METHODS

3.1 Materials used

3.1.1 Surfactants

Two non-ionic surfactants were used for preparing the micro and nanobubbles. Span 60 (sorbitan monostearate) (S7010-1KG, batch # 010M0128) was purchased from Sigma Aldrich (St.Louis, MO) and used without purification. Eastman Vitamin-E TPGS (d-Alpha Tocopheryl polyethylene glycol 1000 succinate) NF grade was purchased from Eastman (Llangefni, Anglesey, United Kingdom) (batch # 78971100) and used without purification.

3.2.2 Buffer

PBS (0.1M) was used as the buffer for preparing and testing the bubbles.

Table 3.1: PBS ingredients

Name of the chemical	Specifics	Quantity (g)
Sodium chloride	(S5886-1KG, Batch # 078K01281) Sigma Aldrich (St.Louis, MO)	8.01
Sodium phosphate dibasic	(S0876-1KG, Batch # 075K0167) Sigma Aldrich (St.Louis, MO)	1.15
Potassium phosphate monobasic	(P5655-500G, Batch # 084K0175) Sigma Aldrich (St. Louis, MO)	0.2
Potassium chloride	(P-4504-500g, Batch # 31K0157) Sigma Aldrich (St. Louis, MO)	0.2

The above chemical were weighed out and transferred to 1L standard flaks and made up to 1L with distilled (DI) water. The pH was adjusted to 7.4 using 1M NaOH and HCl as required followed by filtration using 0.22µm GV Durapore membrane filter (lot # R6AN42605) purchased from Millipore.

3.1.3 Drug

Paclitaxel (Cat No.P-9600, Lot ASM-113) was purchased from LC Laboratories (Woburn, MA) and used without purification.

3.1.4 Other chemicals

Octafluropropane (99.9%) was purchased from American Gas Group (lot # 0327BD09, Toledo, OH) and used after passing through passing through a 0.22µm filter (Nalgene, Rochester, NY). Acetonitrile HPLC Grade (CAS no. 75-05-8) was purchased from Fisher Scientific (Fair Lawn, New Jersey) was used without further purification. Ethyl Acetate HPLC Grade (CAS 141-78-6, Lot no. 032371) was purchased from Fisher Scientific (Fair Lawn, New Jersey) was used without further purification. Thermo scientific Nalgene 0.2 µm syringe filter (Cat. No. 195-2520, Lot no. 1041670) were purchased from Fisher scientific, Newark. 1 ml vial with cap fisher brand (Cat. No. 03-391-23) were purchased from Fisher scientific were used during HPLC. Regular 3ml sterile luer tip syringes (Lot no. 006004) were purchased from Tyco healthcare (Mansfield, MA) used for injecting the extracted paclitaxel in the 1ml vial during HPLC sample injection.

3.2 Methods

Ultrasound contrast agents were prepared using the Standard Operating Procedure (SOP) followed in the laboratory. The United States patent on “Surfactant stabilized microbubble mixtures, process for preparing and methods of using the same” with patent # 5352436 was used with preparation of bubbles with some changes [26].

3.2.1 Standard micro and nanobubble preparation

The SOP for preparing the surfactant stabilized micro and a nanobubble is explained in the appendix B.1. Briefly, calculated amounts of Span 60, TPGS, and sodium chloride were placed in a 300 ml beaker and 50 ml of PBS is added with pH 7.4. The mixture was first heated with constant stirring until the span 60 and TPGS completely dissolved. Then the mixture was autoclaved. The mixture was cooled with continuous stirring to enable proper mixing of the surfactants and to decrease the particle size of span 60 that drops out of solution upon cooling.

The beaker was kept in ice and octafluoropropane was used to purge the mixture. A pipette tip was added to the exit tube of the gas cylinder and placed in the surfactant solution to allow a slow (50 ml/min) stream of gas to bubble through. Later the 1000 µl pipette tip was placed above the solution which was then sonicated for 3 min at 110 W. with a sonicator (Misonix Inc. Farmingdale, NY) employing a CL4 tapped horn probe with 0.5” tip shown in figure 3.1.

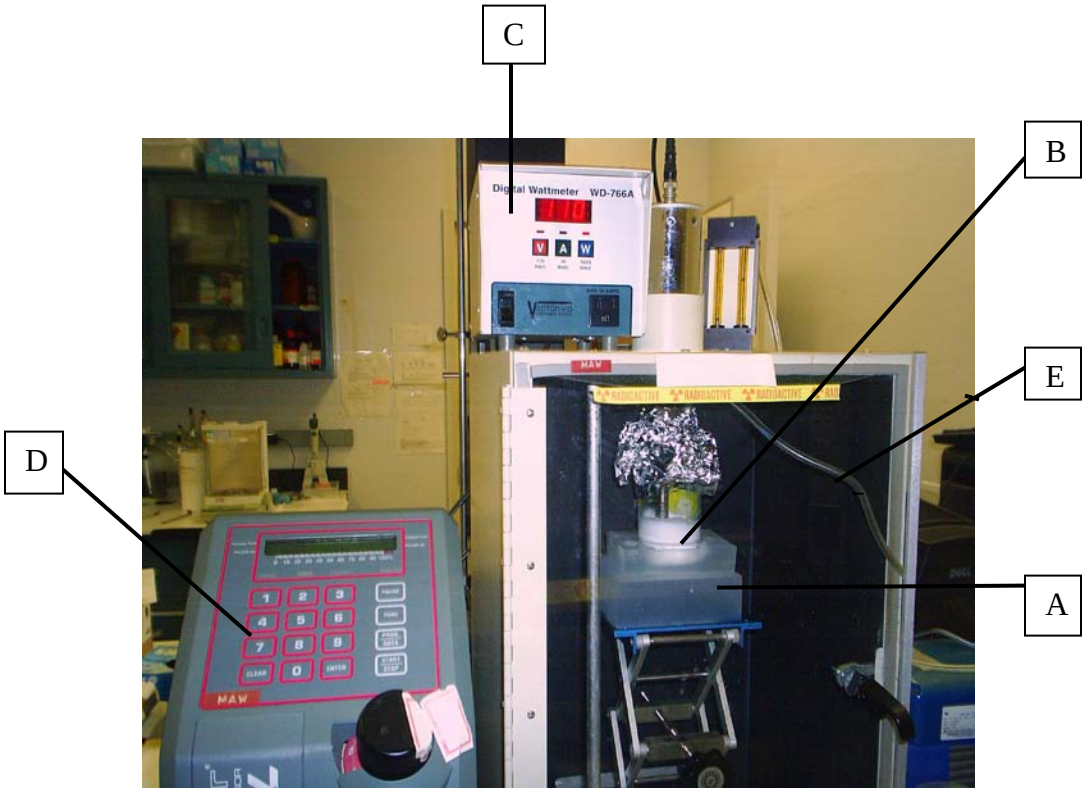

Figure 3.1: Photo of the Paclitaxel loaded SE61 being sonicated at 110W for 3 min using octafluoropropane. The SE61 mixture (B) was placed in ice (A) and covered with foil to hold the tip above the solution. The digital wattmeter was adjusted to 110W (C) and sonication was performed for 3 min (adjusted using instrument D). The pipette tip is connected to exit of gas cylinder and the pipe carries the octafluoropropane gas (E).

The sonicated mixture was poured into a (4^{o}C) separation funnel (A) and 50 ml of 4^{o}C PBS was added to the funnel. This was the first wash with PBS. The bubbles were allowed to separate and after 45 min, 25 ml of solution from the bottom of the separating funnel was discarded and 50-75 ml of the solution is transferred to a second cold (4^{o}C) separation funnel (B). Again both the funnels are washed with 50 ml of cold PBS which was considered as the second wash shown in figure 3.2. After 45 min, 50 ml of the solution was discarded from both the funnels and fresh 50 ml of cold PBS was added to each funnel. This was the third wash with PBS. Finally after a waiting period of 45 min,

from funnel B (containing nanobubbles) 25 ml was discarded and 10 ml was collected in a 50 ml centrifuge tube. This is the standard nanobubble preparation. The solution from funnel A separated into three distinct layers, a lower later containing unused surfactant, a middles, viscous layer containing microbubbles and an upper layer containing foam. The lower layer was drained from the funnel until the middle layer was found. The middle layer (containing the microbubbles) was collected in a 50 ml centrifuge tube. It was later diluted using membrane filtered PBS for acoustic testing of microbubbles

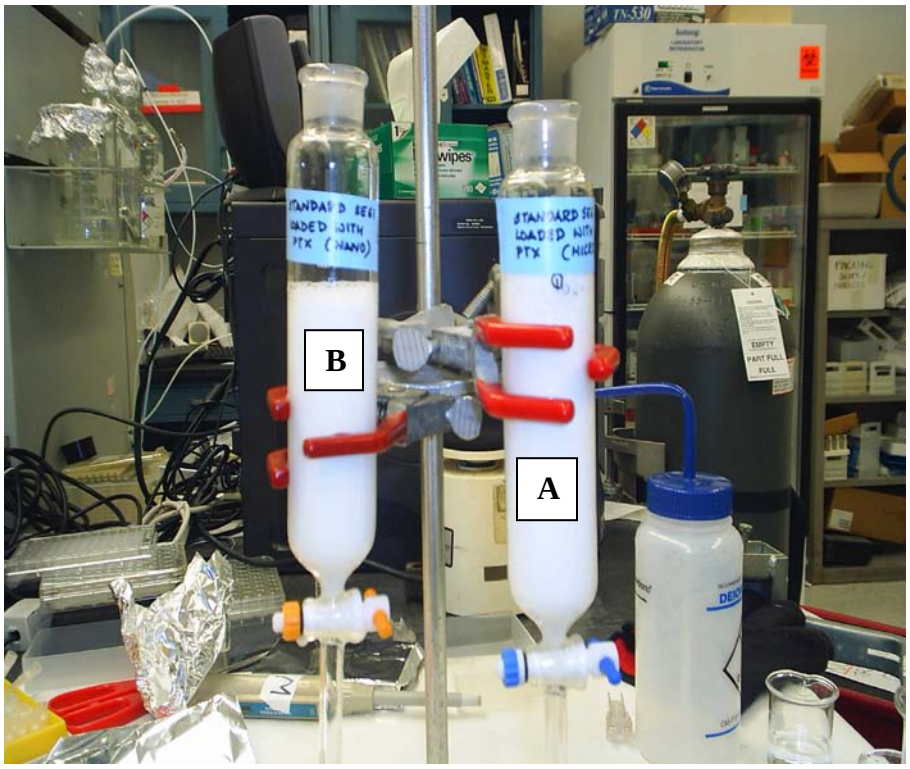

Figure 3.2: Paclitaxel loaded standard micro and nanobubbles in separation funnel after the second wash with 50 ml of cold PBS. Funnel A contains microbubbles and Funnel B contains nanobubbles.

3.2.2 Effect of varying sodium chloride and surfactant

The main goal of thesis was to increase the drug encapsulation efficiency in nanobubbles and get higher nanobubble population. The concentration of total sodium chloride and TPGS were varied to achieve high nanobubble population with higher stability. The first

part of the study involves variation in the amounts of total sodium chloride to find which salt concentration gave the maximum enhancement. In the second part of the study, molar ratio of Span 60: TPGS was varied in the SE61 mixture to find which ratio gave the highest nanobubble population. Also, effects of sodium chloride and TPGS ratios were studied for microbubbles echogenecity and stability.

3.3 Direct Drug loading Method

For direct drug loading, 100 µg/ml of paclitaxel was used which corresponds to 5 mg of paclitaxel in 50 ml of surfactant mixture. The detailed SOP for loading of paclitaxel in the drug is mentioned in Appendix B.7. In brief, paclitaxel was weighed out and added in the stirred autoclaved surfactant mixture. The mixture was heated at about 100° C with constant stirring for 30 min on a magnetic stirrer. The solution was cooled to room temperature by constant stirring for 35-45 min. The mixture was then sonicated as usual and separated using 4°C PBS (pH 7.4).

3.4 Characterization of bubbles and drug loaded bubble

The Standard SE61, varied SE61 (varying total sodium chloride and TPGS ratios) and drug loaded bubbles were tested for in-vitro acoustic properties using echogenecity testing (dose response) and stability. Further characterization of the bubbles and drug loaded bubbles were done using size analysis, zeta potential measurement and turbidity measurement at 610 nm. Three independent trials were conducted for each condition showing repeatability and accuracy in the results.

3.4.1 Dose and Time Response

Initial set up of the function generator was done with pulse repetition frequency being adjusted to 100 Hz, energy to 1 and damping to 3. A 5072 pulser-receiver (Waltham,

MA) was used to generate acoustic pressure with pulse repetition (PRF) frequency of 100 Hz. A Lecroy 9350 A 500 Hz Oscilloscope was used and set to 1µs and 100mV shown in figure 3.3.

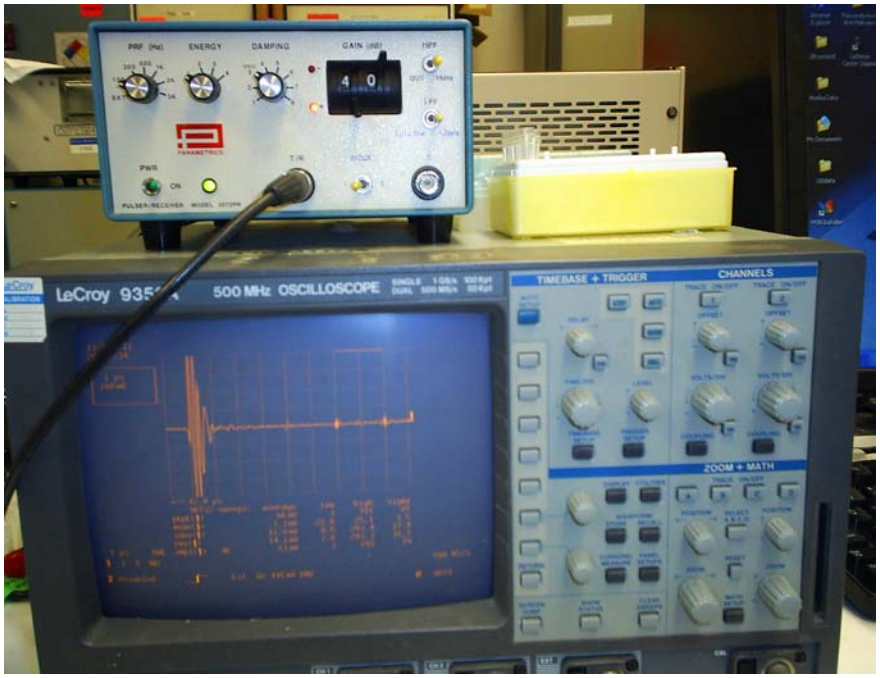

Figure 3.3: Lecroy 500MHz Oscilloscope used during acoustic testing of bubbles. 5MHz transducer was used with delay adjusted to 62µs in the oscilloscope. The gain is adjusted to 40dB for acoustic testing.

A custom built vessel has acoustic window (1.5 inches by 1.5 inches) was used for acoustic testing of micro and nanobubbles. Membrane filtered PBS (50 ml) with pH 7.4 at 37°C was transferred into the custom vessel. This custom vessel was placed in a rectangular tank which is temperature controlled (37°C) and half filled with DI water as shown in figure 3.4. A stir bar was added to the custom vessel and the stirrer is adjusted to level 3. A single Panametric (Waltham, MA) 5 MHz transducer (-6dB bandwidth of 91% and 12.7 mm in diameter) was used with delay being adjusted 62 µs in the oscilloscope. Initially the transducer is focused through the transparent window till a

signal was seen at 20dB gain. Later the gain is adjusted to 40dB. Lab VIEW 7.1 (National Instruments) software was used for analysis.

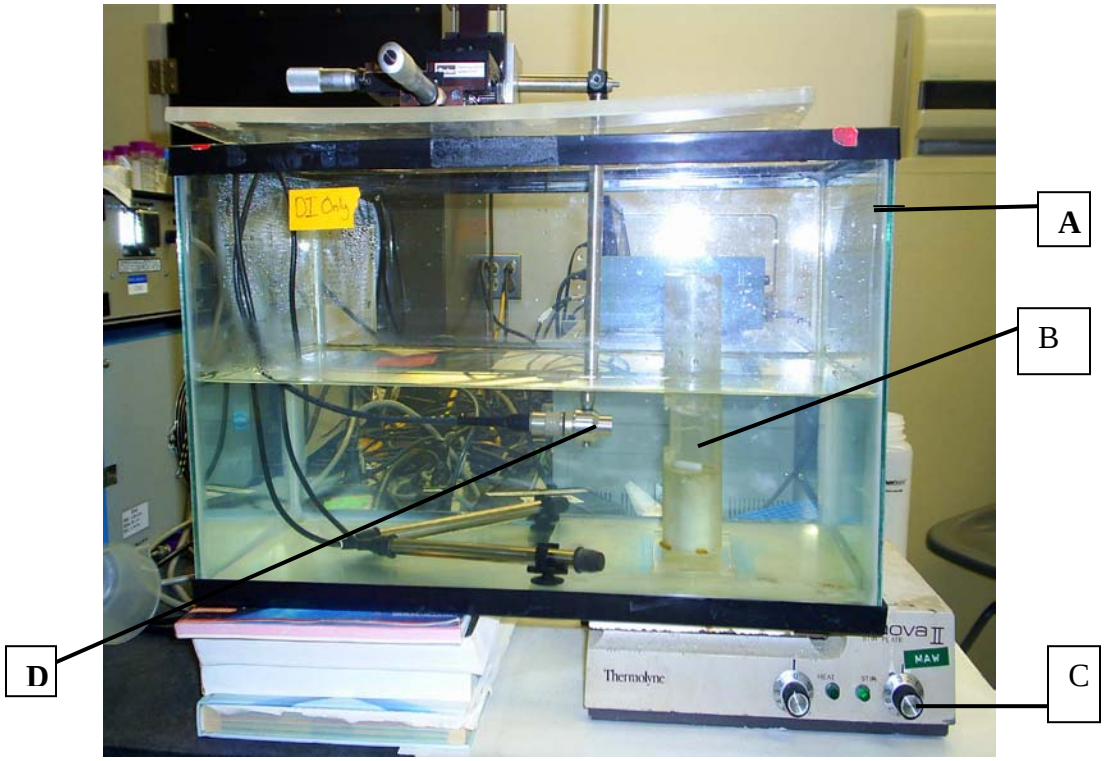

Figure 3.4 Set up of the ultrasound tank for acoustic testing of the bubbles (A). The tank is filled with DI water half way above the 5MHz transducer probe (D). The acoustic window of custom build vessel is shown in (B). Membrane filtered PBS (50 ml) is added to custom built sample vessel and fitted at appropriate position with stirrer level adjusted to 3 (C).

The baseline acquisition was first made (PBS alone) and then the required dose of the SE61 or drug loaded SE61 was added to the sample vessel using a 50-200 µl pipette. Cumulative dose response study was performed where amplification is read at 40dB. For the response with respect to time, a dose on the rise of dose response curve was used. This gave us information about the stability of the bubbles in the ultrasound beam. Data are plotted as dB normalized to the initial values time to account for inter sample variations. The half life of the bubbles were calculated from the point on the

enhancement vs. time curve where initial normalized enhancement drops to 0.5. The stability response for microbubbles was done for 15 min and for nanobubbles stability response was for 10 min.

3.4.2 Size Analysis

The detailed size analysis procedure of bubble and particles is mentioned in Appendix B.4. Briefly, a Zetasizer nano ZS (Malvern Inst., UK) instrument was used for size analysis. For size analysis of mixtures prior to sonication, 1000 µl of room temperature autoclaved SE61 mixture was transferred into tapered cuvettes. In the case of nanobubbles, 1000µl of the nanobubble suspension was taken and transferred directly into the cuvette without dilution. But in case of microbubbles, 200µl of microbubbles is transferred to a 10ml volumetric flask where the volume was made up to the mark with membrane filtered PBS (pH 7.4). After gentle mixing, 1000µl from the 10ml volumetric flask was transferred to the tapered cuvette for size analysis. The measurement was taken three times and the cuvette is gently shaken before each run. The z-average diameter in nm was noted down each time.

Figure 3.5: Photo of the Malvern Zetasizer nano ZS instrument with tapered cuvettes placed in the slot of the instrument (A).

3.4.3 Zeta potential of the particles and bubbles

The magnitude of zeta potential gives information about the charge of the bubbles and the tendency to aggregate, which increases as the value tends to zero. The basic idea of investigating the zeta potential was to study which concentration of total sodium chloride and which Span 60: TPGS molar ratio gave the most stable nanobubbles for drug loading and HPLC studies.

The detailed procedure of zeta potential measurement of bubble and particles is given in Appendix B.5. Briefly, a Zetasizer nano ZS (Malvern Inst., UK) instrument was used for measuring zeta potential. For zeta potential of particles, 1000µl of room temperature autoclaved SE61 mixture was transferred into Zeta sizer Nano series capillary cuvettes (Malvern Inst., UK). In case of nanobubbles, 1000µl of the nanobubbles was taken and transferred directly in the cuvette without dilution. But in case of microbubbles, 200µl of

microbubbles was transferred in 10ml volumetric flask where the volume was made up to the mark with 37°C membrane filtered PBS (pH 7.4). 1000µl from the 10ml volumetric flask was transferred in the cuvette for zeta potential of microbubbles. The measurement was taken three times and the cuvette is gently shaken before each run .The ZP –average in mV is noted down

3.4.4 Turbidity measurement at 610nm

One of the objectives of the thesis was to study the effect of varying total salt concentration and surfactant TPGS ratios on the nanobubble population. Due to difficulty in counting the number of nanobubbles, increase or decrease in the amount of nanobubbles produced was compared by means of turbidity measurement (absorbance scan) at 610nm [112-114]. The detailed procedure for turbidity measurement is mentioned in Appendix B.6. Tecan infinite M 200 (Research Triangle Park, NC) instrument was used as shown in figure 3.6.

Figure 3.6: Photo of the Tecan infinite M 200 instrument (A) with 96 corning flat transparent plate reader (B) on the top of the instrument

Non-sterile Polystyrene, Flat bottom, medium binding costar 96 corning flat transparent plate reader (Corning, NY) was used for turbidity measurement. 10µl of nanobubbles and 190 µl of cold PBS pH 7.4 was added in the well of the plate reader and scanned from 230 nm to 1000 nm.

3.4.5 Efficiency of paclitaxel encapsulation by high performance liquid chromatography

The detailed procedure for studying the efficiency of paclitaxel encapsulation is described in Appendix B.8. In brief, 2.5 ml of ethyl acetate was added to 2.5 ml of paclitaxel loaded bubbles and vortexed for 1 min. Later centrifugation is performed using Beckman Coulter Allegra^{TM} 21 centrifuge with relative centrifugal force being adjusted to 8528 g for 15 min. After centrifugation, 2 separated layers are formed. The upper layer consists of ethyl acetate with paclitaxel in it and the lower layer consists of span 60 and TPGS. Ethyl acetate containing paclitaxel (1.5 ml of the upper layer) was pipette out into a glass bottle and the remaining lower layer containing span 60 and TPGS was discarded out. Ethyl acetate in the glass bottle was evaporated and then 1.5 ml of Acetonitrile was added to glass bottle and sealed with parafilm. The glass bottle is kept for shaking for 24 hours. The extracted paclitaxel in acetonitrile in glass bottle was filtered using thermo scientific Nalgene 0.2 µm syringe filter. Regular 3ml sterile luer tip syringe was used for transferring the paclitaxel extracted into 1 ml vials. Waters 1525 Binary HPLC Pump (reverse-phase) was used to study the efficiency of encapsulation [115] shown in figure 3.7. The HPLC column used was Inertsil ODS column (GL Science, Tokyo, Japan) with 5 µm particle size and dimensions of 250 mm by 4.6 mm. The mobile phase used was 100 % acetonitrile HPLC grade. The flow rate used was 1ml/min [116, 117]. 50µl of the sample is injected and run for 30 min. UV detection at 227 nm is used [116, 117]. From

the salt and surfactant studies, concentration which gave highest population of nanobubbles and microbubbles were chosen. Paclitaxel was loaded in the newly formulated bubbles and the standard micro and nanobubbles. HPLC was used to study the efficiency of paclitaxel encapsulation in newly formulated and standard micro and nanobubbles. The calibration curve of paclitaxel for concentrations 0.0537 to 268.5 µg/ml (prepared by our lab member Boriphat Methachan) with R^2= 0.99 was used for studying the drug encapsulation efficiency. The set up of HPLC is shown in figure 3.7.

Figure 3.7: High Performance Liquid Chromatography (HPLC) used for studying Paclitaxel encapsulation efficiency

3.4.6 Light microscopy

Olympus 1X71 light microscope was used for taking the pictures of SE61 microbubbles and nanobubbles with and without paclitaxel being loaded. SPOT advanced software was used for taking the images.

3.5 Statistical Analysis

All statistical analysis was done using Microsoft excel 2007. t- Tests, one-way and two-way ANOVA were performed for the data sets to give information about the statistical significance of the hypothesis of the experiments. The alpha value used to judge statistical significance is 0.05.

CHAPTER 4: RESULTS AND DISCUSSION

The new agent SE61 was prepared by replacing Tween 80 by TPGS in the standard protocol for preparing ST68. However, the protocol has been changed from the original method for ST68 and despite the successful generation of microbubbles, it was not known what steps affect the yield, properties of SE61, and on generation of the nano population. In the original agent ST68, an initial grinding step was introduced to intimately mix the fatty solid span and the viscous Tween 80 before sonication. However, since the initial studies with ST68 the protocol has been changed to include a heating step and autoclaving, and the salt/grinding step was discontinued. However, it was observed that having no added sodium chloride in the SE61 surfactant mixture appeared to produce fewer nanobubbles. Although the grinding step was discontinued, the same amount of salt was added to the PBS in the solution to be autoclaved, resulting in a total sodium chloride concentration of 650 mM in standard SE61 surfactant mixture.

4.1 Properties of standard SE61 microbubbles

In this section, the dose response, stability, size and zeta potential of microbubbles are studied for standard SE61 in detail.

4.1.1 Acoustic characterization of standard SE61 microbubbles

The acoustic characterization of microbubbles is performed as mentioned in Appendix B.2 and B.3. First the baseline acquisition was made with PBS alone and then the required dose of microbubbles (prepared with 650 mM total sodium chloride concentration and 1: 0.25 molar ratio of span 60: TPGS as in the SOP) was dispensed

into the custom built vessel kept in the ultrasound tank. A cumulative dose response study was performed. For the response with respect to time, a dose on the rise of the dose response curve was used. The stability response for microbubbles was performed for 15 minutes.

4.1.1.1 Dose response of standard SE61 microbubbles

In figure 4.1, dose response of standard SE61 microbubbles is shown. A small degree of shadowing started to occur at a dose of 60 µl/L with maximum contrast enhancement of 25.72 ± 0.855 dB.

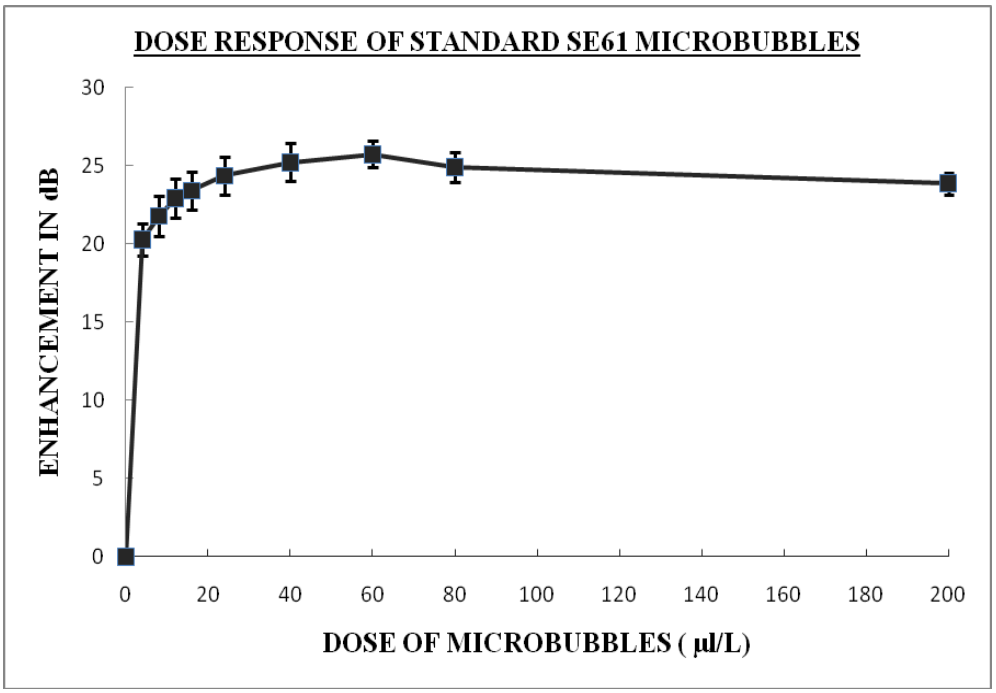

Figure 4.1: Dose response of standard SE61 microbubbles, N=3 independent observations and error bars representing standard error about the mean.

4.1.1.2 Stability response of standard SE61 microbubbles

In the figure 4.2, half life of standard SE61 microbubbles is shown. The dose chosen for stability response was 12 µl/L corresponding to 30 µl of microbubbles added to the

custom built vessel. This dose was chosen because it was found to be in the linear range of dose response curve for both paclitaxel loaded and non-paclitaxel loaded microbubbles. The half lives of the bubbles were calculated from the point on the enhancement vs. time curve where initial normalized enhancement drops to 0.5 as shown in figure 4.2. The half life of standard SE61 microbubbles is 7.75 ± 1.97 minutes.

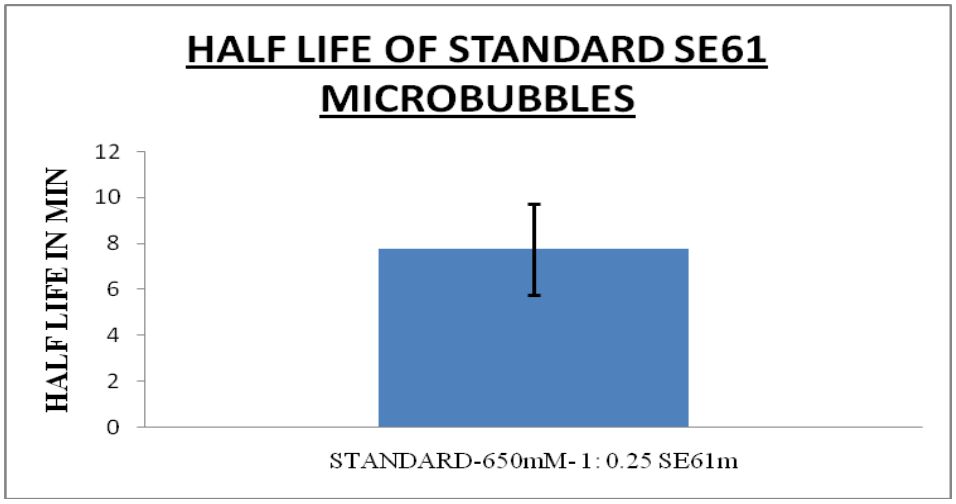

Figure 4.2: Half life of standard SE61 microbubbles, N=3 independent observations and standard error bars representing standard error about the mean.

4.1.2 Size of standard SE61 microbubbles

The average diameter of microbubbles was 2203 ± 95 nm (standard error of mean) for standard SE61 microbubbles.

4.1.3 Zeta potential of standard SE61 microbubbles

The zeta potential of standard SE61 microbubbles was -8.5 ± 0.46 mV.

4.2 Effect of added sodium chloride on SE61 microbubbles

The additional sodium chloride concentration in the entire SE61 mixture was varied to study its effect on microbubble enhancement and stability to form a basis for comparison

with the separated nano component. The sodium chloride concentration in the PBS buffer was kept constant (137 mM) and additional sodium chloride was added to the 50 ml of SE61 surfactant mixture. The effect of additional sodium chloride in the surfactant mixture on microbubble echogenecity, stability, size, zeta analysis is studied in this section.

4.2.1 Acoustic characterization of varying total sodium chloride microbubbles

The acoustic characterization of microbubbles is performed as mentioned in Appendix B.2 and B.3. A cumulative dose response study was performed. For the response with respect to time, a dose on the rise of the dose response curve was used. The stability response of microbubbles was performed for 15 minutes.

4.2.1.1 Dose response of total sodium chloride varying microbubbles

In figure 4.3, dose response of microbubbles are compared at different total (that from the PBS and the added salt) sodium chloride concentrations ($p > 0.05$) at dose of 40 µl/L, implying additional sodium chloride concentration does not have statistically significant effect on enhancement of microbubbles. In the trend, 262 mM total sodium chloride concentration microbubbles shows slightly higher enhancement compared to other salt concentrations. There is no statistically significant difference in the enhancement between 262 mM and 650 mM (standard) total sodium chloride concentration microbubbles ($p > 0.05$) at dose of 40 µl/L. In case of 262 mM total sodium chloride concentration, the maximum contrast enhancement is 28 ± 1.5 dB at dose of 60 µl/L of microbubbles. Shadowing occurred at dose of 60 µl/L with maximum contrast enhancement of 25.72 ± 0.855 dB for standard SE61 microbubbles.

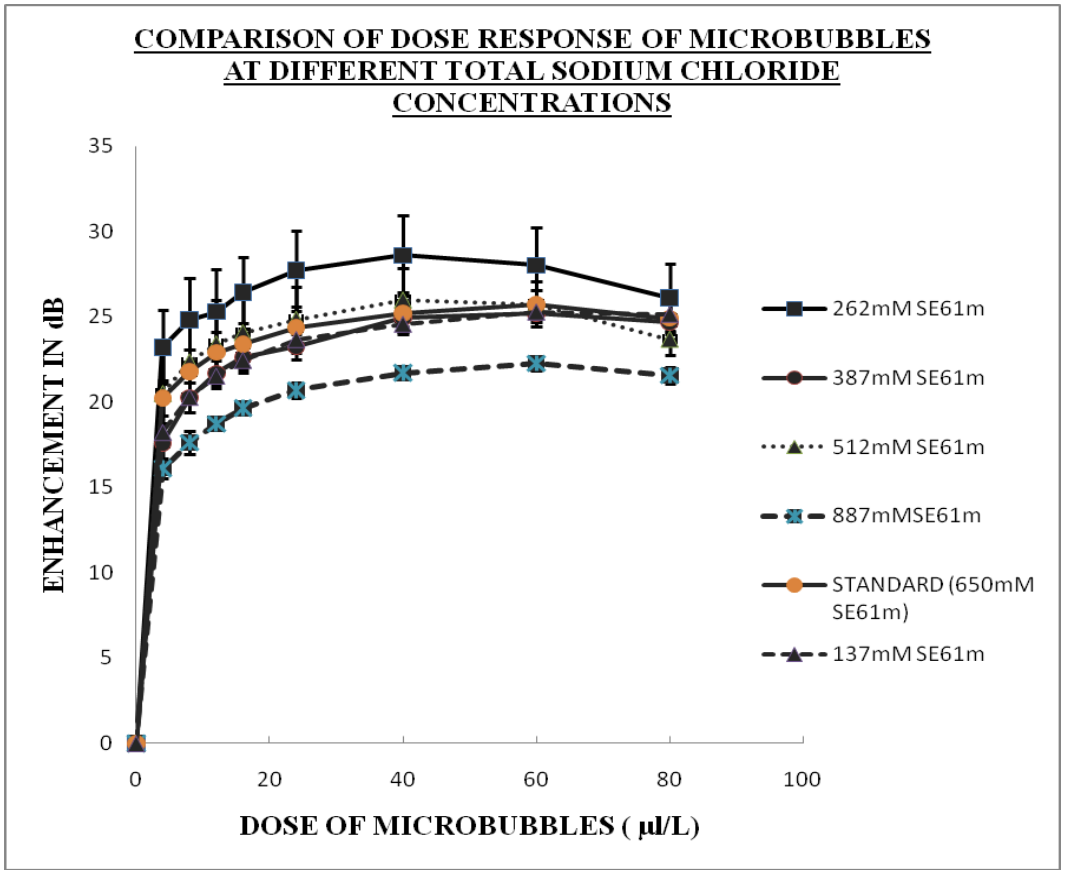

Figure 4.3: Dose response of microbubbles at different total sodium chloride concentration keeping span 60 and TPGS constant, p> 0.05 (one way ANOVA) at dose of 40 µl/L, N=3 independent observations and error bars representing standard error about the mean.

4.2.1.2 Stability response of total sodium chloride varying microbubbles

The dose chosen for stability response was 12 µl/L of microbubbles for non-paclitaxel loaded and paclitaxel loaded microbubbles. The half lives of the bubbles were calculated from the point on the enhancement vs. time curve where initial normalized enhancement drops to 0.5. In figure 4.4, stability of microbubbles at different total sodium chloride concentrations are compared (p> 0.05). The additional sodium chloride added to 50 ml of SE61 mixture does not statistically significant effect on the half life of microbubbles.

There is no statistically significant difference in the half life of microbubbles (p> 0.05) between 262 mM and standard (650 mM) microbubbles. The half life of standard (650 mM) SE61 microbubbles 7.75 ± 1.97 minutes and of 262 mM total sodium chloride is 8.23 ± 2 minutes.

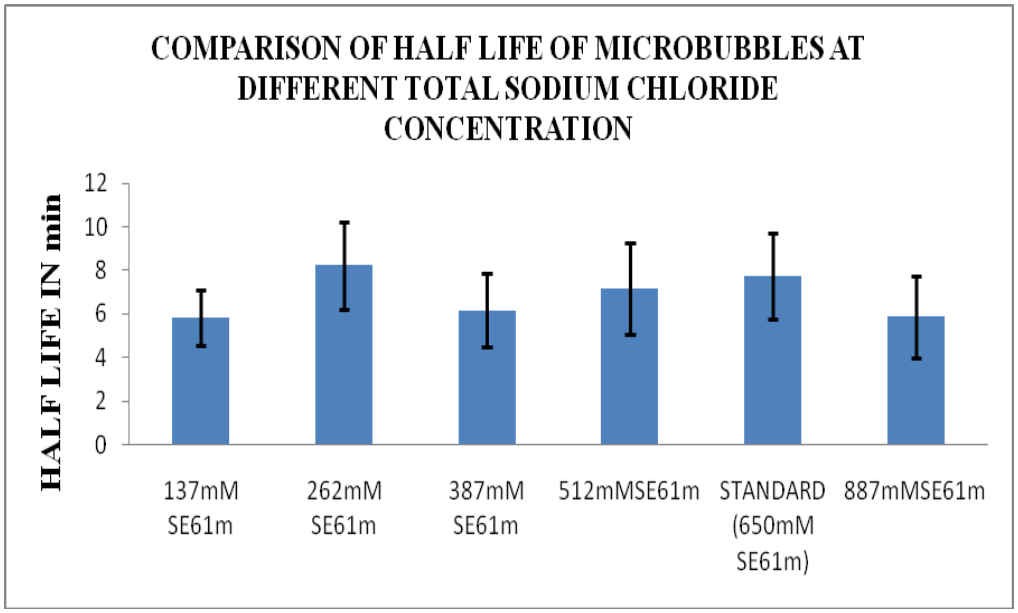

Figure 4.4: Half life of microbubbles at different total sodium chloride concentrations, p> 0.05, N=3 independent observations and error bars representing standard error about the mean**.**

4.2.2 Size of total sodium chloride varying microbubbles

In figure 4.5, size of microbubbles at different total sodium chloride concentrations are compared (p> 0.05). The additional sodium chloride added to SE61 surfactant mixture does not have statistically significant effect on the size of microbubbles.

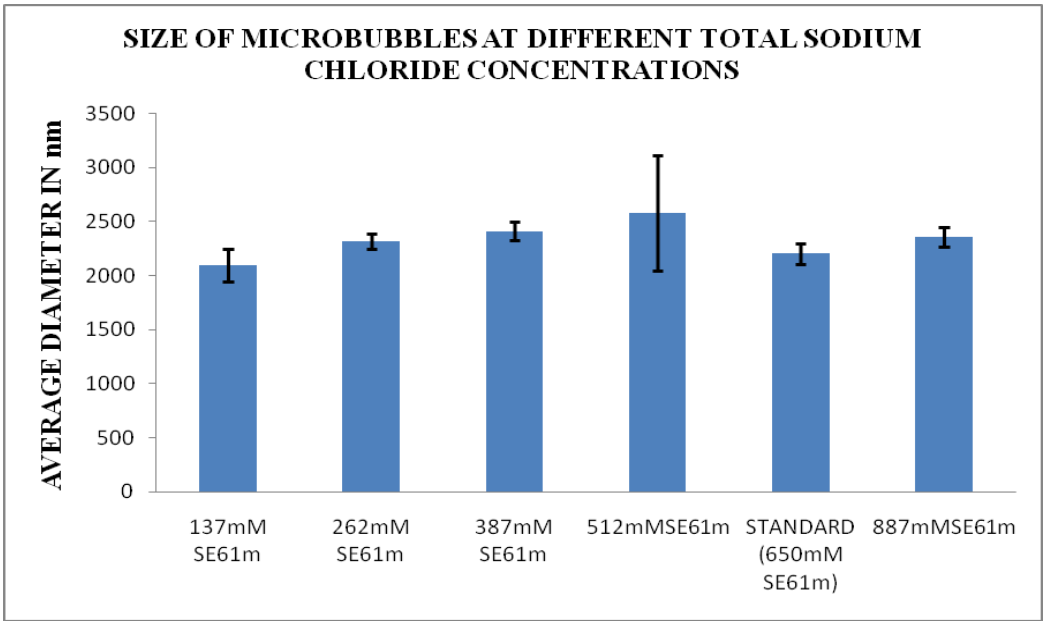

Figure 4.5: Size of microbubbles at different total sodium chloride concentrations, p> 0.05, N=3 independent observations and error bars representing standard error about the mean

4.2.3 Zeta potential of total sodium chloride varying microbubbles

In figure 4.6, zeta potential of microbubbles at different total sodium chloride concentrations are compared with p> 0.05. The additional sodium chloride added to 50 ml of SE61 surfactant mixture does not have statistically significant effect on the zeta potential of microbubbles. The zeta potential of the microbubbles with 262 mM total sodium chloride concentration is -8.8 ± 0.66 mV. The zeta potential of standard SE61 microbubbles is -8.5 ± 0.46 mV. The magnitude of zeta potential of 262 mM total sodium chloride microbubble is slightly higher than standard (650 mM) microbubbles. However, it must of be noted that the presence of sodium chloride could be influencing the results by shielding the actual charge.

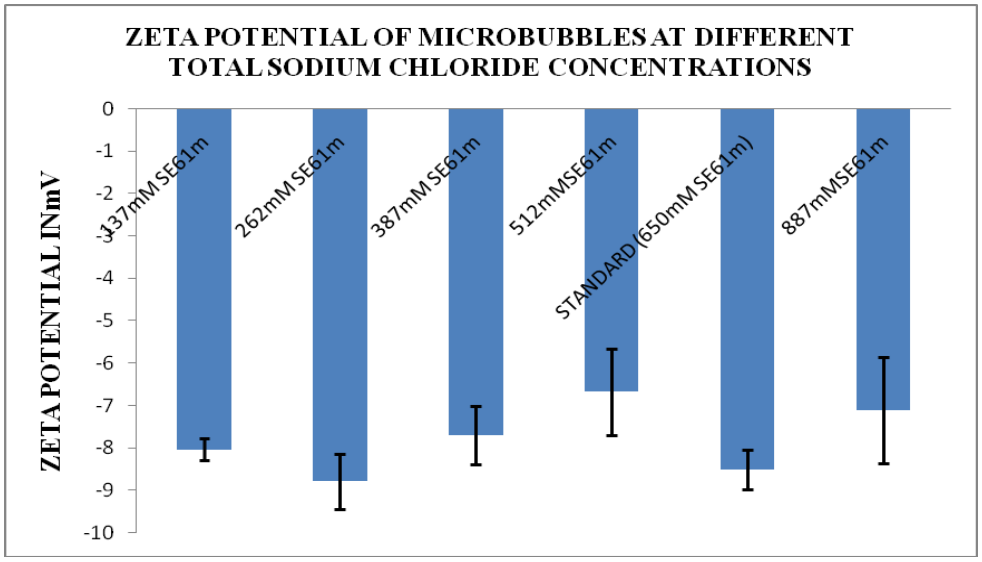

Figure 4.6: Zeta potential of microbubbles at different total sodium chloride concentrations, p> 0.05, N=3 independent observations and error bars representing standard error about the mean

4.2.4 How are newly formulated microbubbles different from standard SE61 microbubbles from the salt study:

In the newly formulated microbubbles, the total sodium chloride concentration chosen is 262 mM over the standard 650 mM total sodium chloride concentration. In case of 262mM total sodium chloride concentration, the maximum contrast enhancement is 28 ± 1.5 dB at dose of 60 µl/L of microbubbles. Shadowing occurred at dose of 60 µl/L with maximum contrast enhancement of 25.72 ± 0.855 dB for standard SE61 microbubbles. The half life of standard (650mM) SE61 microbubbles 7.75 ± 1.97 minutes which is slightly lower than 262 mM total sodium chloride (8.23 ± 2 minutes) microbubbles.

4.3. Effect of surfactant ratio on microbubbles

The TPGS concentration was varied in the SE61 surfactant mixture keeping span 60 and total sodium chloride concentration same as used in standard SE61 microbubbles.

4.3.1 Acoustic characterization of microbubbles with different surfactant ratio

The acoustic characterization of microbubbles is performed as mentioned in Appendix B.2 and B.3

4.3.1.1. Dose response of microbubbles

In the graph shown in figure 4.7, dose response of standard (1: 0.25) SE61, 1: 0.43 and 1: 0.67 molar ratio microbubbles are compared with $p < 0.05$. Shadowing occurred at dose of 60 μl/L with maximum contrast enhancement of 25.72 ± 0.855 dB for standard (1: 0.25) SE61 microbubbles. The maximum contrast enhancement for 1: 0.43 and 1: 0.67 molar ratio microbubbles are 24.9 ± 1.36 dB (dose of 60 μl/L) and 20.8 ± 0.36 dB (dose of 80 μl/L) respectively.

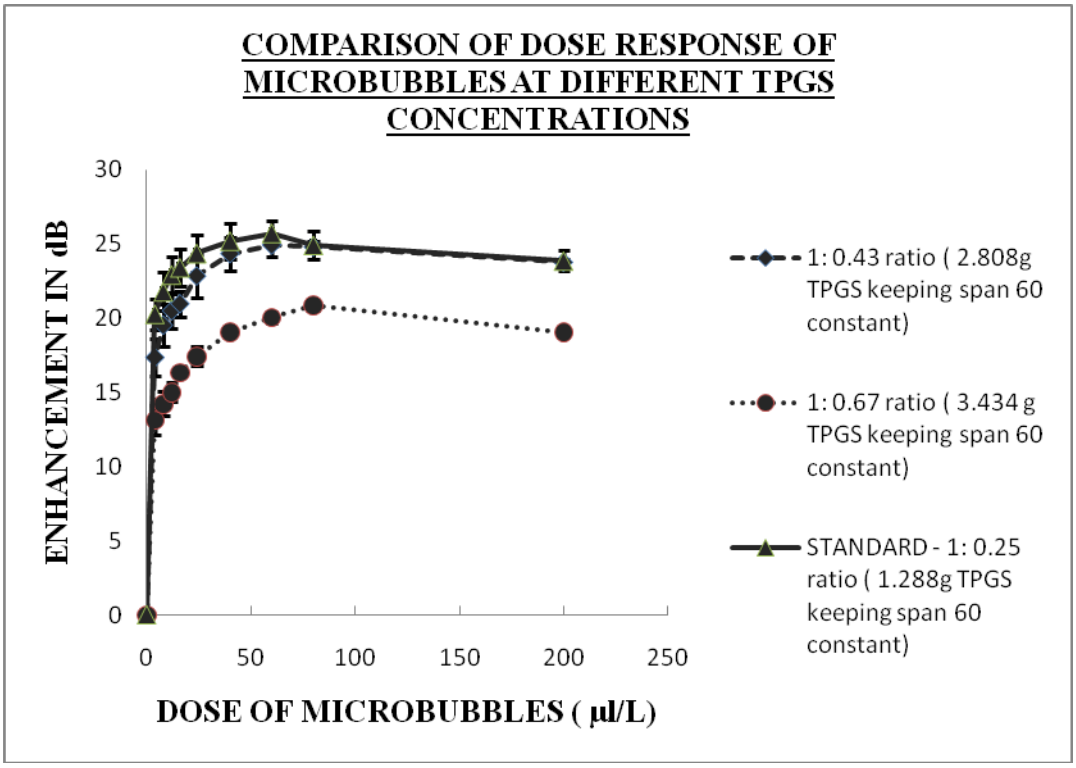

Figure 4.7: Comparison of dose response of microbubble at different TPGS concentrations, $p < 0.05$ at dose of 200 µl/L (One way ANOVA), N=3 independent observations and error bars representing standard error about the mean.

4.3.1.2. Stability response of microbubbles

In figure 4.8, half life of the microbubbles are compared at different TPGS concentrations, using one way ANOVA with $p > 0.05$. There is no statistically significant difference in half life of microbubbles having standard (1: 0.25) and 1: 0.43 molar ratio of span 60: TPGS. The half life of microbubbles having 1: 0.67 molar ratios is 3.3 ± 0.72 minutes.

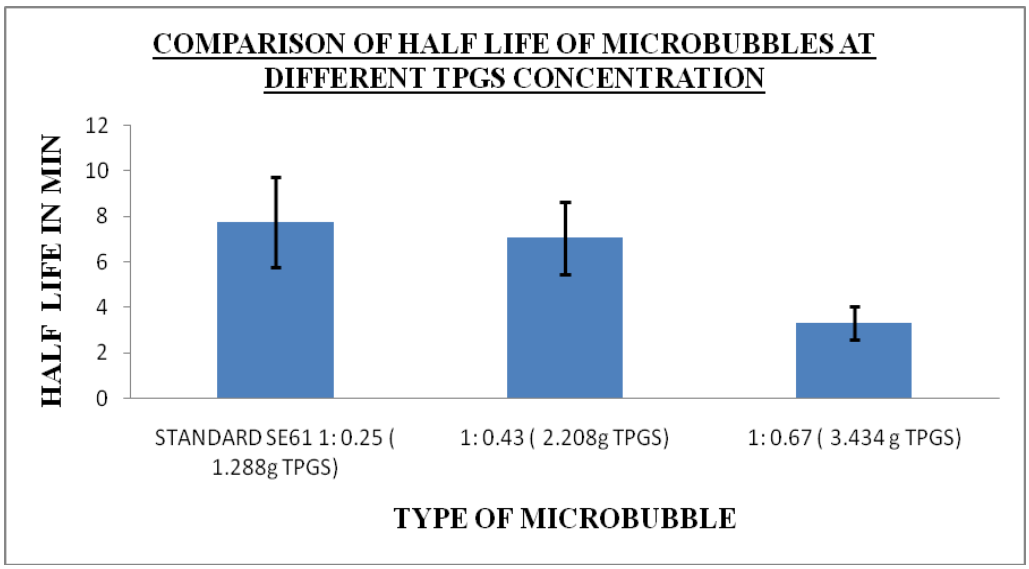

Figure 4.8: Half life of the microbubbles at different TPGS concentrations, One way ANOVA: $p > 0.05$, N=3 independent observations and error bars representing standard error about the mean.

Increasing the TPGS concentration in SE61 mixture does not have statistically significant effect on the half life of the microbubbles.

4.3.2 Size of microbubbles at different TPGS concentrations.

In figure 4.9, size of microbubbles is compared at different TPGS concentrations using one way ANOVA with $p < 0.05$. Increasing the TPGS concentration has statistically significant effect on the size of microbubbles. The size of 1: 0.67 molar ratio microbubbles is significantly smaller with average diameter of 1227 ± 99 nm.

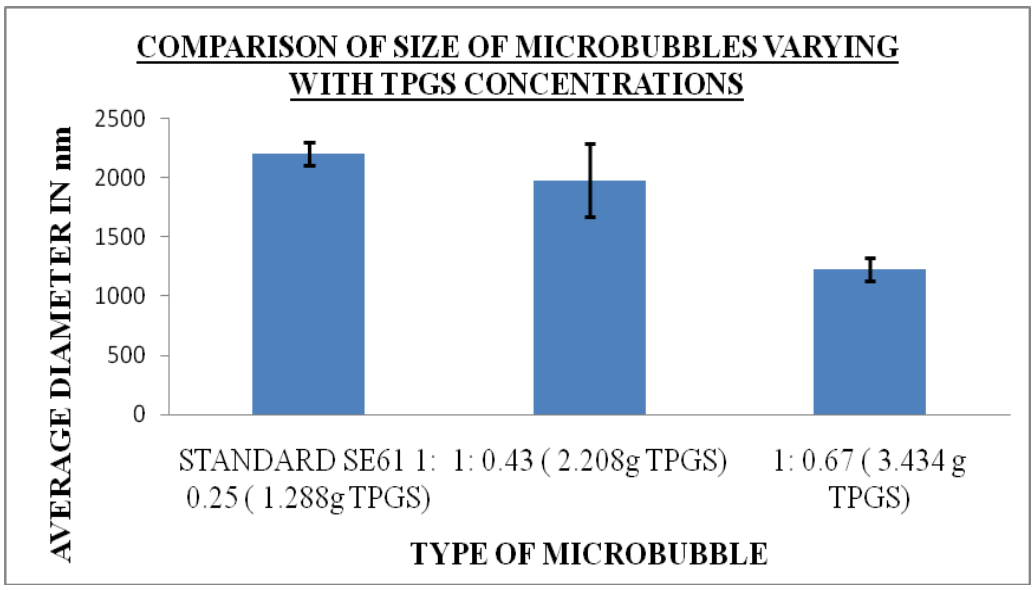

Figure 4.9: Comparison of size of microbubbles at different TPGS concentrations, $p < 0.05$ (One way ANOVA), N=3 independent observations and error bars representing standard error about the mean.

4.3.3 Zeta potential of microbubbles

The zeta potential of microbubbles is compared in Figure 4.10 with $p < 0.05$.

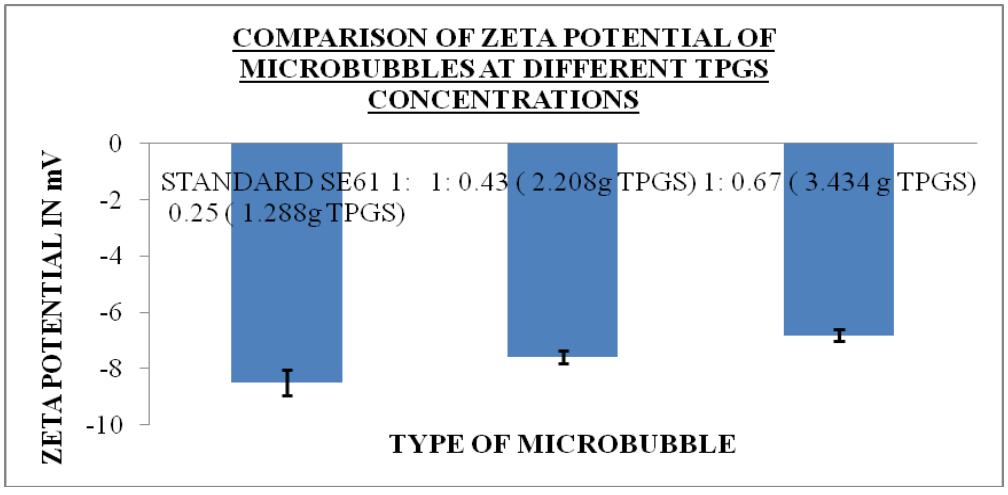

Figure 4.10: Comparison of zeta potential of microbubbles at different TPGS concentrations, $p < 0.05$ (One way ANOVA), N=3 independent observations and error bars representing standard error about the mean

The zeta potential of 1: 0.67 molar ratio nanobubbles is significantly lower with value of -6.8 ± 0.19 mV.

4.3.4. How is newly formulated microbubble different from the standard SE61 microbubbles

From the TPGS study, 1: 0.25 molar ratio of span60: TPGS is chosen over concentrations Also, 1: 0.43 did not have statistically significant difference when compared with standard (1: 0.25) for echogenecity, half life and zeta potential of microbubbles.

4.4 Paclitaxel encapsulation in microbubbles

The second aim of the thesis was to investigate the possibility of incorporating a hydrophobic drug in to the microbubbles with the possibility of using the agent to deliver drug directly to a tumor in the presence of ultrasound.

4.4.1 Acoustic characterization of paclitaxel loaded microbubbles

The acoustic characterization of microbubbles is performed as mentioned in Appendix B.2 and B.3.

4.4.1.1 Dose response of paclitaxel loaded microbubbles

Paclitaxel was loaded into the newly formulated microbubbles (with 262 mM total sodium chloride concentration and 1: 0.25 molar ratio of span: TPGS) and standard SE61 microbubbles in figure 4.11. At maximum dose of 200 µl/L, there is statistically significant difference in the contrast enhancement with $p < 0.05$, with the new formulation showing a great extent of shadowing.

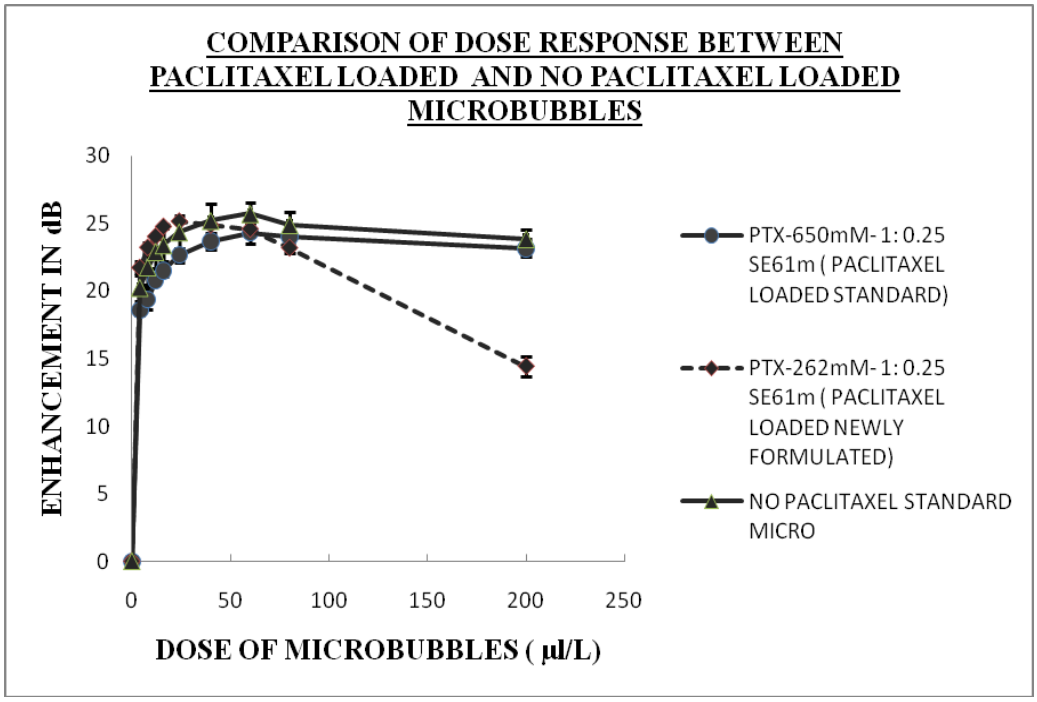

Figure 4.11: Comparison of dose response of paclitaxel loaded standard SE61; paclitaxel loaded newly formulated and standard SE61 microbubbles, $p < 0.05$ at dose of 200 µl/L, N=3 independent observations and error bars representing standard error about the mean.

The maximum enhancement of paclitaxel loaded standard SE61 and without drug standard SE61 are 24.3 ± 0.77dB and 25.72 ± 0.855 dB respectively at dose of 60 µl/L. There is no statistically significant difference in enhancement between paclitaxel loaded in standard SE61 and no-drug standard SE61 microbubbles.

4.4.1.2 Stability response of paclitaxel loaded microbubbles

The half life of the paclitaxel standard SE61microbubbles and paclitaxel loaded newly formulated microbubbles are compared in figure 4.12 with $p > 0.05$.

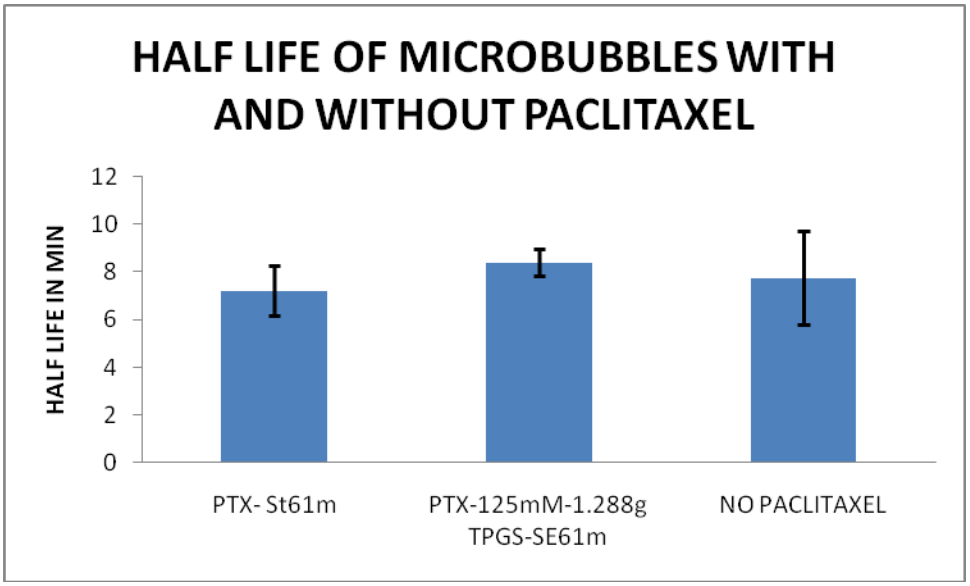

Figure 4.12: Half life of paclitaxel loaded standard SE61 and paclitaxel loaded newly formulated microbubbles, $p>0.05$, N=3 independent observations and error bars representing standard error about the mean.

When considering stability, we would like the bubbles to break easily and release the drug, i.e., to be unstable in the US beam, so in the case of the two agents described here, it would appear that there is no distinct advantage stability-wise of using one over the other. Also, there is no statistically significant difference in half life of paclitaxel loaded and no paclitaxel loaded microbubbles.

4.4.2. Size of paclitaxel loaded microbubbles

The different molar ratios of surfactants did not appear to influence the microbubble size, as seen in figure 4.13. The size of microbubble is not statistically significantly affected by paclitaxel loading.

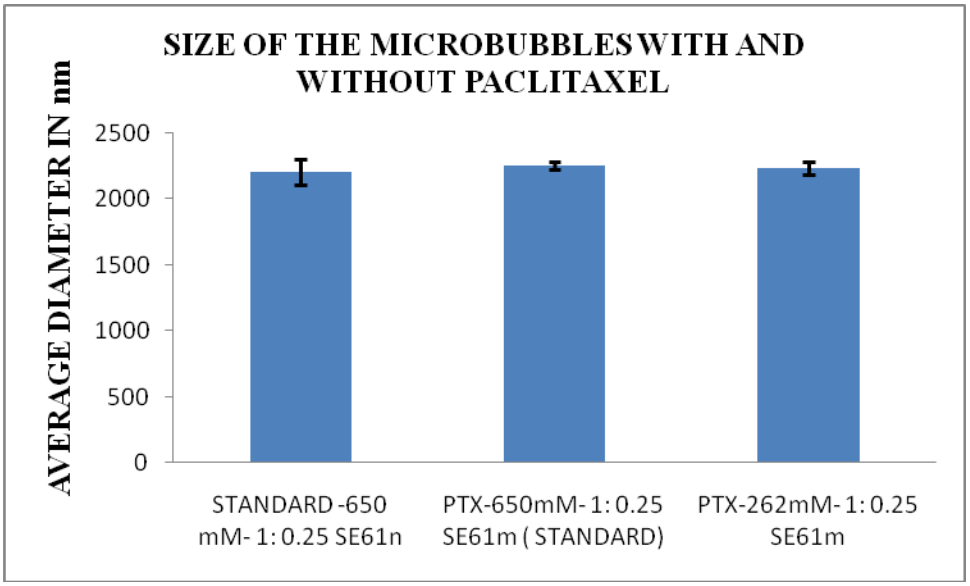

Figure: 4.13: Size of paclitaxel loaded standard SE61 and newly formulated microbubbles, p> 0.05, N=3 independent observations and error bars representing standard error about the mean.

4.4.3 Zeta potential of paclitaxel loaded microbubbles

In figure 4.14, zeta potential of paclitaxel loaded standard SE61 and paclitaxel loaded newly formulated microbubbles (p> 0.05) are compared. Also the zeta potential of paclitaxel loaded standard SE61 and non-paclitaxel loaded SE61 are not statistically significant.

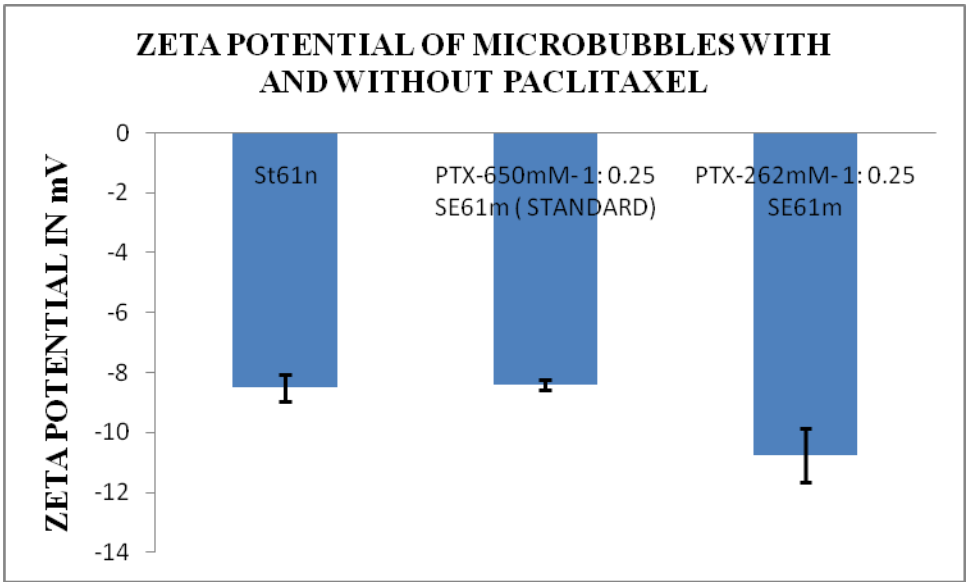

Figure 4.14: Zeta potential of paclitaxel loaded standard SE61 and newly formulated microbubbles, p> 0.05, N=3 independent observations and error bars representing standard error about the mean.

4.4.4 Encapsulation efficiency of paclitaxel in the micro bubbles by high performance liquid chromatography

Initial paclitaxel concentration loaded into 50 ml of SE61 surfactant mixture prior to sonication was 100 µg/ml. The calibration curve for paclitaxel concentrations from 0.0537 to 268.5 µg/ml (R^2= 0.99) was constructed using HPLC, and used for studying the encapsulation efficiency. A comparison in the paclitaxel encapsulation efficiency was made between standard (STANDARD-650 mM- 1: 0.25 SE61) microbubble and newly formulated (PTX-262mM- 1: 0.25 SE61) microbubble in figure 4.15. However, there is no statistically significant difference in the encapsulation efficiency with p > 0.05.

$$\% \text{ encapsulation efficiency} = \frac{\text{Amount of paclitaxel encapsulated in the bubbles}}{\text{Total amount of paclitaxel added initially}} * 100$$

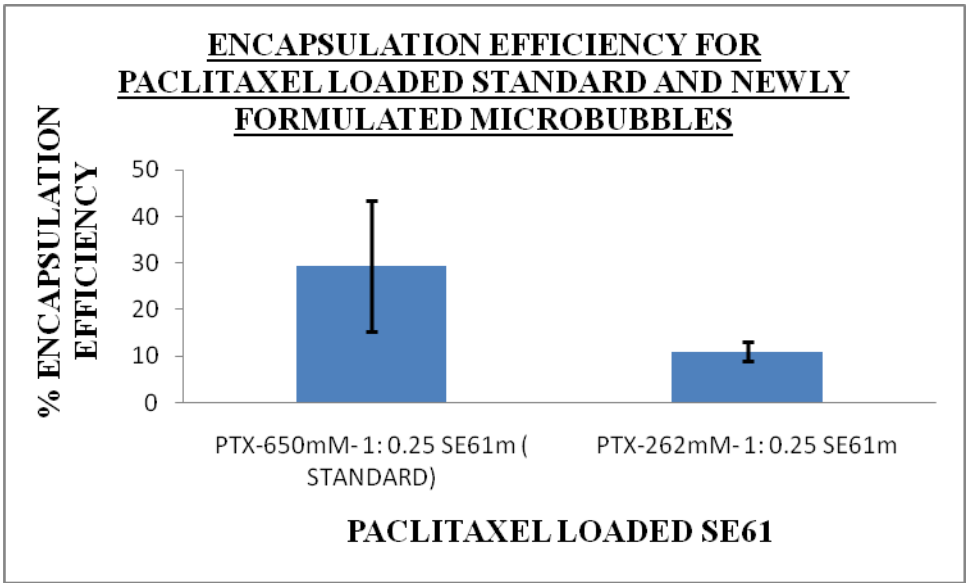

Figure 4.15: Paclitaxel encapsulation in standard SE61 and newly formulated microbubbles, $p>0.05$, N=3 independent observations and error representing standard error about the mean.

One of the aims of the thesis was to investigate parameters that increase the nanobubble population. Also, investigating the effects that changing the parameters has on the particles in suspension after the autoclaving step may shed light on the mechanism of bubble stabilization. The first step was to document the properties of the nanobubbles that were formed by using this current, standard method (SOP) of contrast agent preparation.

4.5 Properties of standard SE61 nanobubbles

It was evident from the start that when Tween 80 was replaced by TPGS, the population of nano sized bubbles that were generated increased. This was evident from two

observations, 1) the very distinct middle band of microbubbles that formed in the mixture after sonication with ST68 was not present with SE61, rather a more diffuse band was observed, and 2) if the sonicated mixture was separated as usual, but then the lower layer that was usually discarded was collected in a second separation funnel, the nanobubbles it contained slowly rose to form a layer on top of the liquid. This rather dilute layer was collected as is and tested as the nano population.

The dose response, stability, size analysis, zeta potential and turbidity measurement were performed for this sub population of nanobubbles after the micron sized bubbles had risen to the middle layer after sonication.

4.5.1. Acoustic in-vitro testing of standard SE61 nanobubbles

First the baseline acquisition was made with PBS alone and then the required dose of nanobubbles (prepared with 650 mM total sodium chloride concentration and 1: 0.25 molar ratio of span60: TPGS as in the SOP) was dispensed into the custom built vessel in the ultrasound tank as described in the methods section. A cumulative dose response study was performed. For the response with respect to time, a dose on the rise of the dose response curve was used. The stability response for nanobubbles was performed for 10min.

4.5.1.1 Dose response of standard SE61 nanobubbles

The dose response of standard SE61 nanobubbles is shown in figure 4.16. Shadowing occurred at a dose of 400 µl/L of nanobubbles giving maximum enhancement of 22.40 ± 0.86 dB.

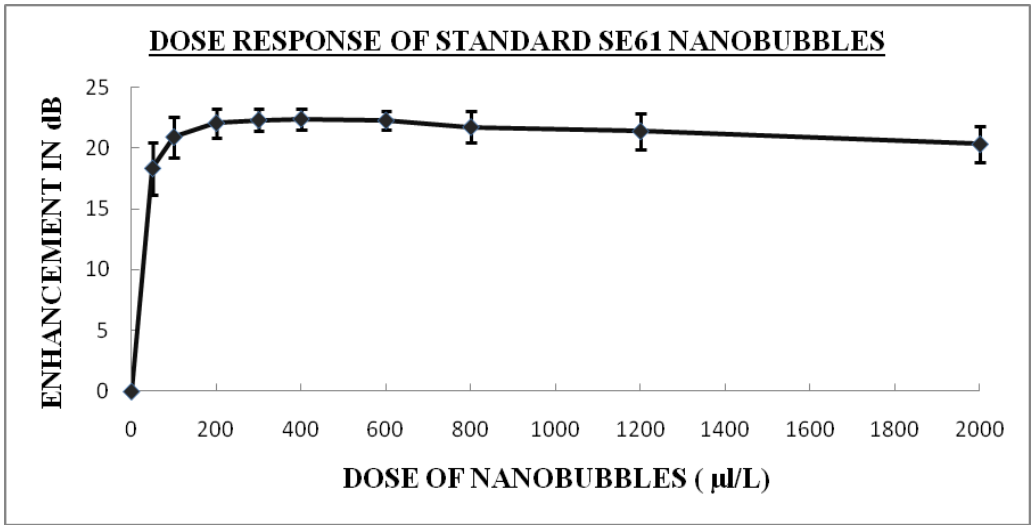

Figure 4.16: Dose response of standard SE61 nanobubbles with 650mM total sodium chloride concentration (513mM additional sodium chloride added and 137mM sodium chloride in PBS) and 1: 0.25 molar ratio of span 60: TPGS, N=3 independent observations and error bars representing standard error about the mean.

Compared to the standard microbubble preparations of SE61, the nanoparticles agent produces equally strong acoustic reflections (with maximum enhancement of 22.40 ± 0.86 dB) vs. 25.72 ± 0.855 dB (standard microbubbles) but are obviously much more dilute, since a dose of close to 500 µl is required to reach maximum signal, compare to 60 µl/L for the micron SE61. This could also be a function of the small size to the bubbles.

The scattering cross section σ of a gas bubble (a measure of how strongly it reflects ultrasound) is given by the born equation (equation 4.1).

$$\sigma = \frac{4\pi}{9} k^4 r^6 \left[\left(\frac{\kappa_s - \kappa}{\kappa} \right)^2 + \frac{1}{3} \left(\frac{3(\rho_s - \rho)}{2\rho_s + \rho} \right)^2 \right] \qquad \text{Equation 4.1}$$

where: σ is scattering cross-section (m^2), r is the radius (m), k is the wave number ($2\pi/\lambda$), $kr<<1$, K_s is the compressibility of the scatterer, K is the compressibility of the

suspending medium, ρ_s is the density of the scatterer, and ρ is the density of the suspending medium. It can be seen that σ is strongly dependent on radius (r^6).

4.5.1.2 Stability response of standard SE61 nanobubbles

The stability response of standard SE61 nanobubbles is shown in figure 4.17. The dose chosen for stability response was 100 µl/L of nanobubbles. This dose was chosen because it was found to be in the linear range of dose response curves for both paclitaxel loaded and non-paclitaxel loaded nanobubbles. The half life of the bubbles were calculated from the point on the enhancement vs. time curve where initial normalized enhancement drops to 0.5 shown in figure 4.17. The average half life of the nanobubble was found to be 0.95 minutes.

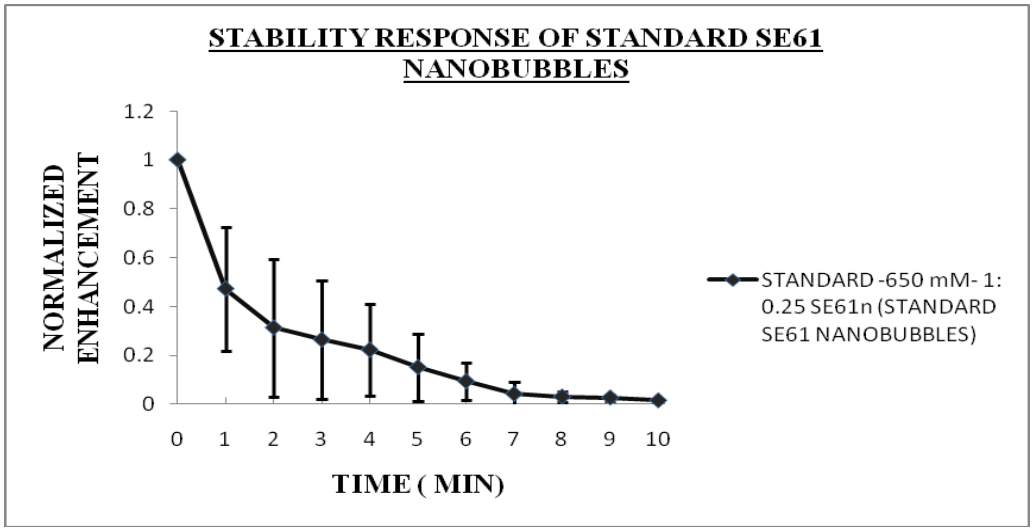

Figure 4.17: Stability response of standard SE61 nanobubbles with 650mM total sodium chloride concentration and 1: 0.25 molar ratio of span 60: TPGS , N=3 independent observations and error bars representing standard error about the mean.

The most notable property of the stability of nano bubbles in the ultrasound beam is that they are considerably less stable than the micro bubbles with half life of 0.95 minutes as

compared to 7.75 ± 1.97 minutes for standard microbubbles. The pressure difference between the inside and outside of a spherical bubble of radius r is described by the Young-Laplace (Y-L) described in equation 4.2.

$$P_{vap} - P_{liq} = 2\,\gamma^{\circ}/r = \Delta P \qquad \text{(Equation 4.2)}$$

Where: P_{vap} and P_{liq} are the pressure inside (vapor phase) and outside (liquid phase) of the bubble, γ° is the surface tension.

This is considered to be accurate for larger, micron sized bubbles, where the pressure difference is inversely proportional to radius, but appears to be unsatisfactory for nano sized bubbles. This can be seen when considering a free bubble in water (γ' = 0:073 N/m) of, for example 10 nm which would have an unsustainable ΔP of 1.5 10^{7} Pa (~150 atm) [118] . So with surfactant stabilized bubbles, the combined surfactants must be lowering the surface tension considerably, but still the effect of radius is still important, leading to the difference in stability compared to the micron bubbles.

4.5.2 Physical analysis

This involved size analysis and measurement of zeta potential of nanobubbles. Both measurements were performed using Zetasizer nano ZS instrument.

4.5.2.1 Size of standard SE61 nanobubbles

The average diameter of standard SE61 nanobubbles ranged from 350-480 nm (figure 4.18) which can easily pass through the capillaries and enter the target site for imaging.

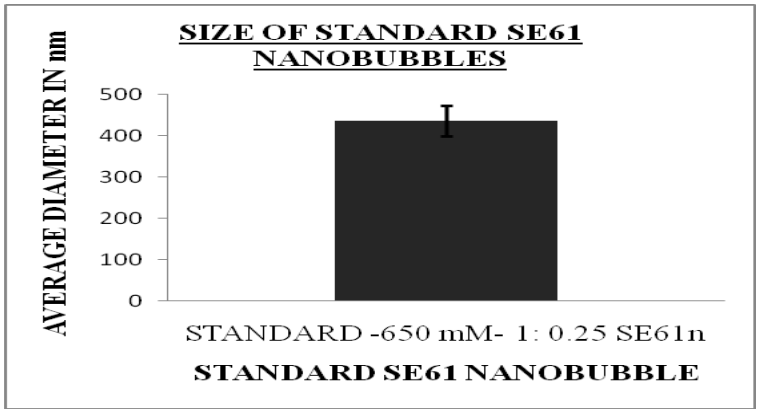

Figure 4.18: Size of standard SE61 nanobubbles with 650mM total sodium chloride concentration and 1: 0.25 molar ratio of span 60: TPGS , N=3 independent observations and error bars representing standard error about the mean.

4.5.2.2 Zeta analysis of nanobubbles

The zeta potential was measured to give information about the stability of the nanobubbles. The magnitude of zeta potential gives information about the charge of the bubbles and the tendency to aggregate, which increases as the value tends to zero. Higher is the absolute value of zeta potential, higher the surface charge of the bubbles and hence higher stability of the bubbles [30]. The zeta potential of standard SE61nanobubbles ranged from -7.79 to -6.67 mV (figure 4.19).

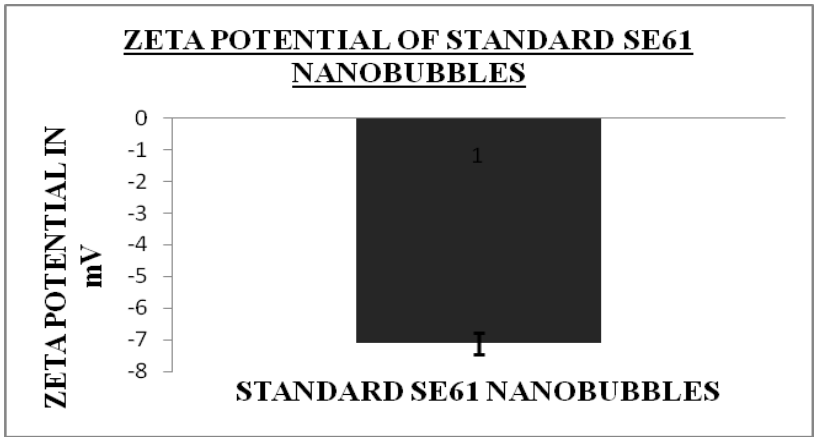

Figure 4.19: Zeta potential of standard SE61 nanobubbles, N=3 independent observations and error bars representing standard error about the mean.

The zeta potential of standard SE61 microbubbles is -8.5 ± 0.46 mV.

4.5.3 Size of standard SE61 particles prior to sonication

The particles of span 60 play an important role in stabilization of bubbles. Studying the particle size prior to sonication could give us information about the mechanism of bubble stabilization. The zeta potential of particles prior to sonication also gives information about the stability of particles in the suspension. Both size and zeta potential of particles are measured using Zetasizer nano instrument.

4.5.3.1 Size of particles

In figure 4.20, average diameter of standard SE61 particles prior to sonication are measured. The average diameter of particles ranged from 25-35 nm.

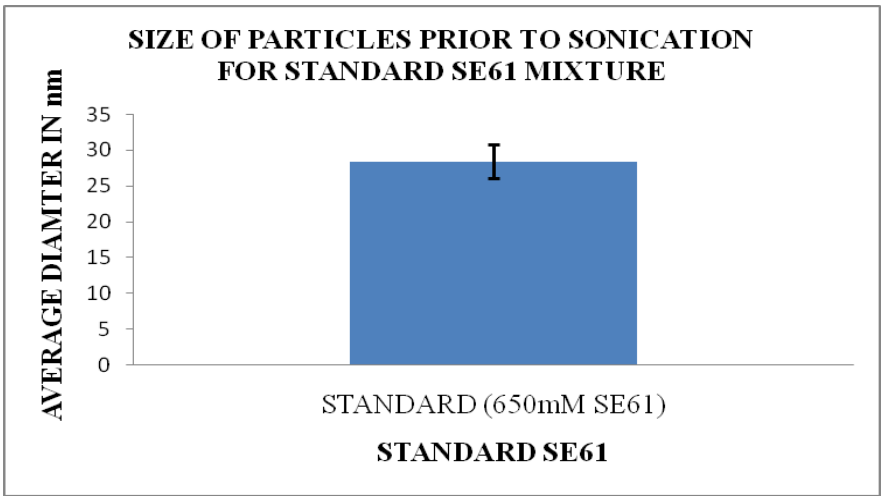

Figure 4.20: Size of standard SE61 particles prior to sonication with 650mM total sodium chloride concentration (N=3 independent observations and error bars representing standard error about the mean.

4.5.3.2 Zeta potential of particles

The zeta potential of particles prior to sonication gives information about the stability of particles that lead to bubble stabilization. The zeta potential for standard SE61 particles ranged from -1.7 to -1.8 mV shown in figure 4.21.

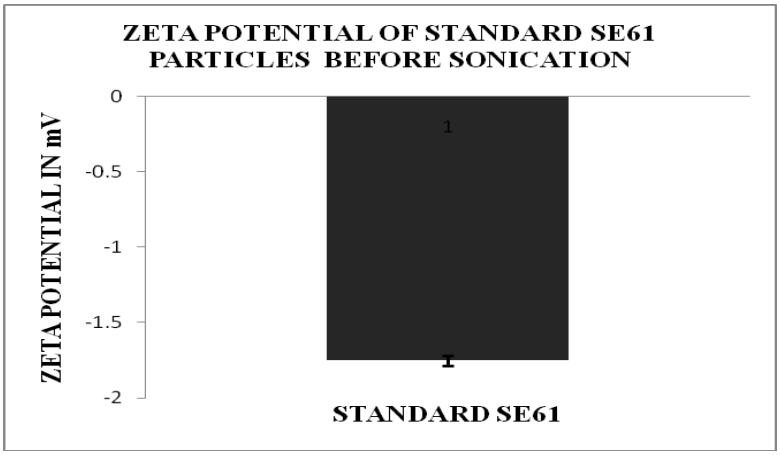

Figure 4.21: Zeta potential of standard SE61 particles before sonication, N=3 independent observations and error bars representing standard error about the mean.

4.6 Effect of added salt on the nanobubble population

As mention at the start of the results section, addition of sodium chloride to the solution to be autoclaved appeared to increase the nano population. In order to characterize the extent of this effect, the additional sodium chloride concentration in the nano samples of SE61 mixture was varied to study its effect. The effects of sodium chloride concentration in the SE61 mixture on nanobubble echogenecity, stability, size, and zeta analysis and nanobubble population are studied in this section.

4.6.1 Acoustic characterization of nanobubbles prepared at various sodium chloride concentrations

The acoustic characterization of nanobubbles is performed as mentioned in Appendix B.2 and B.3.

4.6.1.1 Dose response of nanobubbles

In figure 4.22, dose response of nanobubbles is studied at different total sodium chloride concentrations keeping span 60 and TPGS constant in the preparation steps.

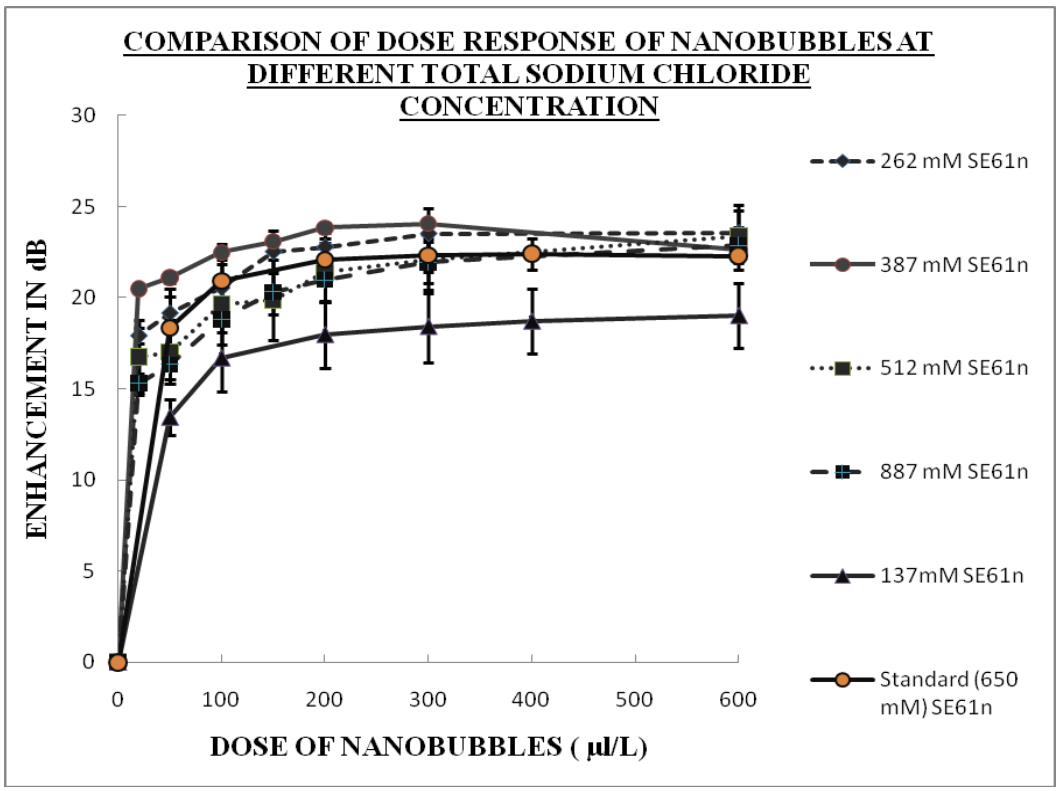

Figure 4.22: Dose response of nanobubbles prepared at different total sodium chloride concentrations keeping span 60 and TPGS constant, $p < 0.05$ at dose of 50 µl/L (one way ANOVA), N=3 independent observations and error bars representing standard error about the mean.

The additional sodium chloride added during preparation of SE61 nano has statistically significant difference at $\alpha = 0.05$ (figure 4.22) at dose of 50 µl/L of nanobubbles. A trend can be observed with 387 mM total sodium chloride concentration giving maximum enhancement of 24 ± 0.16 dB at dose of 300 µl/L of nanobubbles compared to other salt concentrations (figure 4.24). Also, 137 mM total sodium chloride concentration (regular PBS) nanobubbles with no additional sodium chloride added in SE61 mixture gave lower enhancement compared to standard SE61, which is in agreement with the observation that additional salt in the initial mixture to be autoclaved appeared to generate fewer nano bubbles. The exact physical reason for this is not immediately apparent, but is appears

that a threshold ionic strength has to be reached to stabilize the nano bubbles. Also, the nanobubble suspension is very dilute with shadowing occurring around 1200 µl/L representing dose of maximum contrast enhancement. An extended version of figure 4.22 is shown in figure 4.23

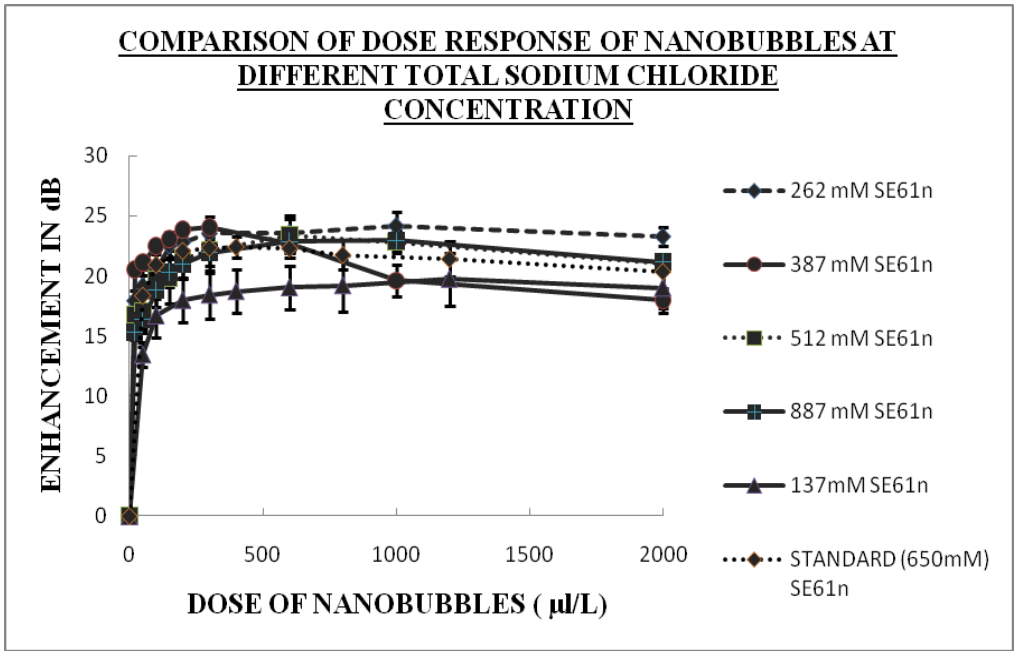

Figure 4.23: Extended version of figure 4.7 till dose of 2000 µl/L: Dose response of nanobubbles at different total sodium chloride concentrations keeping span 60 and TPGS constant, $p < 0.05$ at dose of 50 µl/L (one way ANOVA), N=3 independent observations and error bars representing standard error about the mean.

In case of microbubbles, the additional sodium chloride added to surfactant mixture did not have statistically significant effect on the dose response of microbubbles. Comparing 387 mM total sodium chloride concentration and standard SE61 with 650 mM sodium chloride concentration at dose of 50 µl/L gives $p > 0.5$. However, 387 mM total sodium chloride concentration gave slightly higher maximum enhancement of 24 ± 0.16 dB at dose of 300 µl/L than standard (650 mM) SE61. Shadowing occurred at a dose of 400 µl/L for standard (650 mM) nanobubbles giving maximum enhancement of 22.40 ± 0.86

dB. Hence, in the newly formulated SE61, the total sodium chloride concentration chosen was 387 mM in 50 ml of surfactant mixture.

4.6.1.2 Stability response of nanobubbles at different additional sodium chloride concentrations

The dose chosen for stability response was 100 µl/L of nanobubbles for all different total sodium chloride concentrations. The half lives of the bubbles were calculated from the point on the enhancement vs. time curve where initial normalized enhancement drops to 0.5 shown in figure 4.24. The data were normalized to allow inter sample comparison. In figure 4.24, the half life of nanobubbles at different total sodium chloride concentrations keeping span 60 and TPGS concentrations constant are compared. The additional sodium chloride concentration has statistically significant effect on half life of nanobubbles with $p < 0.05$ between different salt concentrations (one way ANOVA). In the trend (figure 4.24), 387 mM total sodium chloride concentration nanobubbles have higher half life compared to other salt concentrations. The mean half life of nanobubble with 387 mM total sodium chloride concentration is 1.52 minutes. The mean half life of standard SE61 nanobubbles with 650 mM (SOP) total sodium chloride concentration is 0.95 minutes. Statistically significant difference in half life is observed with ($p< 0.05$) between nanobubbles with 387 mM and standard 650 mM total sodium chloride concentrations. In the newly formulated nanobubbles, 387 mM total sodium chloride concentration is chosen over standard 650 mM total sodium concentrations because nanobubbles are more stable with higher half life than standard SE61 nanobubbles.

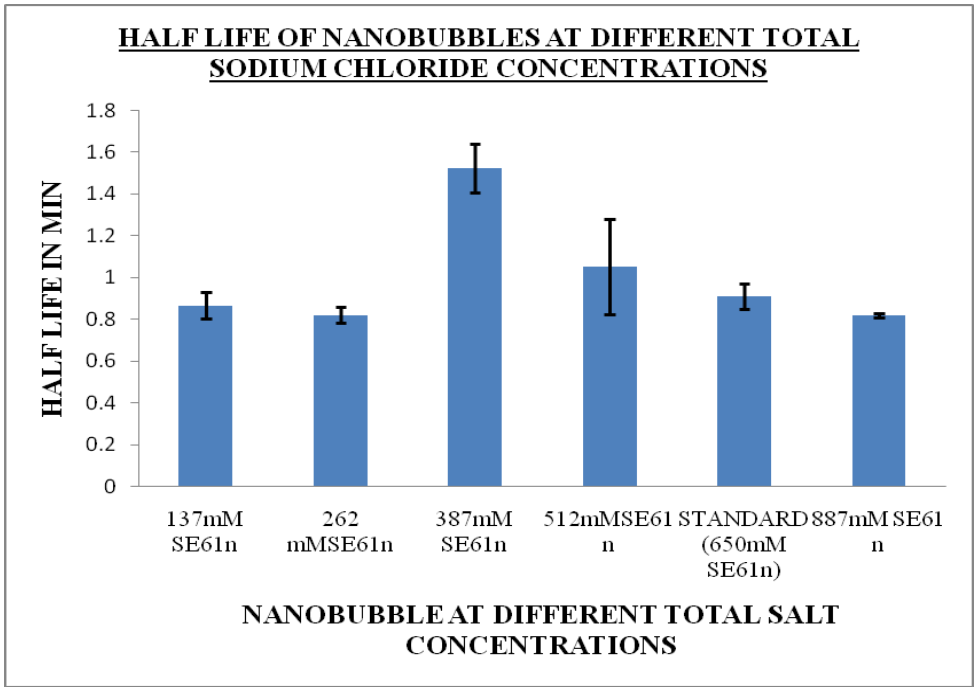

Figure 4.24: Half life of nanobubbles at different total sodium chloride concentrations keeping span 60 and TPGS constant in the SE61 surfactant mixture, $p < 0.05$ (one way ANOVA), N=3 independent observations and error bars representing standard error about the mean.

4.6.2 Physical characterization of nanobubbles

The effect of adding sodium chloride on size and zeta potential of nanobubbles was studied in this section. Size and zeta potential of nanobubbles were studied using Zetasizer nano ZS instrument.

4.6.2.1 Size of the nanobubbles

The size of all nanobubbles at different total sodium chloride concentrations are in range of 350-550 nm ideal as ultrasound contrast agent and tumor imaging as they can easily pass through the capillaries. In figure 4.25, a comparison is made of size of nanobubbles at different total sodium chloride concentrations keeping span 60 and TPGS constant in SE61 surfactant mixture. The additional sodium chloride added to the SE61 mixture has statistically significant effect on the size of nanobubbles with $p < 0.05$.

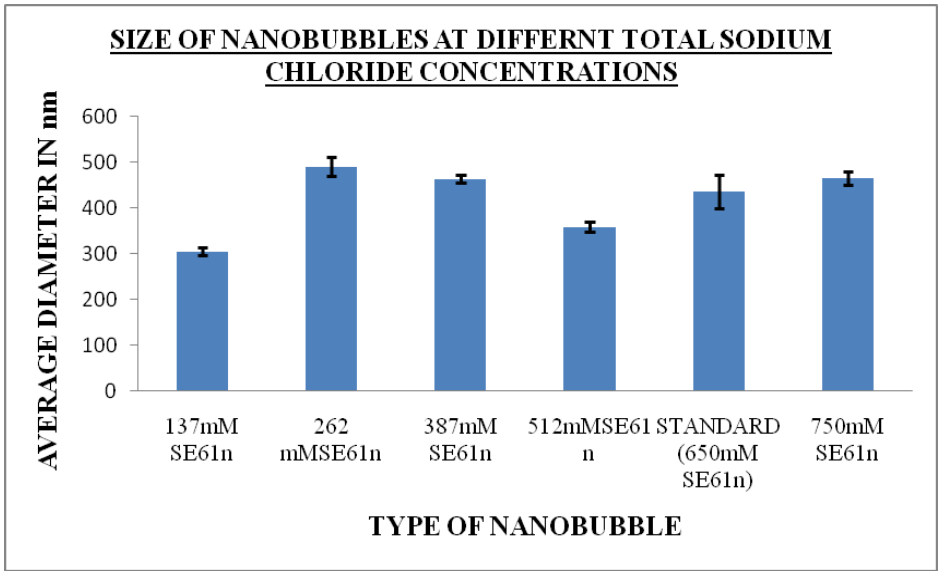

Figure 4.25: Size of SE61 nanobubbles at different total sodium chloride concentrations keeping span 60 and TPGS constant, $p < 0.05$ (One way ANOVA), N=3 independent observations and error bars representing standard error about the mean.

The 137 mM total sodium chloride concentration nanobubbles with no additional sodium chloride are smaller compared to other salt concentrations in the trend (figure 4.25). There is no statistically significant difference in size of nanobubbles between 387 mM and standard 650 mM total sodium chloride concentrations with $p > 0.05$.

4.6.2.2 Zeta potential of nanobubbles

The zeta potential of nanobubbles at different total sodium chloride concentrations is shown in figure 4.28 ($p > 0.05$). In the trend 387 mM total sodium chloride concentration shows slightly higher magnitude of average zeta potential compared to other salt concentrations. Since zeta potential gives information about the stability of bubbles, 387mM total sodium chloride nanobubbles are slightly more stable compared to other salt concentrations shown in figure 4.26.

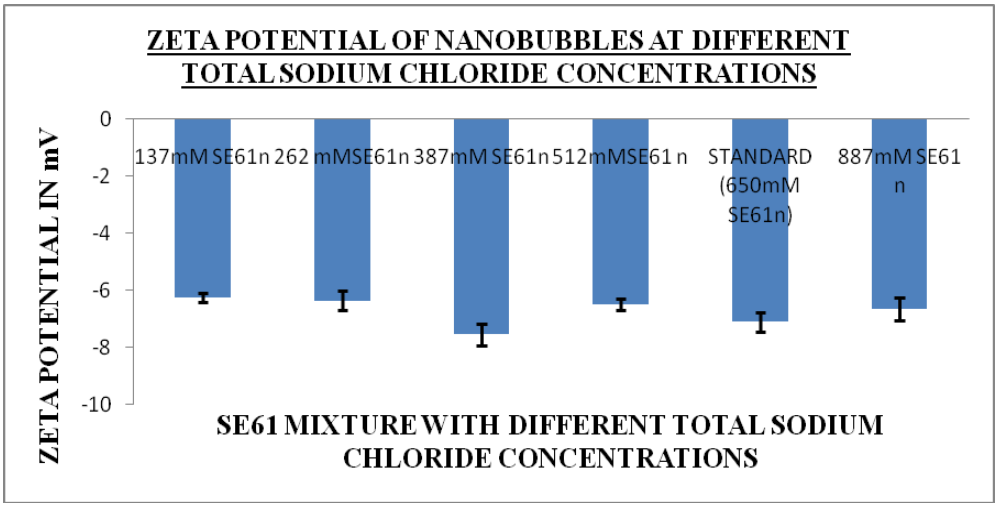

Figure 4.26: Zeta potential of SE61 nanobubbles at different total sodium chloride concentrations keeping span 60 and TPGS constant, $p > 0.05$ (one way ANOVA), N=3 independent observations and error bars representing standard error about the mean.

There is no statistically significant difference in the zeta potential of nanobubbles at 387 mM and 650 mM total sodium chloride concentrations with $p> 0.05$. The zeta potential of 387 mM total sodium chloride nanobubbles is -7.55± 0.37 mV and for standard (650 mM) SE61 nanobubbles is -7.1± 0.3 mV. Since the higher magnitude of zeta potential means higher stability of bubbles, 387 mM total sodium chloride nanobubbles are slightly more stable than standard (650 mM) SE61 nanobubbles.

4.6.3. Nanobubble population measured by turbidity

Turbidity measurement of the nanobubble suspensions were done to give a measure of comparative magnitudes of the nanobubble populations. The wavelength chosen was 610 nm as the standard value for all our measurements. In figure 4.27, turbidity at 610 nm was compared for nanobubbles at different total sodium chloride concentrations keeping span 60 and TPGS constant in SE61 mixture ($p< 0.05$). This implies the additional

sodium chloride has significant effect on the nanobubble population. In the trend, 387 mM total sodium chloride concentration gives higher nanobubble population compared to other salt concentrations. This is in agreement with the observations that these conditions gave the highest echogenecity. Also, 137 mM sodium chloride concentration with no additional salt added in SE61 mixture yields lower nanobubble population with lower turbidity value at 610 nm (figure 4.27) There is statistically significant difference in turbidity at 610 nm ($p < 0.05$) between 387 mM and standard 650 mM total sodium chloride nanobubbles. In the newly formulated nanobubbles, 387 mM is the total sodium chloride concentration chosen as the turbidity values are statistically significantly different from standard 650 mM total sodium chloride concentration.

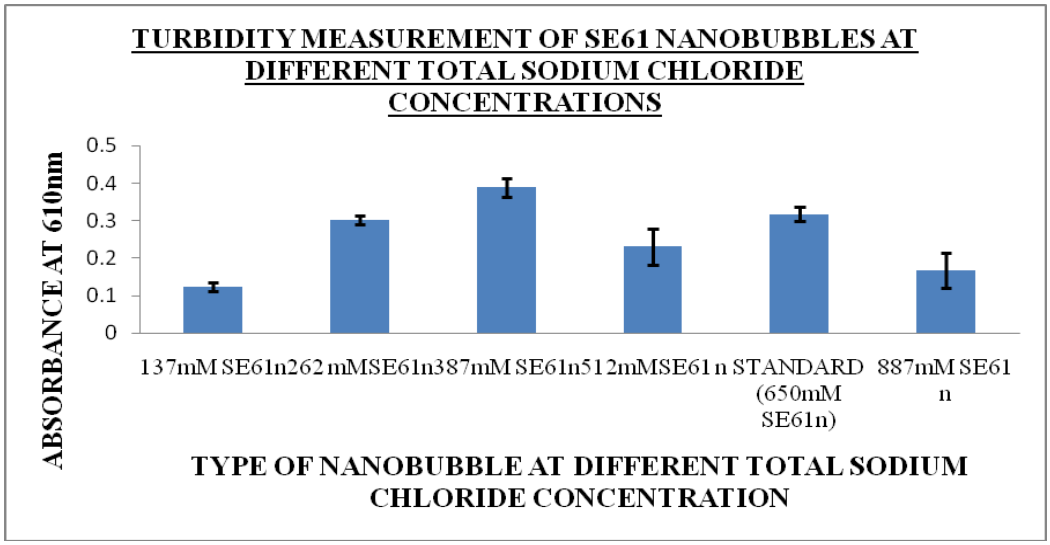

Figure 4.27: Turbidity measurement of nanobubbles at different total sodium chloride concentrations keeping span 60 and TPGS constant, $p < 0.05$ (one way ANOVA), N=3 independent observations and error bars representing standard error about the mean.

4.6.4. Size of particles after autoclave

In figure 4.28, size of the particles prior to sonication at different total sodium chloride concentrations ($p > 0.05$) are compared. A trend can be observed with 137 mM sodium

chloride with no additional sodium chloride added in 50 ml of SE61 mixture have particle size slightly higher compared to other salt concentrations. And 887 mM total sodium chloride SE61 particles having lowest particle size in the trend shown in figure 4.28. However there is no statistical difference.

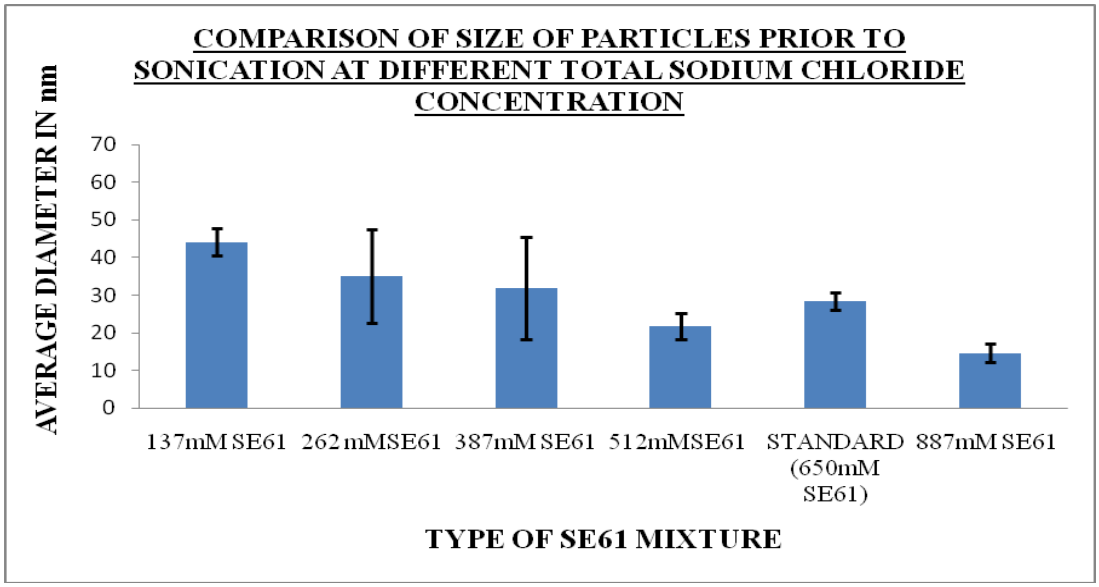

Figure 4.28: Comparison of size of particles prior to sonication at different total sodium chloride concentrations in SE61 mixture, p> 0.05 (One way ANOVA), N=3 independent observations and error bars representing standard error about the mean.

4.6.5 Zeta potential of particles prior to sonication

Zeta potential of particles prior to sonication is done to study the stability of particles. In figure 4.29, zeta potential of particles at different sodium chloride concentrations are compared ($p < 0.05$). In the trend shown below, 387 mM total sodium chloride particles has higher magnitude of average zeta potential compared to other salt concentrations.

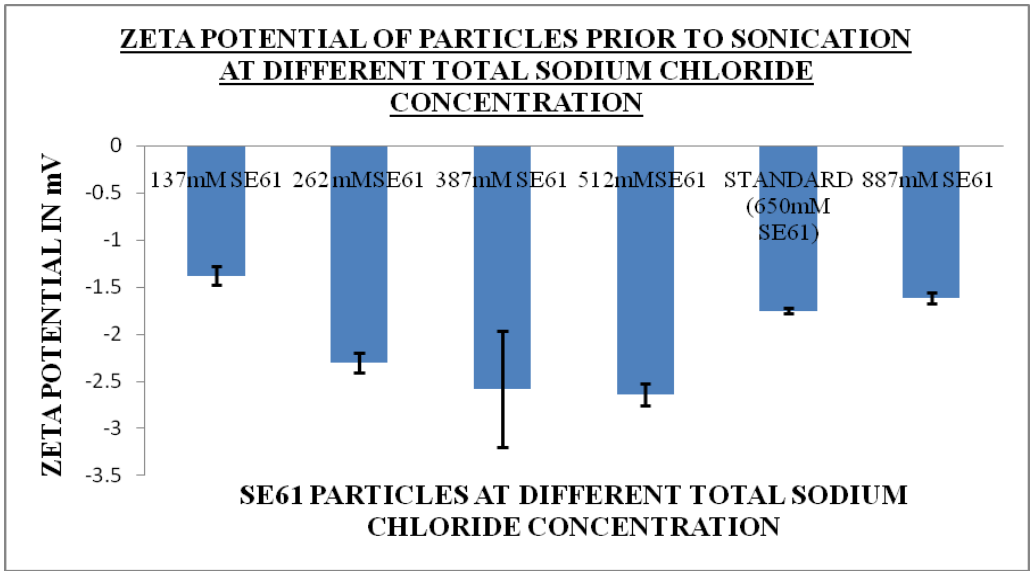

Figure 4.29: Zeta potential of SE61 particles prior to sonication with different total sodium chloride concentrations keeping span 60 and TPGS constant, $p < 0.05$ (one way ANOVA), N=3 independent observations and error bars representing standard error about the mean.

There is no statistically significant difference in zeta potential of particles prior to sonication between 387 mM and standard 650 mM total sodium chloride concentrations ($p > 0.05$). The zeta potential of particles at 387 mM total sodium chloride concentration is -2.58 ± 0.61 mV. The zeta potential of standard 650 mM) a SE61 particle is -1.75 ± 0.03 mV. The magnitude of zeta potential of 387 mM total sodium chloride nanobubbles is slightly higher and hence slightly more stable than standard (650 mM) nanobubbles.

4.6.6 How the new formulated nanobubbles different from standard nanobubbles

In the newly formulated nanobubbles, 387mM total sodium chloride concentration is chosen over standard 650 mM total sodium concentrations because nanobubbles are more stable with higher half life than standard SE61 nanobubbles ($p < 0.05$). 387 mM total sodium chloride concentration gave slightly higher maximum enhancement of 24 ± 0.16 dB at dose of 300 µl/L than standard (650 mM) SE61. Shadowing occurred at a dose of

400 µl/L for standard (650 mM) nanobubbles giving maximum enhancement of 22.40 ± 0.86 dB. Also, there is statistically significant difference in turbidity at 610 nm ($p < 0.05$) at these two salt concentrations.

4.7 Effect of surfactant ratio on the nanobubbles

The ratio of Span to TPGS used in the contrast agent preparation was based on that used in the original ST68 agent. We now wish to produce an agent with a large population of nano bubbles, and so it is important to investigate the effect, if any, that changing the span 60: TPGS molar ratio has on this population.

4.7.1 Acoustic characterization of nanobubbles prepared at different Span 60: TPGS ratios

The acoustic characterization of nanobubbles is performed as mentioned in Appendix B.2 and B.3.

4.7.1.1 Dose response of nanobubbles

The TPGS concentration was varied keeping span 60 and total sodium chloride concentration constant in 50 ml of surfactant mixture used in the sonication step. The standard SE61 has a molar ratio of 1: 0.25. The TPGS concentration was increased in SE61 mixture keeping span 60 constant represented as 1: 0.43 (2.808g TPGS) and 1: 0.67 (3.434g TPGS), and the dose response curves are shown in figure 4.30. A comparison was made in dose response of nanobubbles with different TPGS concentrations ($p > 0.05$ at dose of 50 µl/L and maximum dose of 2000 µl/L) in figure 4.30. There is no statistically significant difference in enhancement between standard (1: 0.25) and 1: 0.43 ratio nanobubbles with $p > 0.05$. In the figure 4.30, 1: 0.43 ratio nanobubbles (2.208g TPGS) nanobubbles gives slightly higher maximum enhancement

(24.2 ± 0.62 dB) than standard (1: 0.25) nanobubbles (22.4 ± 0.86 dB) at dose of 400 µl/L.

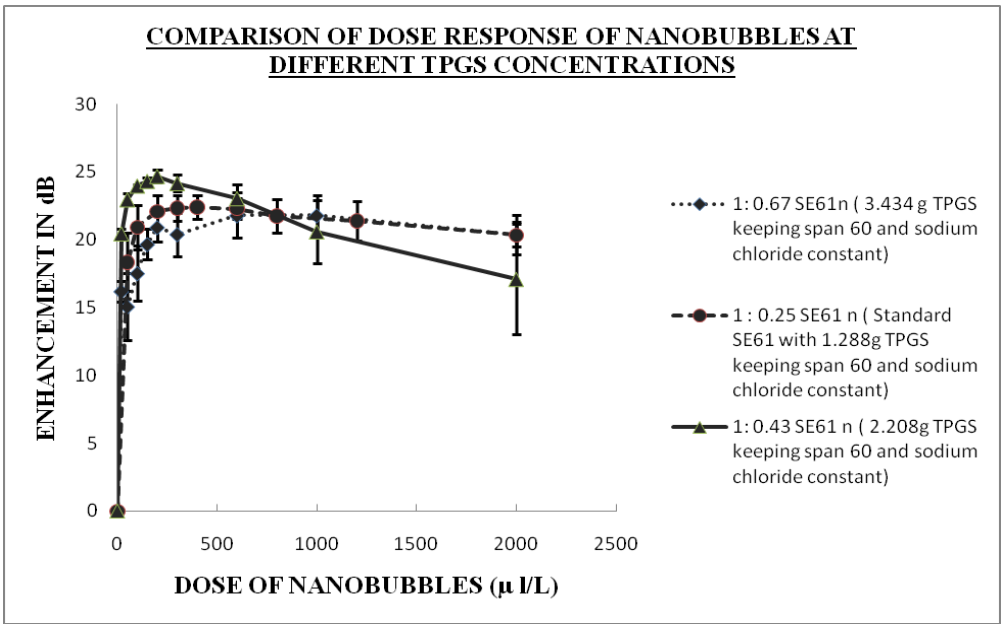

Figure 4.30: Dose response of nanobubbles at different TPGS concentrations keeping span 60 and sodium chloride constant, p > 0.05 at dose of 50 µl/L and maximum dose of 2000 µl/L, N=3 independent observations and error bars representing standard error about the mean.

This result shows that even if the ratio of surfactant has an effect on the number of nano bubbles produced, the acoustic contribution is not distinguishable.

4.7.1.2 Stability response of nanobubbles

The half lives of standard (1: 0.25), 1: 0.43, 1: 0.63 molar ratio nanobubbles are compared in figure 4.31 with p> 0.05. Also, there is no statistically significant difference in the half life of nanobubbles between standard (1: 0.25) and 1: 0.43 molar ratios with p> 0.05. The half life of 1: 0.43 molar ratio nanobubbles is 1.25 ± 0.25 min which is slightly higher than half life of standard (1: 0.25) nanobubbles (0.9 ± 0.062 minutes).

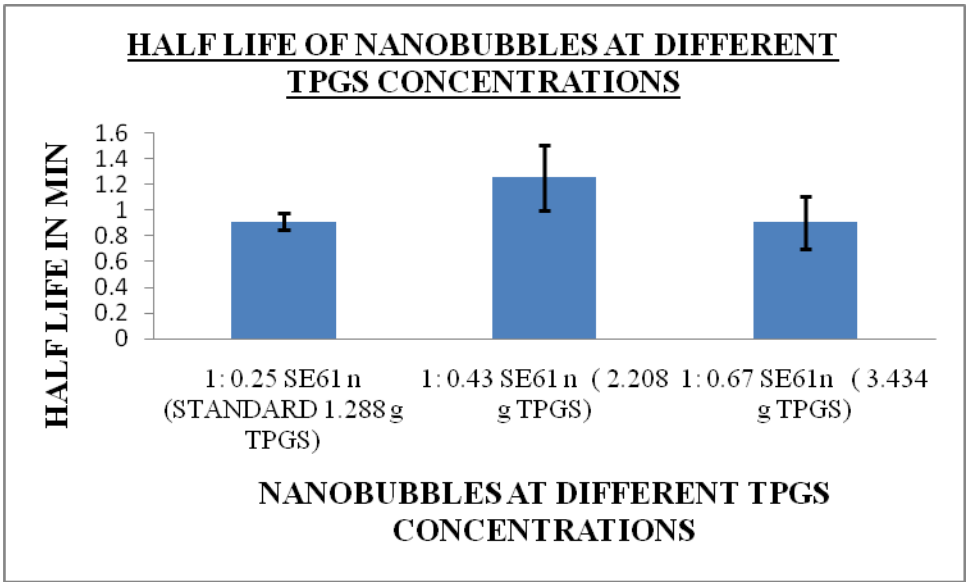

Figure 4.31: Half life of nanobubbles at different TPGS concentrations keeping span 60 and sodium chloride constant, p> 0.05, N=3 independent observations and error bars representing standard error about the mean.

4.7.2 Physical characterization of nanobubbles

The effect of adding higher TPGS on size and zeta potential of nanobubbles is studied in this section. Size and zeta potential of nanobubbles are studied using Zetasizer nano ZS instrument.

4.7.2.1 Size of the nanobubbles

The size of nanobubbles between standard (1: 0.25), 1:0.43 and 1:0.67 molar ratio of span 60: TPGS are compared in figure 4.34 with p< 0.05. The size of nanobubbles at different TPGS concentrations range from 350-600 nm which are ideal for tumor imaging. In the figure 4.32, 1: 0.43 nanobubbles corresponding to 70 (span 60): 30 (TPGS) molar ratio have larger size compared to other TPGS concentrations. Also, there is statistically significant difference in size of nanobubbles (p< 0.05) between standard (1: 0.25) and 1:

0.43 nanobubbles. Therefore changing the TPGS concentration has statistically significant effect on the size of nanobubbles (figure 4.32)

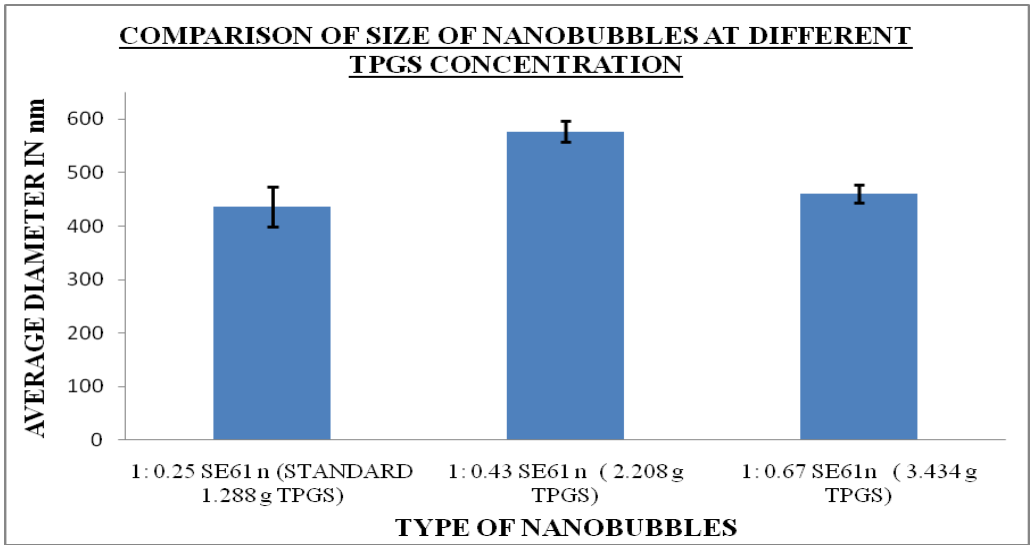

Figure 4.32: Comparison of size of nanobubbles at different TPGS concentrations keeping span 60 and sodium chloride constant, $p<0.05$ (one way ANOVA), N=3 independent observations and error bars representing standard error about the mean.

This is a somewhat unexpected result, since size usually influences echogenecity. However, with such small sizes of bubbles (and hence small differences in diameter, in the nanometer range), it would appear that the influence is not distinguishable in our measurements of acoustic properties (dose and stability response). However, the result does indicate that the molar ratio of the surfactants present during the preparation (sonication) stage does influence the packing of surfactant around the gas bubbles, and hence the size.

4.7.2.2 Zeta potential of nanobubbles

In figure 4.33, zeta potential of standard (1: 0.25), 1:0.43 and 1:0.67 molar ratio nanobubbles are compared ($p< 0.05$). There is no statistically significant difference in magnitude of average zeta potential between standard (1: 0.25) and 1: 0.43 molar ratio

nanobubbles with p>0.05. The zeta potential of 1: 0.43 nanobubbles is -7.53 ±0.22 mV which is slightly higher compared to standard (1: 0.25) nanobubbles (-7.11 ± 0.34mV). Higher magnitude of zeta potential means higher stability of bubbles. The nanobubbles with 1: 0.43 molar ratio of span: TPGS are slightly more stable than standard (1: 0.25) nanobubbles.

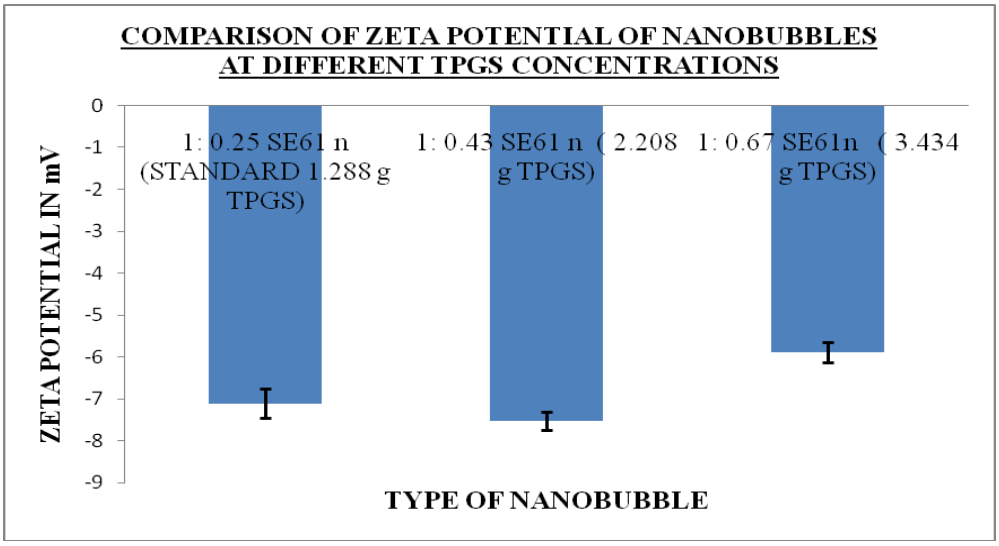

Figure 4.33: Comparison of zeta potential of nanobubbles at different TPGS concentrations keeping Span 60 and sodium chloride constant, p<0.05 (one way ANOVA), N=3 independent observations and error bars representing standard error about the mean.

4.7.3 Nanobubble population measured by turbidity

One way ANOVA was used to study statistical significance between nanobubbles with different TPGS concentrations (p< 0.05) shown in figure 4.34. The average turbidity measurement for 1: 0.43 nanobubbles at 610 nm is 0.4 and for standard (1: 0.25 ratio) SE61 nanobubbles is 0.32. There is no statistically significant difference in nanobubble population (p> 0.05) compared between standard (1: 0.25) and 1: 0.43 nanobubbles. The turbidity value at 610 nm for 1: 0.43 molar ratio nanobubbles is 0.39 ± 0.6 and for standard (1: 0.25) nanobubbles is 0.32 ± 0.2. The turbidity value for 1: 0.67 molar ratio

nanobubbles at 610 nm is 0.22 ± 0.2. There is statistically significant difference in the nanobubble population when standard (1: 0.25), 1: 0.43 and 1: 0.67 molar ratio nanobubbles are compared with $p < 0.05$.

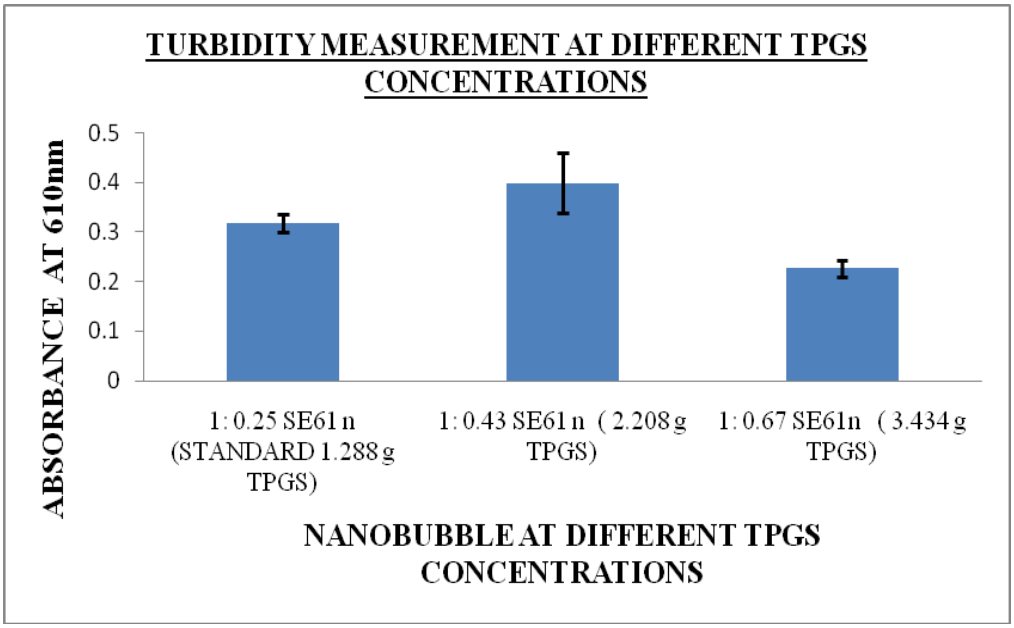

Figure 4.34: Turbidity measurement at 610nm for SE61nanobubbles with different TPGS concentrations keeping span 60 and sodium chloride constant, $p < 0.05$ (one way ANOVA), N=3 independent observations and error bars representing standard error about the mean.

4.7.4 Size of particles after autoclave

In figure 4.35, sizes of particles prior to sonication are compared for standard (1: 0.25), 1: 0.43 and 1: 0.67 SE61 mixtures. There is no statistically significant difference in the size of particles prior to sonication between standard (1: 0.25 molar ratios), 1: 0.43 and 1: 0.67 molar ratio SE61 mixtures with $p > 0.05$. Also, there is no statistically significant difference in the size of particles between standard SE61 (1: 0.25 ratio of span: TPGS) and 1: 0.43 SE61 with $p > 0.05$.

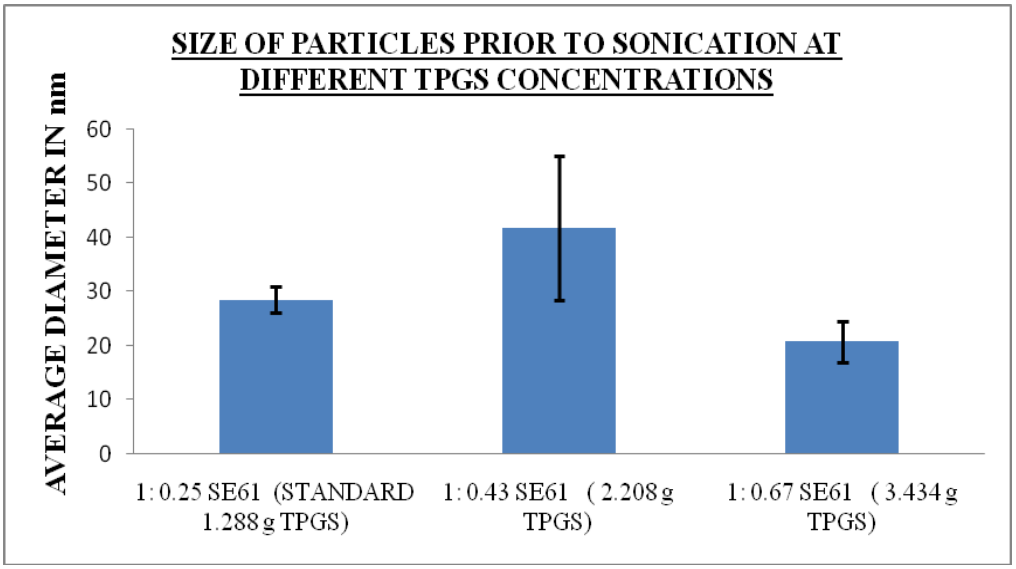

Figure 4.35: Size of particles prior to sonication at different TPGS concentrations keeping span60 and sodium chloride constant, p> 0.05 (one way ANOVA), N=3 independent observations and error bars representing standard error about the mean.

4.7.5 Zeta potential of particles prior to sonication

In figure 4.36, zeta potential of particles prior to sonication is compared for standard (1: 0.25), 1: 0.43 and 1: 0.67 SE61 mixtures with $p< 0.05$. There is no statistically significant difference in the zeta potential between standard SE61 (1: 0.25 ratio of span: TPGS) and 1: 0.43 SE61 with $p > 0.05$. The zeta potential of standard (1: 0.25) particles is -1.75 ± 0.54 mV and for 1: 0.43 molar ratio particles is -1.98 ± 0.36mV.

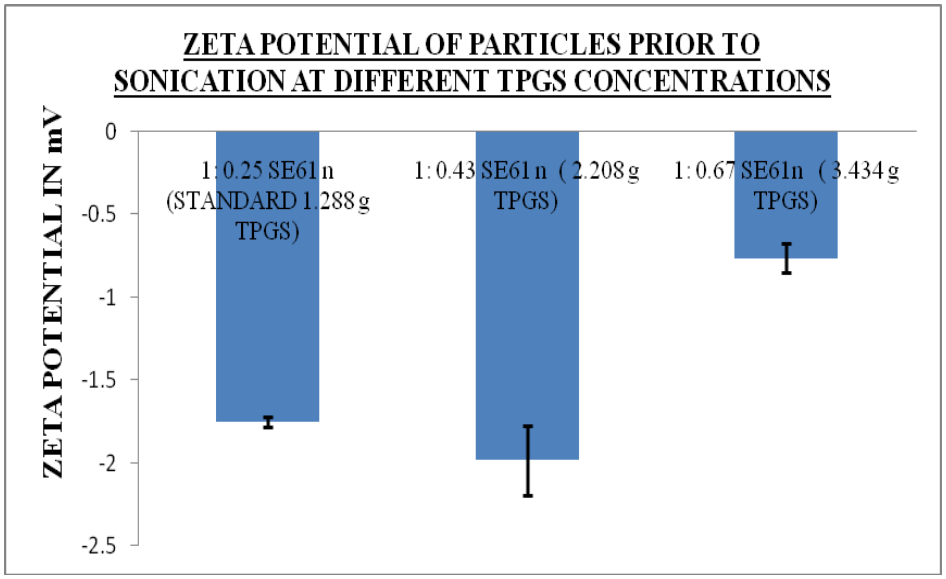

Figure 4.36: Zeta potential of particles prior to sonication at different TPGS concentrations keeping span60 and sodium chloride constant, $p < 0.05$ (one way ANOVA), N=3 independent observations and error bars representing standard error about the mean.

4.7.6 How the new formulated nanobubbles from surfactant study different from standard nanobubbles

In the newly formulated nanobubbles, 1: 0.43 ratio of span60: TPGS is used over the standard SE61 (1: 0.25 ratio) formulation. There is no statistically significant difference in enhancement, turbidity and half life with $p > 0.05$ between the two concentrations. But 1: 0.43 ratio nanobubbles (2.208g TPGS) nanobubbles gave slightly higher maximum enhancement (24.2 ± 0.62 dB) than standard (1: 0.25) nanobubbles (22.4 ± 0.86 dB) at dose of 400 µl/L. The half life of 1: 0.43 molar ratio nanobubbles is 1.25 ± 0.25 min which is slightly higher than half life of standard (1: 0.25) nanobubbles (0.9 ± 0.062 minutes).

4.8 New formulated nanobubbles (from salt and surfactant study)

In the newly formulated nanobubbles, the total sodium chloride concentration chosen was 387 mM sodium chloride and 1: 0.43 ratio keeping amount of span 60 constant (as standard SE61mixture).

4.9 Paclitaxel encapsulation in the nanobubbles

Paclitaxel was encapsulated in the nanobubbles and later the efficiency of paclitaxel encapsulation was studied by high performance liquid chromatography.

4.9.1 Acoustic characterization of paclitaxel loaded nanobubbles

The acoustic characterization of nanobubbles is performed as mentioned in Appendix B.2 and B.3.

4.9.1.1 Dose response of paclitaxel loaded nanobubbles

In figure 4.37, dose response of paclitaxel loaded standard SE61 (with 650 mM total sodium chloride and 1: 0.25 ratio of span: TPGS), paclitaxel loaded newly formulated SE61 (with 387 mM total sodium chloride and 1: 0.43 ratio of span: TPGS) and standard SE61 nanobubbles without paclitaxel are compared. There is statistically significant difference at dose of maximum dose of 2000 µl/L when all three conditions are compared in figure 4.37. In case of standard SE61 nanobubbles without paclitaxel loaded into it, shadowing occurred at a dose of 400 µl/L giving maximum enhancement of 22.40 ± 0.86 dB. Shadowing occurred at dose of 300 µl/L for both paclitaxel loaded standard SE61 and paclitaxel loaded newly formulated nanobubbles with maximum contrast enhancement as 22.8 ± 0.45 dB and 22.58 ±0.188 dB respectively.

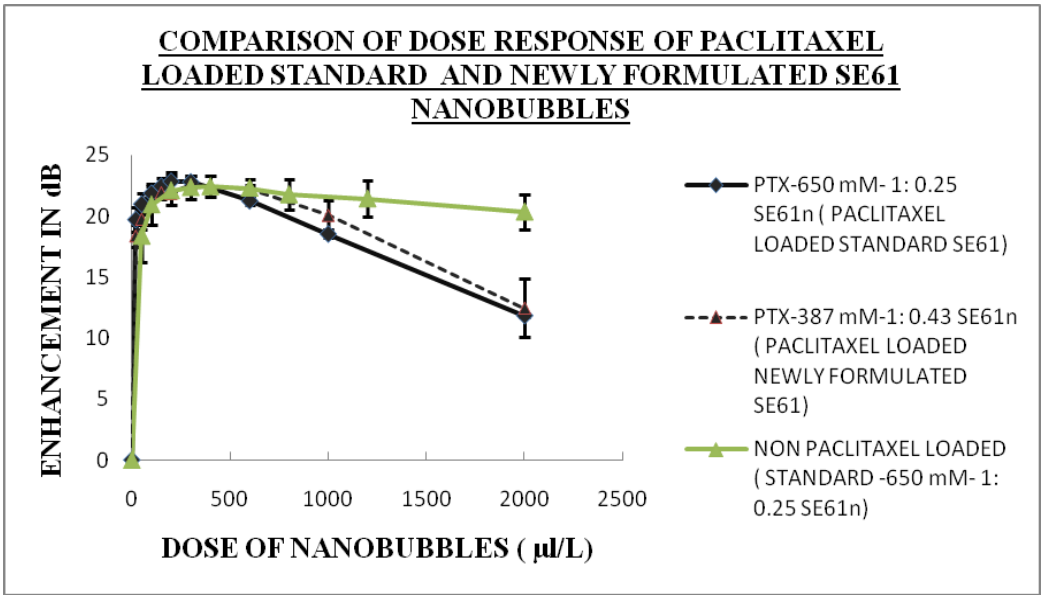

Figure 4.37: Dose response of paclitaxel loaded standard SE61nanobubbles (with 650mM total sodium chloride concentration and 1: 0.25 ratio of span 60 and TPGS), paclitaxel loaded newly formulated SE61 nanobubbles (with 387mM total sodium chloride concentration and 1: 0.43 ratio of span 60 and TPGS) and standard SE61 nanobubbles without drug, $p<0.05$ at dose of 2000 µl/L, N=3 independent observations and error bars representing standard error about the mean.

4.9.1.2 Stability response of paclitaxel loaded nanobubbles

In figure 4.38, paclitaxel loaded standard SE61, paclitaxel loaded newly formulated nanobubbles and standard SE61 without paclitaxel are compared with $p< 0.05$. The average half life of standard SE61 nanobubbles is 0.95 min. From the figure 4.38, half life of paclitaxel loaded standard SE61 is around 1.4 ± 0.6 minutes. There is statistically significant difference in half life of nanobubbles with $p< 0.05$ between paclitaxel loaded standard SE61 and non-paclitaxel loaded standard SE61 nanobubbles. This implies that paclitaxel loaded nanobubbles are more stable in ultrasound beam than standard SE61 nanobubbles. There is statistically significant difference in the half lives of paclitaxel loaded standard SE61 and paclitaxel loaded newly formulated nanobubbles with $p <0.05$.

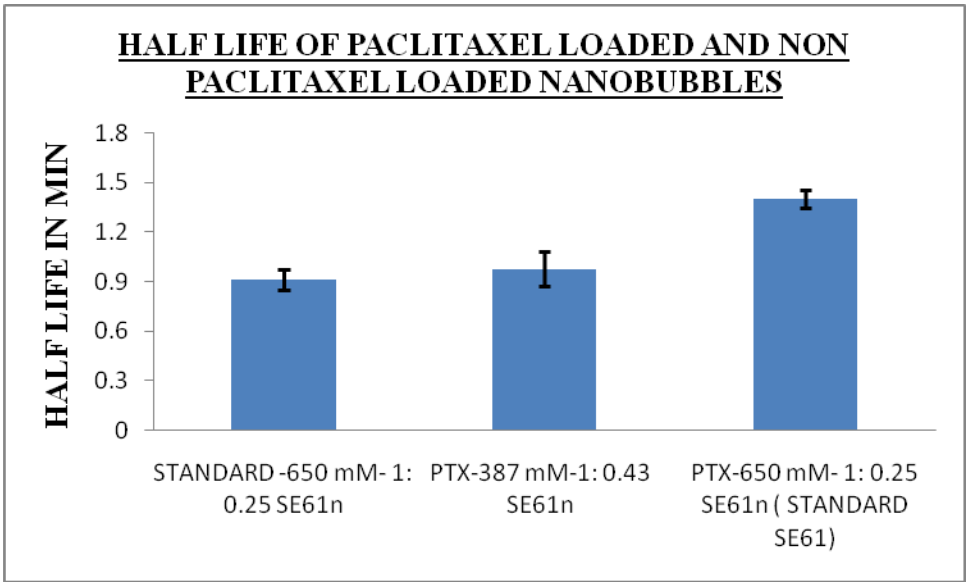

Figure 4.38: Half life of paclitaxel loaded standard SE61nanobubbles, standard nanobubbles and paclitaxel loaded newly formulated nanobubbles, $p < 0.05$, N=3 independent observations and error bars representing standard error about the mean.

4.9.2 Physical characterization of paclitaxel loaded nanobubbles

The size and zeta potential of paclitaxel loaded nanobubbles are studied in this section. Size and zeta potential of paclitaxel loaded nanobubbles are studied using Zetasizer nano ZS instrument.

4.9.2.1 Size of the paclitaxel loaded nanobubbles

In figure 4.39, size of paclitaxel loaded standard SE61, paclitaxel loaded newly formulated nanobubbles and standard SE61 nanobubbles are compared ($p > 0.05$). There is no statistically significant difference is size of paclitaxel loaded standard SE61 and paclitaxel loaded newly formulated nanobubbles.

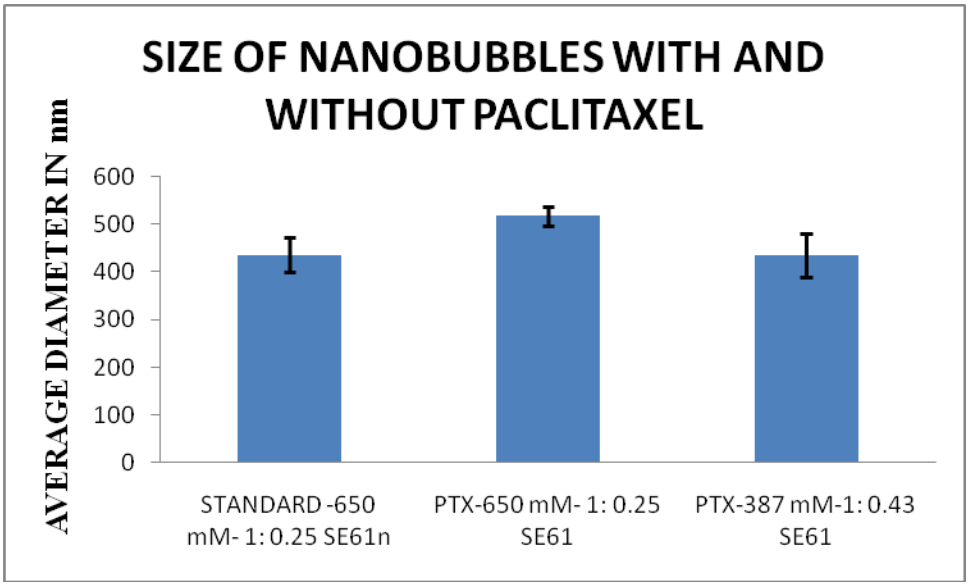

Figure 4.39: Size of paclitaxel loaded standard , paclitaxel loaded newly formulated nanobubbles and standard SE61 nanobubbles without paclitaxel , p> 0.05, N=3 independent observations and error bars representing standard error about the mean.

4.9.2.2 Zeta potential of paclitaxel loaded nanobubbles

In figure 4.40, zeta potential of paclitaxel loaded standard SE61, paclitaxel loaded newly formulated SE61 and standard SE61 nanobubbles are compared with p< 0.05. The zeta potential of standard SE61 nanobubbles is -7.11 ± 0.34mV. There is no statistically significant difference in the zeta potential between paclitaxel loaded standard SE61 and non-paclitaxel loaded standard SE61 with p > 0.05. The zeta potential of paclitaxel loaded standard SE61 is – 7.86 ± 0.15 mV. But the magnitude of zeta potential is slightly higher than standard SE61 implying the paclitaxel loaded standard SE61 nanobubbles are slightly more stable than standard SE61 nanobubbles. The zeta potential of paclitaxel loaded a newly formulated nanobubble is -6.57 ± 0.11mV. There is statistically significant difference in zeta potential between paclitaxel loaded newly formulated nanobubbles and paclitaxel loaded standard SE61 nanobubbles. The newly formulated nanobubbles loaded with paclitaxel are less stable because of less negative value of zeta

potential compared to paclitaxel loaded standard SE61 nanobubbles, which indicated a greater potential to coalesce.

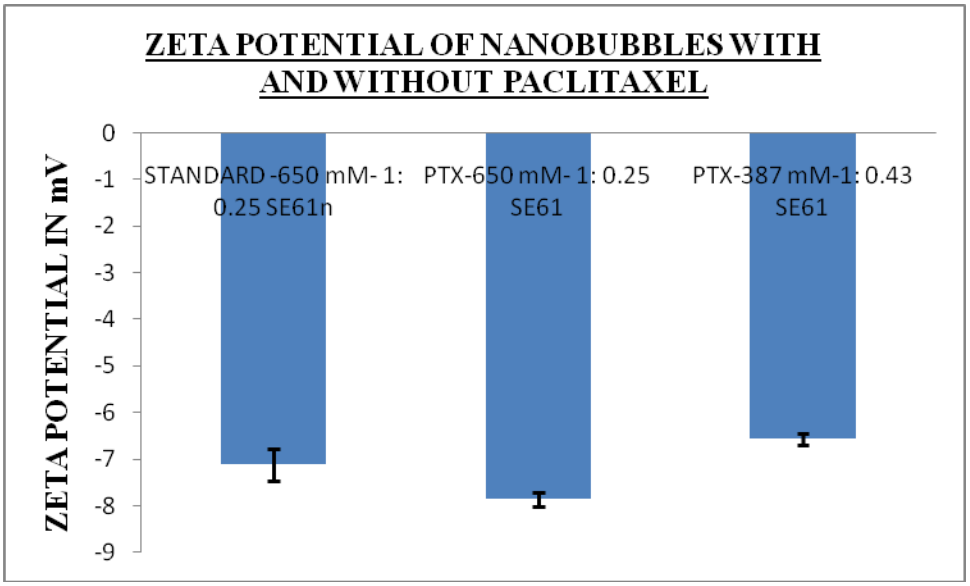

Figure 4.40: Zeta potential of paclitaxel loaded standard SE61nanobubbles, paclitaxel loaded newly formulated SE61 nanobubbles and non-paclitaxel loaded standard SE61 nanobubbles , $p< 0.05$, N=3 independent observations and error bars representing standard error about the mean

4.9.3 Paclitaxel loaded nanobubble population measured by turbidity

In figure 4.41, the turbidity of paclitaxel loaded standard SE61 and paclitaxel loaded newly formulated nanobubbles are compared with $p> 0.05$. Comparing turbidity values between standard SE61 and paclitaxel loaded standard SE61 gives $p> 0.05$.

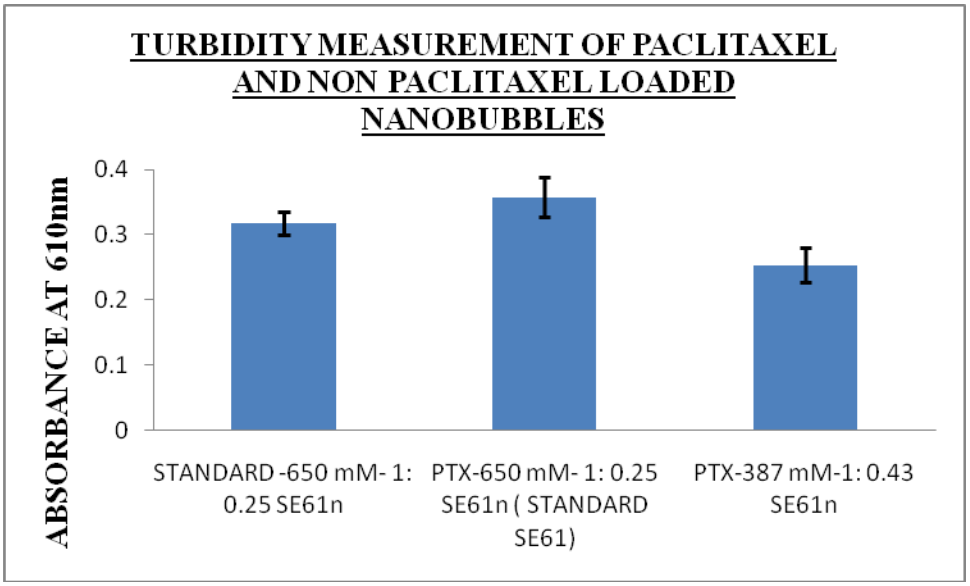

Figure 4.41: Turbidity measurement between paclitaxel loaded standard SE61 (with 650mM total sodium chloride concentration and 1: 0.25 ratio of span 60:TPGS), paclitaxel loaded newly formulated nanobubbles (with 387mM total sodium chloride concentration and 1: 0.43 ratio of span 60: TPGS) and standard SE61 nanobubbles, $p > 0.05$, N=3 independent observations and error bars representing standard error about the mean.

Based on turbidity, it would appear that the size of the population of nano bubbles is not affected by the formulation.

4.9.4 Size of paclitaxel added SE61 particles prior to sonication

The size of paclitaxel loaded SE61 particles are shown in figure 4.42. The size of particles in non paclitaxel loaded standard SE61 is 28 ± 2.4 nm. In case of paclitaxel loaded SE61 particles 24 ± 4.2 nm. But in case of newly formulated paclitaxel loaded particles size of particles is around 14.65 ± 2.4 nm.

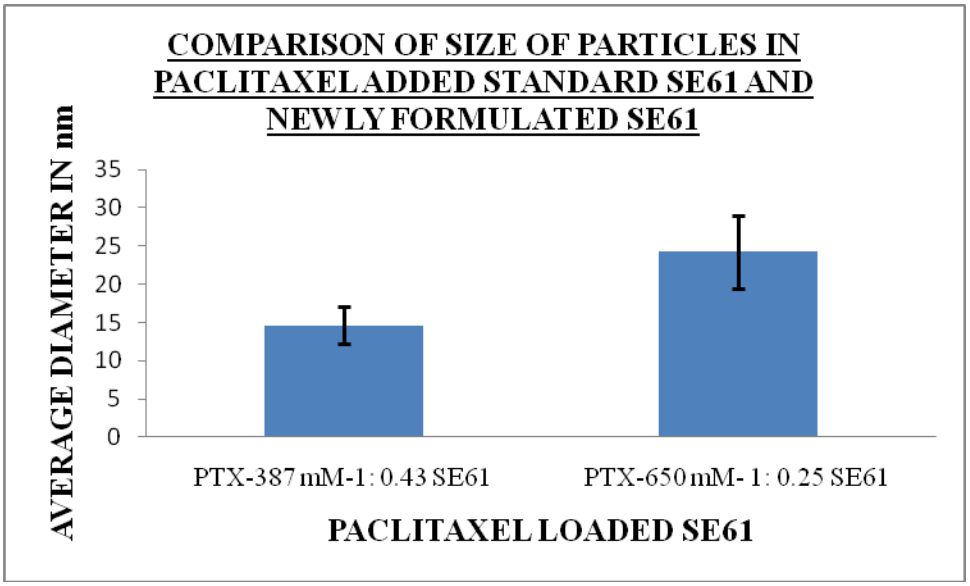

Figure 4.42: Comparison of size of particles in paclitaxel added standard SE 61 and paclitaxel added newly formulated SE61 (with 387mM total sodium chloride concentration and 1: 0.43 ratio of span 60 and TPGS in the mixture), $p > 0.05$, N=3 independent observations and error bars representing standard error about the mean.

4.9.5 Zeta potential of paclitaxel added SE61 particles prior to sonication

The zeta potential of paclitaxel added SE61 particles prior to sonication is shown in figure 4.43. There is no statistically significant difference in paclitaxel loaded standard SE61 and paclitaxel loaded newly formulated nanobubbles with $p > 0.05$. The zeta potential of standard (650 mM) SE61 particles is -1.75 ± 0.03 mV.

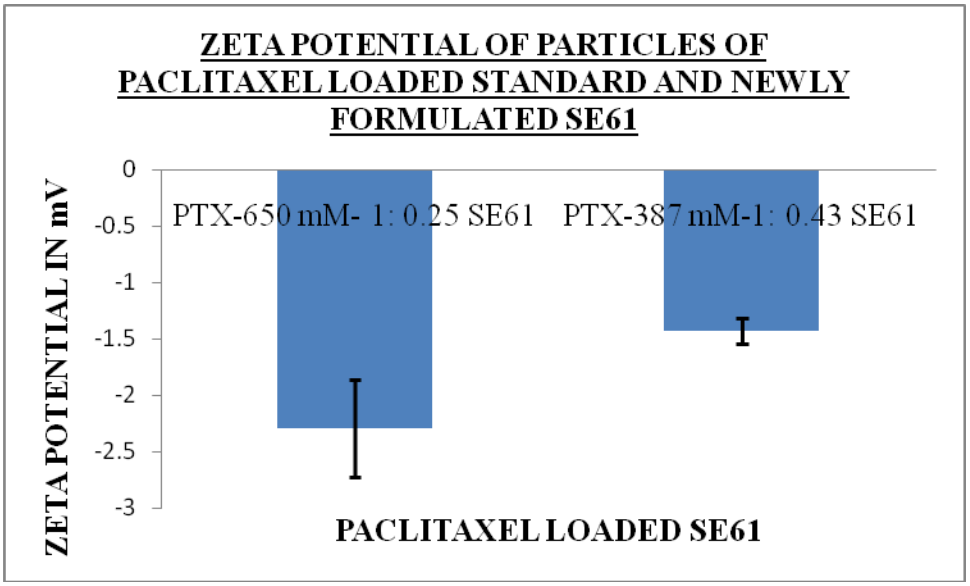

Figure 4.43: Zeta potential of particles prior to sonication for paclitaxel added standard SE61 and newly formulated SE61, p> 0.05, N=3 independent observations and error bars representing standard error about the mean.

4.9.6 Encapsulation efficiency of paclitaxel in the nanobubbles by high performance liquid chromatography

Efficiency of paclitaxel encapsulated in the nanobubbles were calculated. Initial paclitaxel concentration loaded into 50 ml of SE61 surfactant mixture was 100 µg/ml. The calibration curve by height for paclitaxel concentrations from 0.0537 to 268.5 µg/ml (R^2= 0.99) was used for studying the encapsulation efficiency. The amount of paclitaxel encapsulated in the bubbles is found from the high performance liquid chromatography.

$$\% \text{ encapsulation efficiency} = \frac{\text{Amount of paclitaxel encapsulated in the bubbles}}{\text{Total amount of paclitaxel added initially}} * 100$$

There is no statistically significant difference in the encapsulation efficiency for both the nanobubbles with p>0.05 (figure 4.44)

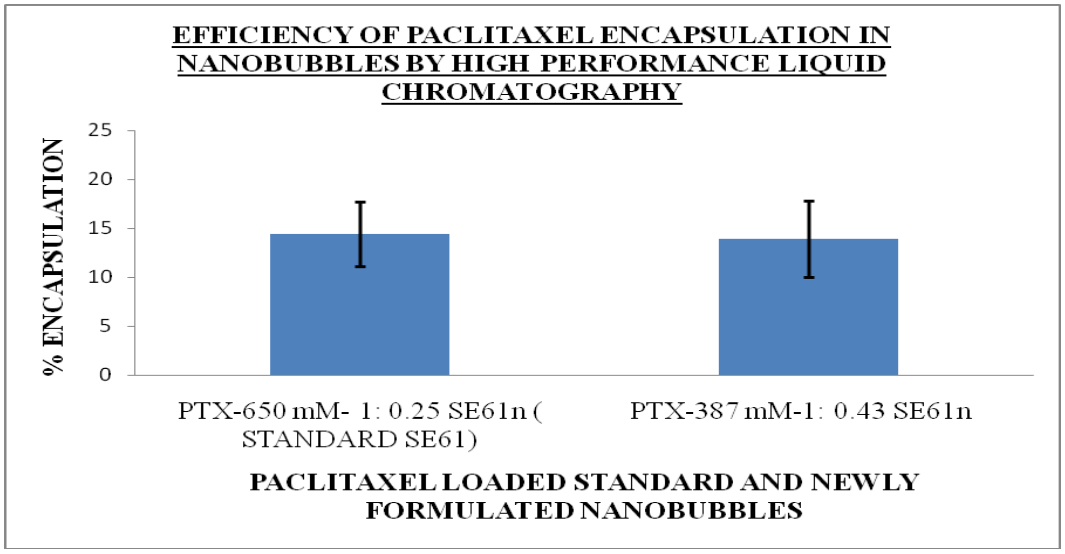

Figure 4.44: Paclitaxel encapsulation efficiency compared between standard SE61 and 250mM sodium chloride, 2.208g TPGS nanobubbles, p> 0.05, N=3 independent observations and error bars representing standard error about the mean.

When compared with microbubbles, paclitaxel loaded in standard SE61 microbubbles was 29.4% and in paclitaxel loaded newly formulated microbubbles was 10.98%. In case of nanobubbles, formulation change did not affect paclitaxel encapsulation efficiency. The encapsulation efficiency of paclitaxel loaded into standard SE61 nanobubbles was 14.4% and in paclitaxel loaded newly formulated nanobubbles was 13.9%.

4.10. Light Microscopy

Light microscope was used to obtain pictures of microbubbles and nanobubbles with and without paclitaxel. Spot Advanced software was used for obtaining the pictures.

4.10.1. Microbubbles

The microbubbles in the size 3 μm are shown in figure 4.45. These are 1: 0.43 SE61 (non-paclitaxel loaded) microbubbles representing 70: 30 molar ratio of span 60: TPGS.

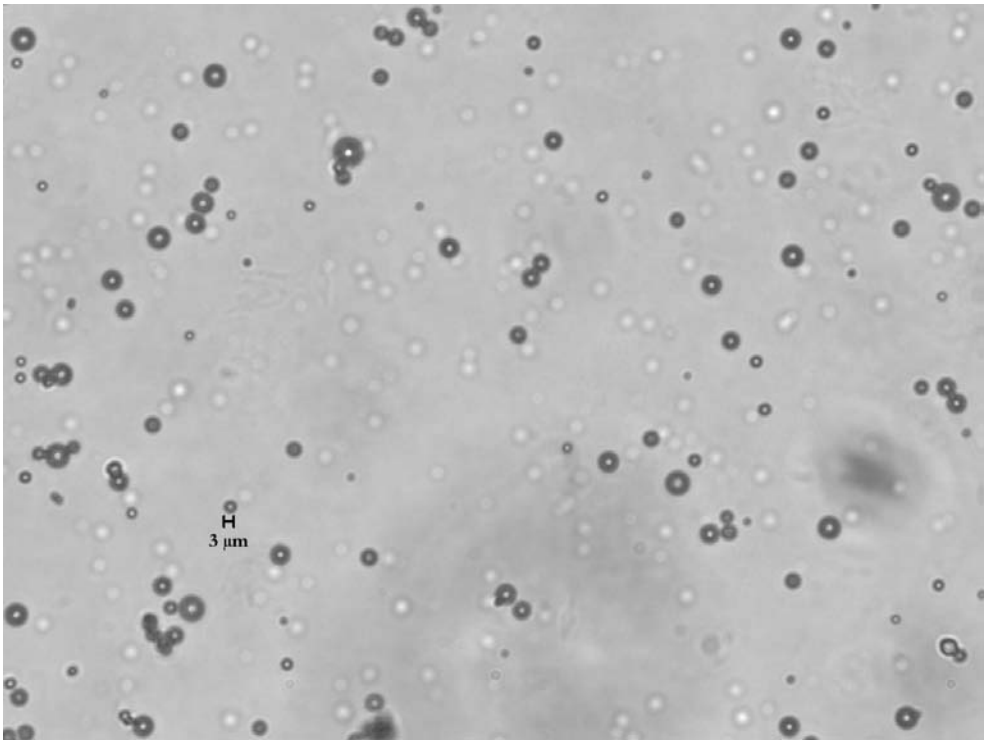

Figure 4.45: Image of 1: 0.43 SE61 microbubbles with 2.208 g TPGS keeping span 60 and sodium chloride concentration constant (No paclitaxel and no Ultrasound). Magnification: 40 X

The microbubbles with and without paclitaxel being encapsulated cannot be distinguished since SE61 surfactant mixture and paclitaxel are both white in colour. The paclitaxel loaded microbubbles with average diameter of 3µm are shown in Figure 4.46.

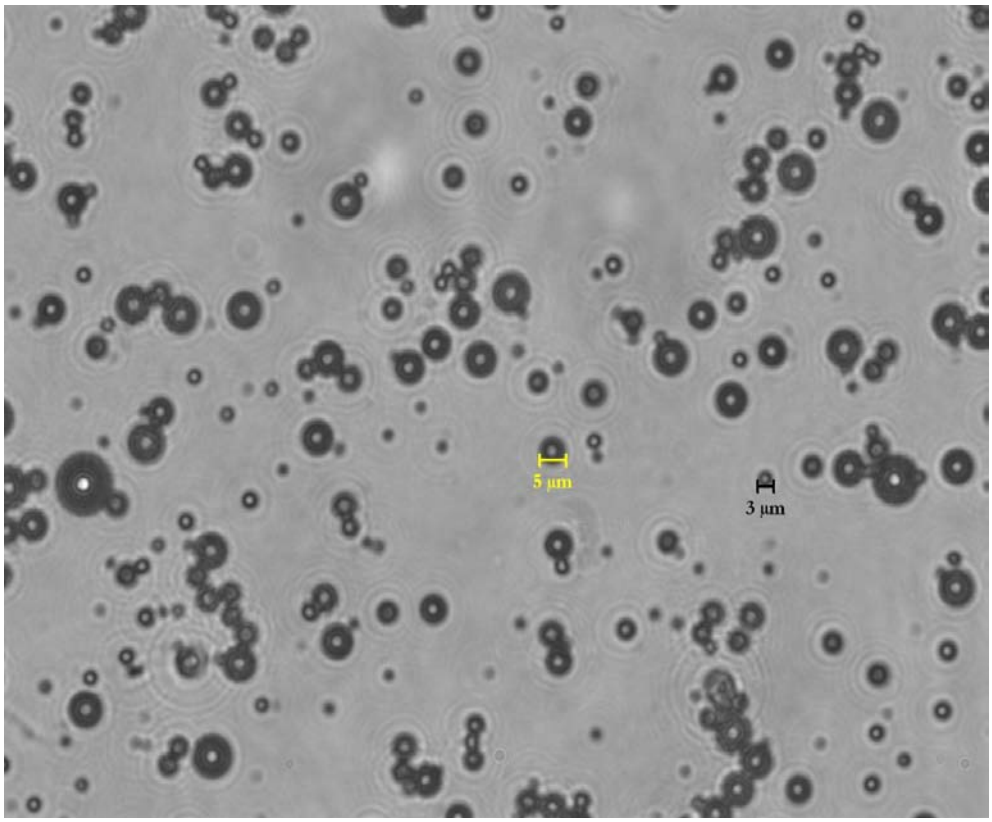

Figure 4.46: Standard (1: 0.25) SE61 microbubbles loaded with paclitaxel (No ultrasound). Magnification of 40 X and 1.6 X

4.10.2 Nanobubbles

The bubbles with average diameter of about 1μm are shown in figure 4.47

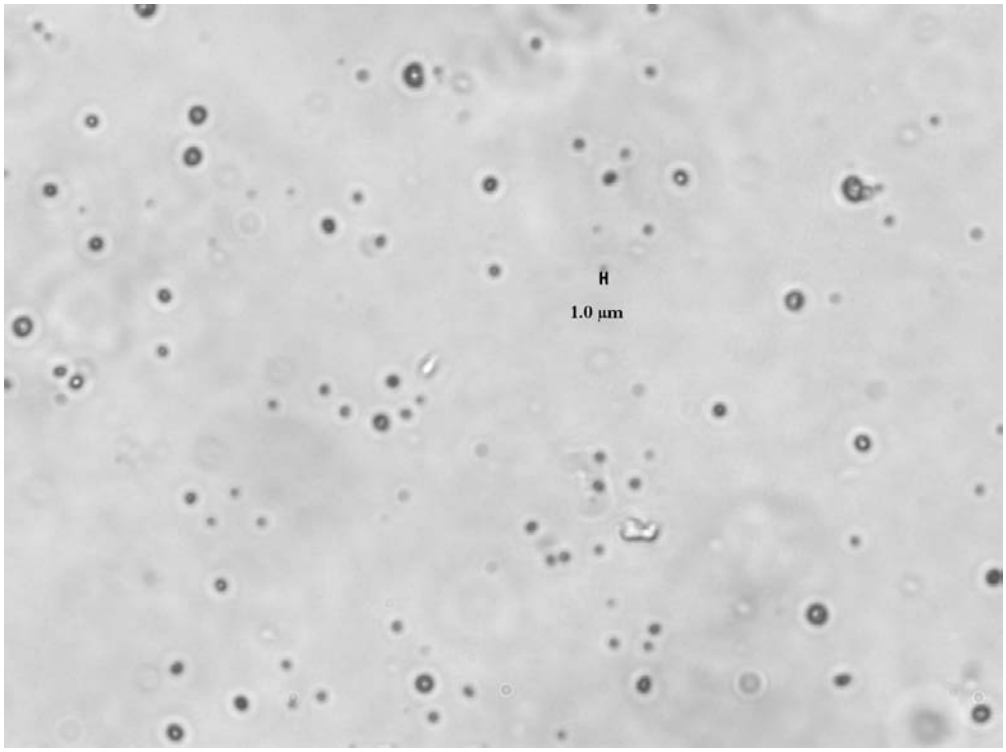

Figure 4.47: Image of 1: 0.43 SE61 nanobubbles with 2.208 g TPGS keeping span 60 and sodium chloride concentration constant (No paclitaxel and no Ultrasound). Magnification: 40 X and 1.6 X

The nanobubbles are not clearly observed and currently work in going on observing the nanobubbles clearly. Also, the nanobubbles with and without paclitaxel cannot be identified when figure 4.47 and figure 4.48 are compared.

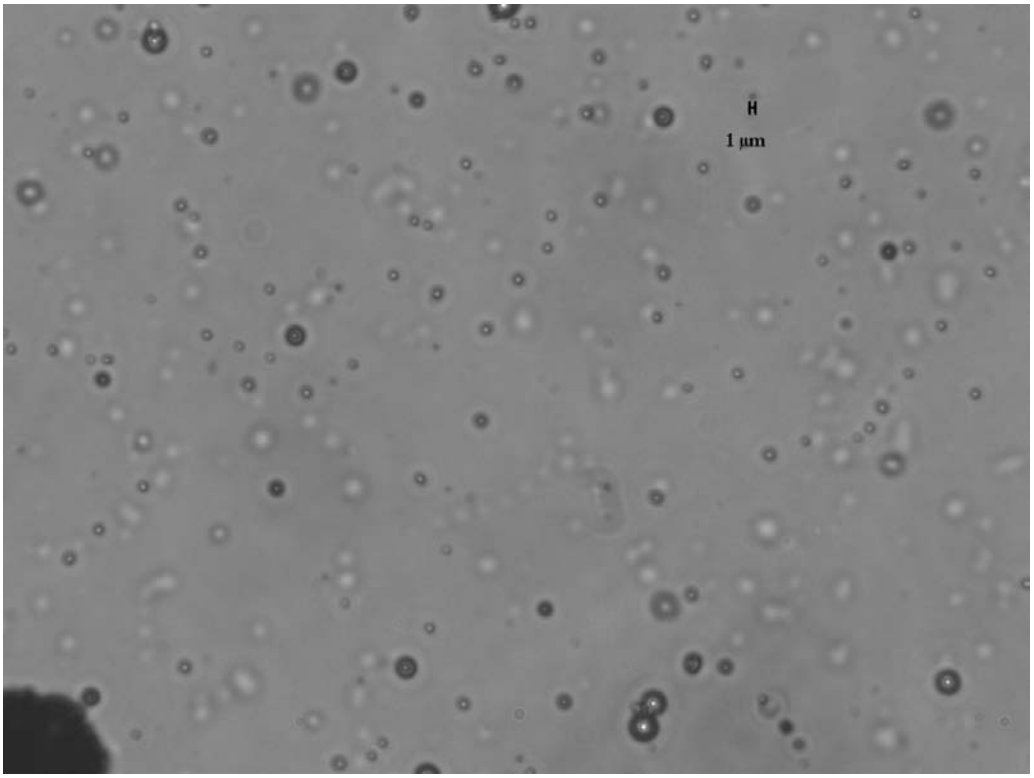

Figure 4.48: Image of paclitaxel loaded newly formulated SE61 nanobubbles (No ultrasound) .Magnification 40X and 1.6 X

CHAPTER 5: CONCLUSIONS

The acoustic characterization of standard SE61 micro and nanobubbles was studied. The average diameter of standard SE61 microbubbles was 2-2.3 μm and provided contrast enhancement between 18- 24 dB. Nanobubbles with mean diameter of 350-480 nm were separated from the primary mixture and provided contrast enhancement between 18-23 dB.

The effect of additional sodium chloride concentration in the SE61 mixture was studied for micro and nanobubbles. In case of nanobubbles, the additional sodium chloride had statistically significant effect on enhancement at dose of 50 μl/L. However, additional sodium chloride did not have statistically significant effect on enhancement of microbubbles with $p > 0.05$. From the salt study, 387 mM total sodium chloride concentration gave maximum enhancement of 24 ± 0.16 dB at dose of 300 μl/L of nanobubbles. Also, higher nanobubble population was observed at this particular concentration. In case of microbubbles, 262 mM total sodium chloride gave maximum contrast enhancement is 28 ± 1.5 dB at dose of 60 μl/L. From the surfactant study, 1: 0.43 (for nanobubbles) and 1: 0.25 (for microbubbles) molar ratio of span 60: TPGS were chosen as ratio in the newly formulated bubbles.

In the thesis, it has been shown that paclitaxel was incorporated into the SE61 micro and nanobubbles, ultrasound contrast agents. The acoustic properties of microbubbles with and without paclitaxel were studied and did not reveal statistically significant difference. Paclitaxel was loaded into the microbubbles without altering their structure and acoustic stability in ultrasound beam. In case of standard SE61 nanobubbles without paclitaxel

loaded into it, shadowing occurred at a dose of 400 µl/L giving maximum enhancement of 22.40 ± 0.86 dB. Shadowing occurred at dose of 300 µl/L for both paclitaxel loaded standard SE61 and paclitaxel loaded newly formulated nanobubbles with maximum contrast enhancement as 22.8 ± 0.45 dB and 22.58 ±0.188 dB respectively. Also, the half life of paclitaxel loaded standard SE61 nanobubbles was 1.4 ± 0.6 minutes which is higher than standard SE61 nanobubbles (0.95 min) with $p < 0.05$.

High performance liquid chromatography was used to study paclitaxel encapsulation efficiency in micro and nanobubbles. In case of nanobubbles, formulation change did not affect paclitaxel encapsulation efficiency. The encapsulation efficiency of paclitaxel loaded into standard SE61 nanobubbles was 14.4% and in newly formulated nanobubbles was 13.9%. When compared with microbubbles, paclitaxel loaded in standard SE61 microbubbles was 29.4% and in paclitaxel loaded newly formulated microbubbles was 10.98%.

The images of paclitaxel loaded and non-paclitaxel loaded bubbles were observed under light microscope. Since the colour of SE61 contrast agent and paclitaxel is the same, paclitaxel loaded into the hydrophobic region of the bubble was not distinguishable.

CHAPTER 6: RECOMMENDATIONS

In my thesis work, only one concentration of paclitaxel was used and loaded into micro and nanobubbles. Different concentrations of paclitaxel can be loaded into the bubbles to see which concentration gives highest encapsulation efficiency in the bubbles.

The effect of total sodium chloride and TPGS were studied on the population of nanobubbles keeping span 60 concentration constant. Since span 60 plays an important role in maintaining the structure of bubbles, effect of span 60 concentration on nanobubble population can be studied.

Since paclitaxel and SE61 mixture are both white in colour, the images under light microscope were not clear with paclitaxel loaded into the hydrophobic region of the bubble. Paclitaxel can be linked to some targeting dye specific to paclitaxel which shows the paclitaxel being loaded into the bubbles. Although ultrasound meditated paclitaxel delivery enables targeted cancer therapy, increase in specificity towards tumor targeting can be done by attaching ligands specific to tumor receptors.

Also, studies where another anti-cancer drug can be encapsulated along with paclitaxel can be done.

APPENDIX A: LIST OF NOMENCLATURE USED

Table A.1: Nomenclature of standard SE61 bubbles with total sodium chloride concentration and span 60: TPGS molar ratios

Name	Type of bubble	Represented as
Standard nanobubble with 650mM sodium chloride and 1: 0.25 ratio of span 60 and TPGS	Nano	STANDARD-650mM- 1: 0.25 SE61n
Standard microbubble with 650mM sodium chloride and 1: 0.25 ratio of span 60 and TPGS	Micro	STANDARD-650mM- 1: 0.25 SE61m

Table A.2: Amount of additional sodium chloride added and total sodium chloride concentration in 50 ml of SE61 surfactant mixture.

Type of mixture	Additional salt added in 50 ml of surfactant mixture		Sodium chloride in 1L of PBS		Total sodium chloride concentration in 50 ml of SE61 mixture
	(g)	(mM)	(g)	(mM)	(mM)
137mM sodium chloride SE61	0	0	8.01	137	137
262 mM sodium chloride SE61	0.366	125	8.01	137	262
387mM sodium chloride SE61	0.730	250	8.01	137	387
512mM sodium chloride SE61	1.097	375	8.01	137	512
Standard (650mM sodium chloride) SE61	1.5	513	8.01	137	650
887mM sodium chloride SE61	2.192	750	8.01	137	887

Table A.3: Types of bubbles at different total sodium chloride concentrations keeping Span 60 and TPGS constant

Name	Type of the bubble	Represented as
137 mM sodium chloride SE61 keeping span 60 and TPGS constant	Nano	137mM SE61n
262 mM sodium chloride SE61 keeping span 60 and TPGS constant	Nano	262 mM SE61n
387mM sodium chloride SE61keeping span 60 and TPGS constant	Nano	387 mM SE61n
512mM sodium chloride SE61 keeping span 60 and TPGS constant	Nano	512 mM SE61n
Standard (650mM sodium chloride) SE61 keeping span 60 and TPGS constant	Nano	Standard (650 mM) SE61n
887mM sodium chloride SE61 keeping span 60 and TPGS constant	Nano	887 mM SE61n
137 mM sodium chloride SE61 keeping span 60 and TPGS constant	Micro	137mM SE61m
262 mM sodium chloride SE61 keeping span 60	Micro	262 mM SE61m

and TPGS constant		
387mM sodium chloride SE61keeping span 60 and TPGS constant	Micro	387 mM SE61m
512mM sodium chloride SE61 keeping span 60 and TPGS constant	Micro	512 mM SE61m
Standard (650mM sodium chloride) SE61 keeping span 60 and TPGS constant	Micro	Standard(650mM) SE61m
887mM sodium chloride SE61 keeping span 60 and TPGS constant	Micro	887 mM SE61m

Table A.4: Molar ratio of span 60 and TPGS in surfactant study (changing amount of TPGS keeping span 60 and total sodium chloride constant in 50 ml of SE61 mixture)

Type of mixture	Molar ratio of surfactant Span 60	Molar ratio of surfactant TPGS
Standard (1.288g TPGS) SE61	80	20
2.208 g TPGS keeping span 60 and total sodium chloride constant	70	30
3.434 g TPGS keeping Span60 and total sodium chloride constant	60	40

Table A.5: Nomenclature for TPGS study keeping span 60 and sodium chloride constant in surfactant mixture

Name	Type of bubble	Represented as
Standard (1.288g TPGS) SE61	Nano	1 : 0.25 SE61 n
2.208 g TPGS keeping span 60 and total sodium chloride constant	Nano	1: 0.43 SE61 n
3.434g TPGS keeping Span60 and total sodium chloride constant	Nano	1: 0.67 SE61n
Standard (1.288g TPGS) SE61	Micro	1: 0.25 SE61m
2.208 g TPGS keeping span 60 and sodium chloride constant	Micro	1: 0.43 SE61 m
3.434 g TPGS keeping Span60 and sodium chloride constant	Micro	1: 0.67 SE61m

Table A.6: Encapsulation of paclitaxel into newly formulated bubbles

Name	Type of bubble	Represented as
Paclitaxel loaded nanobubble with 387mM sodium chloride and 1: 0.43 ratio of span 60 and TPGS (newly formulated)	Nano	PTX-387 mM-1: 0.43 SE61n
Paclitaxel loaded standard nanobubble with 650mM sodium chloride and 1: 0.25 ratio of span 60 and TPGS	Nano	PTX-650 mM- 1: 0.25 SE61n
Paclitaxel loaded microbubble with 262 mM sodium chloride and 1: 0.25 ratio of span 60 and TPGS (newly formulated)	Micro	PTX-262mM- 1: 0.25 SE61m
Paclitaxel loaded standard microbubble with 650mM sodium chloride and 1: 0.25 ratio of span 60 and TPGS	Micro	PTX-650mM- 1: 0.25 SE61m

APPENDIX B: STANDARD OPERATING PROCEDURES

B.1.Micro and Nanobubble Preparation

1. To a clean 300 ml beaker, add calculated amounts of Sodium chloride, TGPS and span 60 in 50 ml of PBS. The pH of the PBS (PBS) is adjusted to 7.4 before usage.

Table B.1: Amount of span 60, TPGS and additional sodium chloride added to 50 ml of SE61 mixture

Type of mixture	Span 60 (g)	TPGS (g)	Additional sodium chloride (g)	PBS (ml)
137mM sodium chloride SE61	1.464	1.288	0	50
262 mM sodium chloride SE61	1.464	1.288	0.366	50
387mM sodium chloride SE61	1.464	1.288	0.730	50
512mM sodium chloride SE61	1.464	1.288	1.097	50
Standard (650mM sodium chloride and 1: 0.25 molar ratio of span60:	1.464	1.288	1.5	50

TPGS) SE61				
887mM sodium chloride SE61	1.464	1.288	2.192	50
1: 0.43 SE61	1.464	2.208	1.5	50
1: 0.67 SE61	1.464	3.434	1.5	50

2. Add a stir bar to the beaker
3. Cover the beaker with aluminum foil and put 1 inch piece of autoclave tape
4. Heat the solution with continuous stirring until span 60 and TPGS completely dissolve.
5. Autoclave: Take out the inner part of the autoclave and measure the water level. The water level should be between the 2-2.5 inch mark, if not, adjust the water level accordingly. Turn the heat to maximum so that the water begins heating. After putting in the beakers, put the top back on the autoclave and screw all the knobs in place. Wait until seeing the water boils and water vapor comes from the ventilation valve. When this happens close the ventilation value and wait until the pressure inside reaches the green zone, adjust the heat to 4, and count 35 minutes from there. After that close the autoclave switch and let the pressure come down. Also, be sure to wear the mitts to avoid causing injury. Autoclaving is done to reduce the particle size of span 60.
6. Keep the PBS (pH 7.4) in 4° C refrigerator

7. After this allow the solution to cool by constant stirring the mixture at room temperature for 35-45 min.
8. Keep the separation funnel attached to a clamp in 4° C refrigerator
9. Place the beaker in ice and purge the mixture with octafluoropropane until the bubbles cover the solution by placing the tip in the solution. When sonicating, the tip supplying the gas will not be in the solution, only the sonication probe will be submerged.
10. For sonication place the pipette tip above the solution and purge the solution with octafluoropropane for 3 min at 110 W at flow rate of 50 ml/min using Misonix Inc. CL4 tapped horn probe with 0.5" tip, Farmingdale, NY.
11. Pour the sonicated mixture in the cold separation funnel and add 50 ml of cold PBS.
12. Because there is no distinct layer after 45 min after the first wash with 50 ml PBS, the solution is discarded for 25 ml and then 50-75 ml of the solution is transfer to another separation funnel (B). Now we have 2 separation funnels, a previous one that is a remaining after the transfer (A) and a new one with 50-75 ml of solution (B).
13. Add 50 ml of PBS to both the funnels and allow it to separate in the cold fridge for 45min.
14. Discard 50ml of the solution from both funnel A and B after 45 min and again add 50ml of the cold Phosphate buffer in both the funnels.
15. After 45 min, from funnel A remove the solution until you find the middle layer. Collect the layer in the centrifuge tube and place in the cold fridge. The funnel A contains the micro-bubbles. 200µl of the microbubbles from the centrifuge tube (from funnel A) is transferred into 10 ml volumetric flask which is then made up to mark

with 37°C membrane filtered PBS (pH 7.4). The diluted microbubbles is used for dose, time response, size analysis and zeta potential of microbubbles.

16. For funnel B remove 20 ml of the solution and collect 10 ml in centrifuge tube. Place the tube in the cold fridge. The funnel B contains the nanobubbles. The nanobubbles from the centrifuge tube can directly be used for dose response, time response, size analysis of nanobubbles, zeta potential of the bubbles and turbidity measurement at 610nm without further dilution.

B.2. Enhancement studies (Dose response curve)

1) A 5072 pulser-receiver (Waltham, MA) is used to generate acoustic pressure with a pulse repetition frequency of 100Hz.
2) First the initial set up of the function generator is done. The pulse repetition frequency is adjusted to 100Hz, energy to 1 and damping to 3.
3) Lecroy 9350 A 500 MHz Oscilloscope is used and set to 1µs and 100mV.
4) Fill the custom vessel for ultrasound testing with 50 ml of 37°C membrane filtered 1X PBS (pH7.4).
5) A stir-bar is added to the custom vessel to continuously stir the PBS.
6) This vessel is placed into another cubical tank with 20 gallons of distilled water
7) The temperature of this cubical tank is maintained at 37°C
8) The stirrer is adjusted to level 3
9) A 5 MHz transducer is used for the acoustic testing with delay being adjusted to 62µs.
10) Initially the transducer is focused through the transparent window till a signal is seen at 20db gain
11) On the top of the rectangular tank is Parker positioning system (Edmund Scientific, NJ). These adjustable knobs can be used for proper positioning of the transducer and for adjusting the signal seen in the oscilloscope.
12) The gain is adjusted to 40 db
13) Create a new folder for saving the results in the data folder
14) Click Ultrasound --→ main program--→ main ultrasound program---→ main ultrasound program.vi

15) Lab VIEW 7.1 (National Instruments) software is used for acoustic testing
16) Click on the run button
17) Enter the folder path to save the acquired data
18) In the sample name folder write Baseline and click on Make baseline for the acquisition
19) Click acquire
20) In the sample name type the dose of the bubble being injected or bubble with the drug being injected
21) Add the required dose of the bubble or bubble with the drug using 50-200µl pipette in the custom vessel in the cubical tank
22) Click acquire
23) Each time after the previous acquisition replace the PBS in the custom vessel with another 50 ml of membrane filtered 37°C PBS
24) Repeat with different doses and observe where shadowing effect begins to affect enhancement
25) Export the data to folder created and save them.

B.3 Stability Response and half life of the bubble

1) The dose on the rise of dose response curve is used as the dose for time response
2) Click on capture waveform on set time interval
3) Interval between Acquisitions is set to 1 min
4) Number of time points to acquire is set to 11 for nanobubbles and 16 for microbubbles.
5) In the sample name section write the dose being used for time response
6) Press acquire
7) Export the data to the folder
8) Half life in min of the bubble is calculated from the time response data

B.4. Size Analysis

Zetasizer nano ZS (Malvern Institute, UK) was used for size analysis of particles and bubbles. Low volume disposable sizing tapered cuvette was used for size testing.

B.4.1 Size Analysis of particles after autoclave

1) Transfer 1000µl of autoclaved and later cooled SE61 mixture in the tapered cuvette

2) Place the cuvette in the slot of the instrument

3) Choose DTS (Nano) software for size analysis

4) The measurement SOP is chosen from the dropdown menu

5) Choose measure --→ sample and write specifics of the sample whose size is being measured

6) The measurement is taken three times and z-average diameter in nm is noted down

B.4.2 Size Analysis of the bubbles

1) In case of nanobubbles: 1000µl of the nanobubbles is taken and transferred directly in the cuvette without dilution.

2) In case of microbubbles: 200µl of microbubbles is transferred in 10ml volumetric flask where the volume is made up to the mark with 37°C membrane filtered PBS (pH 7.4). 1000µl from the 10ml volumetric flask is transferred in the tapered cuvette for size analysis of microbubbles

3) The cuvette were placed into the slot of the instrument

4) Choose DTS (Nano) software for size analysis

5) The measurement SOP is chosen from the dropdown menu

6) Choose measure --→ sample and write specifics of the sample whose size is being measured

7) The measurement is taken three times and z-average diameter in nm is noted down.

B.5 Zeta potential measurement

Zetasizer nano ZS (Malvern Institute, UK) was used for measuring zeta potential of particles and bubbles. Zeta sizer Nano series Disposable capillary cuvettes (Malvern Inst., UK) were used for measuring zeta potential

B.5.1 Zeta potential of particles

1) Transfer 1000µl of autoclaved and later cooled SE61 mixture in the zeta sizer cuvette

2) Place the cuvette into the slot of the instrument

3) Choose DTS (Nano) software

4) The appropriate Zeta measurement SOP is chosen from the dropdown menu

5) Choose measure --→ sample and write specifics of the sample whose zeta potential is being measured

6) The measurement is taken three times and ZP-average (mV) is calculated from each run.

B.5.2 Zeta Potential of the bubbles

1) In case of nanobubbles: 1000µl of the nanobubbles is taken and transferred directly in the cuvette without dilution.

2) In case of microbubbles: 200µl of microbubbles is transferred in 10ml volumetric flask where the volume is made up to the mark with 37°C membrane filtered PBS (pH 7.4) 1000µl from the 10ml volumetric flask is transferred in the tapered cuvette for size analysis of microbubbles

3) The cuvette is then placed into the slot of the instrument

4) Choose DTS (Nano) software

5) The zeta measurement SOP is chosen from the dropdown menu

6) Choose measure --→ sample and write specifics of the sample whose zeta potential is being measured

7) The measurement is taken three times and ZP-average (mV) is calculated from each run.

B.6 Turbidity measurement of nanobubbles

1) Start the Tecan infinite M 200 machine (Research Triangle Park, NC)
2) Click on Tecan i control 1.3 software
3) Choose Infinite 200 Reader instrument
4) Choose 96 corning Flat Transparent plate reader from the drop down menu
5) Drag Absorbance scan option to the bottom center, set number of reads as 5 and number of steps as 1
6) Scan from 230nm to 1000nm.
7) Non- sterile Polystyrene, Flat bottom, medium binding costar 96 corning Flat transparent plate reader (Corning, NY) is used for the turbidity measurement
8) Put the plate inside with the nanobubbles in concentration (10µl of nanobubbles and 190 µl of cold PBS ph 7.4)
9) Click the start button
10) Absorbance value at 610nm is used to study the nanobubble population.

B.7 Loading of Paclitaxel into the bubbles

1) To a clean 300 ml beaker, add calculated amounts of Sodium chloride, TGPS and Span 60 in 50 ml of PBS. The pH of the PBS is adjusted to 7.4 before usage.

2) Add a stir bar to the beaker

3) Cover the beaker with aluminum foil and put 1 inch piece of autoclave tape

4) Heat the solution with continuous stirring until Span 60 and TPGS dissolves completely.

5) Autoclave: Take out the inner part of the autoclave and measure the water level. The water level should be between the 2-2.5 inch mark, if not, adjust the water level accordingly. Turn the heat to maximum so that the water begins heating. After putting in the beakers, put the top back on the autoclave and screw all the knobs in place. Wait until seeing the water boils and water vapor comes from the ventilation valve. When this happens close the ventilation value and wait until the pressure inside reaches the green zone, adjust the heat to 4, and count 35 minutes from there. After that close the autoclave switch and let the pressure come down. Also, be sure to wear the mitts to avoid causing injury. Autoclaving is done to reduce the particle size of Span 60.

6) Keep the PBS (pH 7.4) in 4°

7) After this allow the solution to cool by constant stirring the mixture at room temperature for 35-45 min.

8) Add 100 μg/ml of Paclitaxel to the stirred mixture which corresponds to 5mg of the drug in the 50 ml autoclaved SE61 surfactant mixture. Heat/ stir the mixture and care should be taken that the solution does not boil. The solution is kept aside for some time and later cooled to room temperature for 30-45 min while constant stirring .

9) Keep the separation funnel attached to a clamp in 4° C refrigerator

10) Place the beaker in ice and purge the mixture with Octafluoropropane until the bubbles cover the solution by placing the tip in the solution. When sonicating, the tip supplying the gas will not be in the solution, only the sonication probe will be submerged.

11) For sonication place the pipette tip above the solution and purge the solution with Octafluoropropane for 3 min at 110 W at flow rate of 50ml/min using Misonix Inc. CL4 tapped horn probe with 0.5" tip, Farmingdale, NY.

12) Pour the sonicated mixture in the cold separation funnel and add 50 ml of cold PBS.

13) Because there is no distinct layer after 45min after the first wash with 50 ml PBS, the solution is discarded for 25 ml and then 50-75 ml of the solution is transfer to another separation funnel (B). Now we have 2 separation funnels, a previous one that is a remaining after the transfer (A) and a new one with 50-75 ml of solution (B).

14) Add 50 ml of PBS to both the funnels and allow it to separate in the cold fridge for 45min.

15) Discard 50ml of the solution from both funnel A and B after 45 min and again add 50ml of the cold Phosphate buffer in both the funnels.

16) After 45 min, from funnel A remove the solution until you find the middle layer. Collect the layer in the centrifuge tube and place in the cold fridge. The funnel A contains the micro-bubbles.

17) For funnel B remove 20 ml of the solution and collect 10 ml in centrifuge tube. Place the tube in the cold fridge. The funnel B contains the nanobubbles.

B.8 Efficiency of Paclitaxel Encapsulation in the bubble by High Performance liquid chromatography

1) Add 2.5 ml ethyl acetate to Paclitaxel loaded bubbles

2) Vortex shaking for 1 min

3) Centrifuge at 9000rpm for 15 min

4) Pipette 1.5ml of ethyl acetate (top layer) to glass bottle and evaporate

5) Add 1.5ml Acetonitrile and then close and seal then shake for 24 hours

6) A reverse phase Inertsil ODS column (250mm x 4.6 mm, 5µm particle size, GL Science) is used.

7) The mobile phase used was 100% Acetonitrile HPLC Grade at flow rate of 1 ml/min.

8) Inject sample 50µl and run for 30 min

9) The column effluent was detected at 227 nm.

APPENDIX C: THEORY BEHIND THE STRUCTURE OF THE BUBBLES

The air-water interface is an excellent reflector of ultrasound beam [13]. In our micro and nanobubbles perfluorocarbon (gas core) is used which strongly reflects the ultrasound beam thus helping in contrast enhancement during imaging. In the old model, microbubble is gas-filled micelle formed by surfactant molecules being arranged with the hydrophobic tail groups arranged to face the relatively hydrophobic gas bubble and hydrophilic head groups facing the aqueous solution [13].

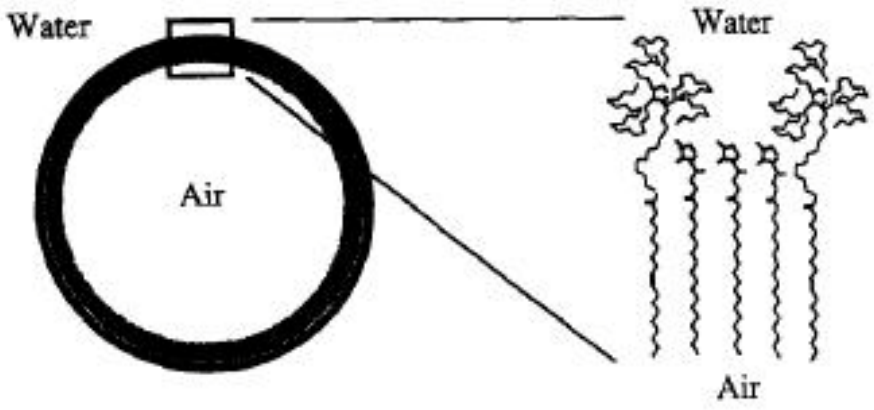

Figure C.1 : Old model of microbubble showing the arrangement of Span 60 and Tween 80 in microbubble [13]

The large polar head groups of Tween put forth mutual repulsive forces and span 60 molecules sandwiched between the Tween molecules to moderate the head group repulsion [13] as shown in the figure.

Unpublished results in our laboratory explain the structure and stability of microbubble with another theory. Pickering emulsions and foams consist of bubbles which are stabilized by small solid particles attached to surface [119-122]. In our case the solid particles are of span 60 and TPGS is attached to the surface of span particles.

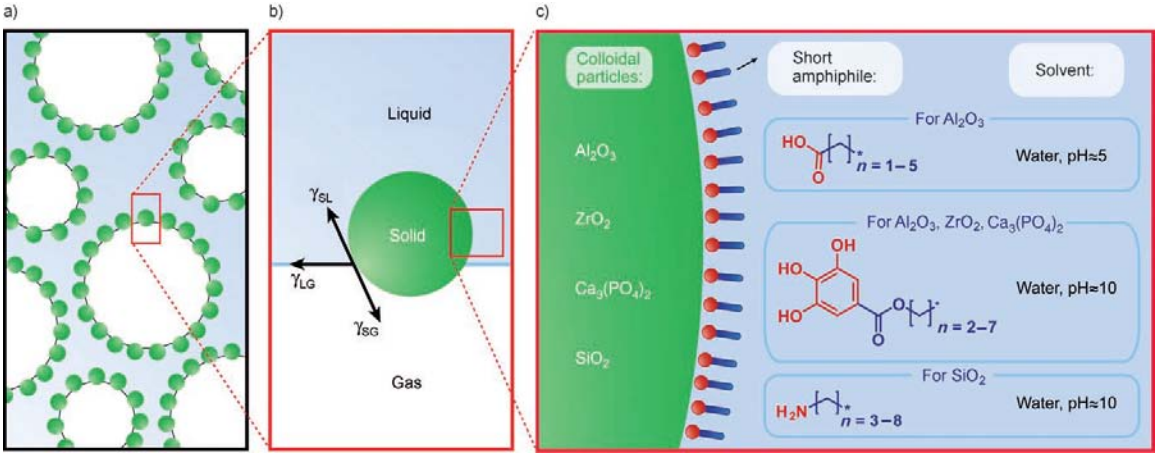

Figure C.2: Solid span 60 attached at the surface of the bubble would stabilize the bubbles [123]

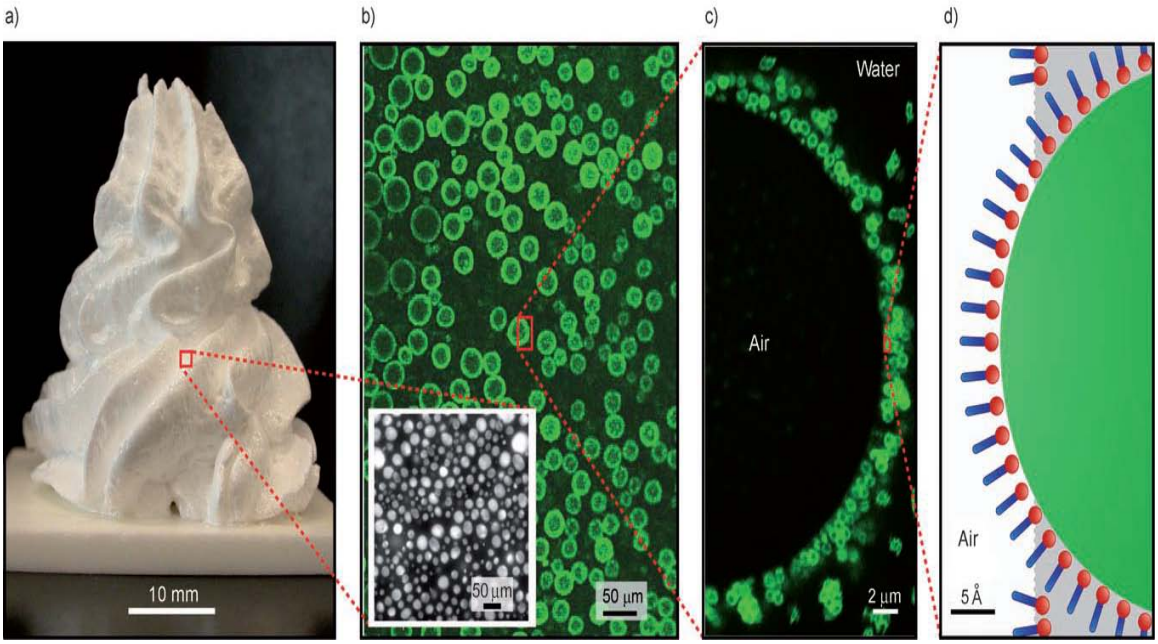

Figure C.3: At the gas-liquid interface span 60 are attached on the bubble surface imparting stability [123]

LIST OF REFERENCES

1. Frinking, P.J.A., et al., *Ultrasound contrast imaging: current and new potential methods.* Ultrasound Med Biol, 2000. **26**(6): p. 965-975.

2. Husseini, G.A. and W.G. Pitt, *The Use of Ultrasound and Micelles in Cancer Treatment.* J Nanosci and Nanotechnol, 2008. **8**(5): p. 2205-2215.

3. Liu, Y., H. Miyoshi, and M. Nakamura, *Encapsulated ultrasound microbubbles: Therapeutic application in drug/gene delivery.* J Control Release, 2006. **114**(1): p. 89-99.

4. Husseini, G.A. and W.G. Pitt, *Ultrasonic-activated micellar drug delivery for cancer treatment.* J Pharm Sci, 2009. **98**(3): p. 795-811.

5. Wheatley, M.A. and S. Singhal, *Structural studies on stabilized microbubbles: development of a novel contrast agent for diagnostic ultrasound.* Reactive Polymers, 1995. **25**(2-3): p. 157-166.

6. Case, T.D., *ULTRASOUND PHYSICS AND INSTRUMENTATION.* Surg Clin N Am, 1998. **78**(2): p. 197-217.

7. Obrienjr, W., *Ultrasound–biophysics mechanisms☆.* Prog Biophys Mol Biol, 2007. **93**(1-3): p. 212-255.

8. Newman, P.G. and G.S. Rozycki, *THE HISTORY OF ULTRASOUND.* Surg Clin N Am, 1998. **78**(2): p. 179-195.

9. Beach, K.W., *1975-2000: A quarter century of ultrasound technology.* Ultrasound Med Biol, 1992. **18**(4): p. 377-388.

10. Humphrey, V., *Ultrasound and matter—Physical interactions.* Prog Biophys Mol Biol, 2007. **93**(1-3): p. 195-211.

11. Wheatley, M.A., et al., *Surfactant-stabilized contrast agent on the nanoscale for diagnostic ultrasound imaging.* Ultrasound Med Biol, 2006. **32**(1): p. 83-93.

12. Ophir, J. and K.J. Parker, *Contrast agents in diagnostic ultrasound.* Ultrasound Med Biol, 1989. **15**(4): p. 319-333.

13. Singhal, S., C.C. Moser, and M.A. Wheatley, *Surfactant-stabilized microbubbles as ultrasound contrast agents: stability study of Span 60 and Tween 80 mixtures using a Langmuir trough.* Langmuir, 1993. **9**(9): p. 2426-2429.

14. Forsberg, F., et al. *Comparison of air and perfluorocarbon filled microbubbles for ultrasound contrast studies*. in *Ultrasonics Symposium, 1996. Proceedings., 1996 IEEE*. 1996.

15. Basude, R. and M.A. Wheatley, *Generation of ultraharmonics in surfactant based ultrasound contrast agents: use and advantages.* Ultrasonics, 2001. **39**(6): p. 437-444.

16. Kaufmann, B.A. and J.R. Lindner, *Molecular imaging with targeted contrast ultrasound.* Curr Opin Biotechnol, 2007. **18**(1): p. 11-16.

17. Dhanikula, A.B. and R. Panchagnula, *Localized paclitaxel delivery.* Int J Pharm, 1999. **183**(2): p. 85-100.

18. Klibanov, A.L., *Microbubble Contrast Agents: Targeted Ultrasound Imaging and Ultrasound-Assisted Drug-Delivery Applications.* Invest Radiol, 2006. **41**(3): p. 354-362 10.1097/01.rli.0000199292.88189.0f.

19. Porter, T.R., et al., *Targeted vascular delivery of antisense molecules using intravenous microbubbles.* Cardiovasc Revasc Med. **7**(1): p. 25-33.

20. Miller, M.W., D.L. Miller, and A.A. Brayman, *A review of in vitro bioeffects of inertial ultrasonic cavitation from a mechanistic perspective.* Ultrasound Med Biol, 1996. **22**(9): p. 1131-1154.

21. Liu, Y., H. Yang, and A. Sakanishi, *Ultrasound: Mechanical gene transfer into plant cells by sonoporation.* Biotech Adv. **24**(1): p. 1-16.

22. Umemura, S., et al., *Recent advances in sonodynamic approach to cancer therapy.* Ultrason Sonochem, 1996. **3**(3): p. S187-S191.

23. Frenkel, V., *Ultrasound mediated delivery of drugs and genes to solid tumors.* Adv Drug Deliv Rev, 2008. **60**(10): p. 1193-1208.

24. Unger, E.C., et al., *Therapeutic applications of microbubbles.* Eur J Radiol, 2002. **42**(2): p. 160-168.

25. Smith, N.B., et al., *Ultrasound-mediated transdermal transport of insulin in vitro through human skin using novel transducer designs.* Ultrasound Med Biol, 2003. **29**(2): p. 311-317.

26. *Wheatley, M.A., B.B. Goldberg, and S. Singhal, SURFACTANT-STABILIZED MICROBUBBLE MIXTURES, PROCESS FOR PREPARING AND METHODS OF USING THE SAME U.S. Patent, Editor. 1994, Drexel University, Philadelphia, Pa: USA. p. 4.*

27. Wick, A.N. and L. Joseph, *Sorbitan Monostearate Metabolism, Lack of Deposition upon Chronic Feeding.* J Agric Food Chem, 1953. **1**(5): p. 398-399.

28. Hendy, R.J., et al., *Long-term toxicity study of sorbitan monostearate (Span 60) in mice.* Food Cosmet Toxicol, 1978. **16**(6): p. 527-534.

29. Li, P.-Y., et al., *Poly(l-lactide)-Vitamin E TPGS Nanoparticles Enhanced the Cytotoxicity of Doxorubicin in Drug-Resistant MCF-7 Breast Cancer Cells.* Biomacromolecules, 2010. **11**(10): p. 2576-2582.

30. Zhang, Z. and S.-S. Feng, *Nanoparticles of poly(lactide)/vitamin E TPGS copolymer for cancer chemotherapy: Synthesis, formulation, characterization and in vitro drug release.* Biomaterials, 2006. **27**(2): p. 262-270.

31. Mu, L. and S.S. Feng, *Vitamin E TPGS used as emulsifier in the solvent evaporation/extraction technique for fabrication of polymeric nanospheres for controlled release of paclitaxel (Taxol®).* J Control Release, 2002. **80**(1-3): p. 129-144.

32. Yan, A., et al., *Tocopheryl polyethylene glycol succinate as a safe, antioxidant surfactant for processing carbon nanotubes and fullerenes.* Carbon, 2007. **45**(13): p. 2463-2470.

33. Constantinides, P.P., J. Han, and S.S. Davis, *Advances in the use of tocols as drug delivery vehicles.* Pharm Res, 2006. **23**(2): p. 243-55.

34. Varma, M.V.S. and R. Panchagnula, *Enhanced oral paclitaxel absorption with vitamin E-TPGS: Effect on solubility and permeability in vitro, in situ and in vivo.* Eur J Pharm Sci. **25**(4-5): p. 445-453.

35. Zhang, Z., S. Huey Lee, and S.-S. Feng, *Folate-decorated poly(lactide-co-glycolide)-vitamin E TPGS nanoparticles for targeted drug delivery.* Biomaterials, 2007. **28**(10): p. 1889-1899.

36. Traber, M.G., et al., *Efficacy of water-soluble vitamin E in the treatment of vitamin E malabsorption in short-bowel syndrome.* Vol. 59. 1994. 1270-4.

37. Ke, W.-T., et al., *Physical characterizations of microemulsion systems using tocopheryl polyethylene glycol 1000 succinate (TPGS) as a surfactant for the oral delivery of protein drugs.* J Control Release, 2005. **102**(2): p. 489-507.

38. Mu, L., et al., *Study on surfactant coating of polymeric nanoparticles for controlled delivery of anticancer drug.* Colloid Polym Sci, 2004. **283**(1): p. 58-65.

39. Dintaman, J.M. and J.A. Silverman, *Inhibition of P-Glycoprotein by D-α-Tocopheryl Polyethylene Glycol 1000 Succinate (TPGS).* Pharm Res, 1999. **16**(10): p. 1550-1556.

40. Bansal, T., et al., *Novel formulation approaches for optimising delivery of anticancer drugs based on P-glycoprotein modulation.* Drug Discovery Today, 2009. **14**(21-22): p. 1067-1074.

41. Wempe, M.F., et al., *Inhibiting efflux with novel non-ionic surfactants: Rational design based on vitamin E TPGS.* Int J Pharm, 2009. **370**(1-2): p. 93-102.

42. Peltier, S., et al., *Enhanced Oral Paclitaxel Bioavailability After Administration of Paclitaxel-Loaded Lipid Nanocapsules.* Pharm Res, 2006. **23**(6): p. 1243-1250.

43. Rowinsky, E.K. and R.C. Donehower, *Paclitaxel (Taxol).* New Engl J Med, 1995. **332**(15): p. 1004-1014.

44. Nicolaou, K.C., W.-M. Dai, and R.K. Guy, *Chemistry and Biology of Taxol.* Angew Chem Int Ed Engl, 1994. **33**(1): p. 15-44.

45. Panchagnula, R., *Pharmaceutical aspects of paclitaxel.* Int J Pharm, 1998. **172**(1-2): p. 1-15.

46. Sonnichsen, D.S. and M.V. Relling, *Clinical pharmacokinetics of paclitaxel.* Clin pharmacokinet, 1994. **27**(4): p. 256-69.

47. Burt, H.M., et al., *Controlled delivery of taxol from microspheres composed of a blend of ethylene-vinyl acetate copolymer and poly (d,l-lactic acid).* Cancer Lett, 1995. **88**(1): p. 73-79.

48. Dordunoo, S.K., et al., *Taxol encapsulation in poly(ε-caprolactone) microspheres.* Cancer Chemother Pharmacol, 1995. **36**(4): p. 279-282.

49. *Release of taxol from poly(epsilon-caprolactone) pastes: effect of water-soluble additives.* J Control Release, 1997. **44**: p. 87-94.

50. Winternitz, C.I., et al., *Development of a Polymeric Surgical Paste Formulation for Taxol.* Pharm Res, 1996. **13**(3): p. 368-375.

51. Trynda-Lemiesz, L., *Paclitaxel-HSA interaction. Binding sites on HSA molecule.* Bioorg Med Chem , 2004. **12**(12): p. 3269-3275.

52. Wani, M.C., et al., *Plant antitumor agents. VI. Isolation and structure of taxol, a novel antileukemic and antitumor agent from Taxus brevifolia.* J Am Chem Soc, 1971. **93**(9): p. 2325-2327.

53. Donehower, R.C. and E.K. Rowinsky, *An overview of experience with taxol* (paclitaxel) in the U.S.A.* Cancer Treat Rev, 1993. **19**(Supplement 3): p. 63-78.

54. Guenard, D., F. Gueritte-Voegelein, and P. Potier, *Taxol and taxotere: discovery, chemistry, and structure-activity relationships.* Acc Chem Res, 1993. **26**(4): p. 160-167.

55. Parekh, H. and H. Simpkins, *The transport and binding of taxol.* General Pharmacology: The Vascular System, 1997. **29**(2): p. 167-172.

56. Band Horwitz, S., *Mechanism of action of taxol.* Trends Pharmacol Sci, 1992. **13**: p. 134-136.

57. van Zuylen, L., J. Verweij, and A. Sparreboom, *Role of Formulation Vehicles in Taxane Pharmacology.* Investigational New Drugs, 2001. **19**(2): p. 125-141.

58. Gelderblom, H., et al., *Cremophor EL: the drawbacks and advantages of vehicle selection for drug formulation.* Eur J Cancer, 2001. **37**(13): p. 1590-1598.

59. Engblom, P., et al., *Effects of paclitaxel with or without cremophor EL on cellular clonogenic survival and apoptosis.* Eur J Cancer, 1999. **35**(2): p. 284-288.

60. Guchelaar, H.J., et al., *Clinical, toxicological and pharmaceutical aspects of the antineoplastic drug taxol: A review.* Clin Oncol, 1994. **6**(1): p. 40-48.

61. Schiff, P.B. and S.B. Horwitz, *Taxol stabilizes microtubules in mouse fibroblast cells.* Proc Natl Acad Sci, 1980. **77**(3): p. 1561-1565.

62. Schiff, P.B., J. Fant, and S.B. Horwitz, *Promotion of microtubule assembly in vitro by taxol.* Nature, 1979. **277**(5698): p. 665-667.

63. Rao, S., et al., *3'-(p-azidobenzamido)taxol photolabels the N-terminal 31 amino acids of beta-tubulin.* J Biol Chem, 1994. **269**(5): p. 3132-3134.

64. Takahashi, M., et al., *Sensitivity to paclitaxel is not related to p53-dependent apoptosis in ovarian cancer cells.* Eur J Cancer, 2000. **36**(14): p. 1863-1868.

65. Javeed, A., et al., *Paclitaxel and immune system.* Eur J Pharm Sci, 2009. **38**(4): p. 283-290.

66. Spratlin, J. and M.B. Sawyer, *Pharmacogenetics of paclitaxel metabolism.* Crit Rev Oncol Hemat, 2007. **61**(3): p. 222-229.

67. Rowinsky, E.K., L.A. Cazenave, and R.C. Donehower, *Taxol: A Novel Investigational Antimicrotubule Agent.* J Natl Cancer Inst, 1990. **82**(15): p. 1247-1259.

68. Brouwer, E., et al., *Measurement of Fraction Unbound Paclitaxel in Human Plasma.* Drug Metab Dispos, 2000. **28**(10): p. 1141-1145.

69. Wiernik, P.H., et al., *Phase I Clinical and Pharmacokinetic Study of Taxol.* Cancer Res, 1987. **47**(9): p. 2486-2493.

70. Glantz, M.J., et al., *Paclitaxel Disposition in Plasma and Central Nervous Systems of Humans and Rats With Brain Tumors.* J Natl Cancer Inst, 1995. **87**(14): p. 1077-1081.

71. Baker, S.D., et al., *Role of Body Surface Area in Dosing of Investigational Anticancer Agents in Adults, 1991–2001.* J Natl Cancer Inst, 2002. **94**(24): p. 1883-1888.

72. Monsarrat, B., et al., *Modification of Paclitaxel Metabolism in a Cancer Patient by Induction of Cytochrome P450 3A4.* Drug Metab Dispos, 1998. **26**(3): p. 229-233.

73. Monsarrat, B., et al., *Hepatic metabolism and biliary excretion of Taxol in rats and humans*. 1993. 39-46.

74. Nielsen, D. and T. Skovsgaard, *P-glycoprotein as multidrug transporter: a critical review of current multidrug resistant cell lines.* Biochimica et Biophysica Acta (BBA) - Molecular Basis of Disease, 1992. **1139**(3): p. 169-183.

75. Gottesman, M.M. and V. Ling, *The molecular basis of multidrug resistance in cancer: The early years of P-glycoprotein research.* FEBS Letters, 2006. **580**(4): p. 998-1009.

76. Callen, D.F., et al., *Localization of the human multiple drug resistance gene, <i>MDR1</i>, to 7q21.1.* Human Genetics, 1987. **77**(2): p. 142-144.

77. Chin, J.E., et al., *Structure and expression of the human MDR (P-glycoprotein) gene family.* Mol cell biol, 1989. **9**(9): p. 3808-20.

78. Hennessy, M. and J.P. Spiers, *A primer on the mechanics of P-glycoprotein the multidrug transporter.* Pharm Res, 2007. **55**(1): p. 1-15.

79. Fiala, R., et al., *P-glycoprotein-mediated multidrug resistance phenotype of L1210/VCR cells is associated with decreases of oligo- and/or polysaccharide contents.* Biochimica et Biophysica Acta (BBA) - Molecular Basis of Disease, 2003. **1639**(3): p. 213-224.

80. Endicott, J.A. and V. Ling, *The Biochemistry of P-Glycoprotein-Mediated Multidrug Resistance.* Annu Rev Biochem, 1989. **58**(1): p. 137-171.

81. Sorrentino, B.P., *Gene therapy to protect haematopoietic cells from cytotoxic cancer drugs.* Nat Rev Cancer, 2002. **2**(6): p. 431-441.

82. Yang, T.-F., et al., *Shell-crosslinked Pluronic L121 micelles as a drug delivery vehicle.* Biomaterials, 2007. **28**(4): p. 725-734.

83. Collnot, E.-M., et al., *Mechanism of Inhibition of P-Glycoprotein Mediated Efflux by Vitamin E TPGS: Influence on ATPase Activity and Membrane Fluidity.* Mol Pharm, 2007. **4**(3): p. 465-474.

84. Lake, R.A. and B.W.S. Robinson, *Immunotherapy and chemotherapy [mdash] a practical partnership.* Nat Rev Cancer, 2005. **5**(5): p. 397-405.

85. Minchinton, A.I. and I.F. Tannock, *Drug penetration in solid tumours.* Nat Rev Cancer, 2006. **6**(8): p. 583-592.

86. Wang, Y. and F. Yuan, *Delivery of Viral Vectors to Tumor Cells: Extracellular Transport, Systemic Distribution, and Strategies for Improvement.* Ann Biomed Eng, 2006. **34**(1): p. 114-127.

87. McDonald, D.M. and P.L. Choyke, *Imaging of angiogenesis: from microscope to clinic.* Nat Med, 2003. **9**(6): p. 713-725.

88. Zhanwen, X. and et al., *The fabrication of novel nanobubble ultrasound contrast agent for potential tumor imaging.* Nanotechnology, 2010. **21**(14): p. 145607.

89. Hobbs, S.K., et al., *Regulation of transport pathways in tumor vessels: Role of tumor type and microenvironment.* Proc Natl Acad Sci, 1998. **95**(8): p. 4607-4612.

90. Jain, R.K., *Normalization of Tumor Vasculature: An Emerging Concept in Antiangiogenic Therapy.* Science, 2005. **307**(5706): p. 58-62.

91. Maeda, H., *The enhanced permeability and retention (EPR) effect in tumor vasculature: the key role of tumor-selective macromolecular drug targeting.* Adv Enzyme Regul, 2001. **41**(1): p. 189-207.

92. Maeda, H., G.Y. Bharate, and J. Daruwalla, *Polymeric drugs for efficient tumor-targeted drug delivery based on EPR-effect.* Eur J Pharm Biopharm, 2009. **71**(3): p. 409-419.

93. Bisht, S. and A. Maitra, *Dextran–doxorubicin/chitosan nanoparticles for solid tumor therapy.* Wiley Interdisciplinary Reviews: Nanomedicine and Nanobiotechnology, 2009. **1**(4): p. 415-425.

94. Folkman, J., *Angiogenesis and apoptosis.* Sem Cancer Biol, 2003. **13**(2): p. 159-167.

95. Rak, J. and J.L. Yu, *Oncogenes and tumor angiogenesis: The question of vascular [`]supply' and vascular [`]demand'.* Sem Cancer Biol, 2004. **14**(2): p. 93-104.

96. Bouck, N., V. Stellmach, and S.C. Hsu, *How Tumors Become Angiogenic,* in *Advances in Cancer Research,* F.V.W. George and K. George, Editors. 1996, Academic Press. p. 135-174.

97. Hanahan, D. and J. Folkman, *Patterns and Emerging Mechanisms of the Angiogenic Switch during Tumorigenesis.* Cell, 1996. **86**(3): p. 353-364.

98. Rak, J., J. Filmus, and R.S. Kerbel, *Reciprocal paracrine interactions between tumour cells and endothelial cells: the [`]angiogenesis progression' hypothesis.* Eur J Cancer, 1996. **32**(14): p. 2438-2450.

99. Jain, R.K., *Normalizing tumor vasculature with anti-angiogenic therapy: A new paradigm for combination therapy.* Nat Med, 2001. **7**(9): p. 987-989.

100. van Moorselaar, R.J.A. and E.E. Voest, *Angiogenesis in prostate cancer: its role in disease progression and possible therapeutic approaches.* Mol Cell Endocrinol, 2002. **197**(1-2): p. 239-250.

101. Campbell, S.C., *ADVANCES IN ANGIOGENESIS RESEARCH: RELEVANCE TO UROLOGICAL ONCOLOGY.* J Urol, 1997. **158**(5): p. 1663-1674.

102. Cvetkovic, D., et al., *Increased hypoxia correlates with increased expression of the angiogenesis marker vascular endothelial growth factor in human prostate cancer*. Urology, 2001. **57**(4): p. 821-825.

103. Huss, W.J., et al., *Angiogenesis and Prostate Cancer: Identification of A Molecular Progression Switch.* Cancer Research, 2001. **61**(6): p. 2736-2743.

104. Zhong, H., et al., *Overexpression of Hypoxia-inducible Factor 1α in Common Human Cancers and Their Metastases.* Cancer Res, 1999. **59**(22): p. 5830-5835.

105. Zhong, H., et al., *Modulation of Hypoxia-inducible Factor 1α Expression by the Epidermal Growth Factor/Phosphatidylinositol 3-Kinase/PTEN/AKT/FRAP Pathway in Human Prostate Cancer Cells: Implications for Tumor Angiogenesis and Therapeutics.* Cancer Res, 2000. **60**(6): p. 1541-1545.

106. Drevs, J., *VEGF and angiogenesis: implications for breast cancer therapy.* Eur J Cancer Suppl, 2008. **6**(6): p. 7-13.

107. Lee, T.-H., et al., *Vascular Endothelial Growth Factor Modulates the Transendothelial Migration of MDA-MB-231 Breast Cancer Cells through Regulation of Brain Microvascular Endothelial Cell Permeability.* J Biol Chem, 2003. **278**(7): p. 5277-5284.

108. Symmans, F.W., *Breast cancer response to paclitaxel in vivo.* Drug Resist Update, 2001. **4**(5): p. 297-302.

109. Milas, L., et al., *Kinetics of mitotic arrest and apoptosis in murine mammary and ovarian tumors treated with taxol.* Cancer Chemother Pharmacol, 1995. **35**(4): p. 297-303.

110. Milross, C.G., et al., *Relationship of Mitotic Arrest and Apoptosis to Antitumor Effect of Paclitaxel.* J Natl Cancer Inst, 1996. **88**(18): p. 1308-1314.

111. Symmans, W.F., et al., *Paclitaxel-induced Apoptosis and Mitotic Arrest Assessed by Serial Fine-Needle Aspiration: Implications for Early Prediction of Breast Cancer Response to Neoadjuvant Treatment.* Clin Cancer Res, 2000. **6**(12): p. 4610-4617.

112. Rattanasomboon, N., et al., *Growth and enumeration of the meat spoilage bacterium Brochothrix thermosphacta.* Int J Food Microbiol, 1999. **51**(2-3): p. 145-158.

113. Sakai, K., et al., *Change in nitrite conversion direction from oxidation to reduction in heterotrophic bacteria depending on the aeration conditions.* J Ferment Bioeng, 1997. **84**(1): p. 47-52.

114. Luxo, C., et al., *Tamoxifen induces ultrastructural alterations in membranes of Bacillus Stearothermophilus.* Toxicol in Vitro. **17**(5-6): p. 623-628.

115. Fonseca, C., S. Simões, and R. Gaspar, *Paclitaxel-loaded PLGA nanoparticles: preparation, physicochemical characterization and in vitro anti-tumoral activity.* J Control Release, 2002. **83**(2): p. 273-286.

116. Danhier, F., et al., *Paclitaxel-loaded PEGylated PLGA-based nanoparticles: In vitro and in vivo evaluation.* J Control Release, 2009. **133**(1): p. 11-17.

117. Kim, S.C., et al., *Sensitive HPLC method for quantitation of paclitaxel (Genexol®) in biological samples with application to preclinical pharmacokinetics and biodistribution.* J Pharmaceut Biomed Anal, 2005. **39**(1-2): p. 170-176.

118. Matsumoto, M. and K. Tanaka, *Nano bubble--Size dependence of surface tension and inside pressure.* Fluid Dynam Res. **40**(7-8): p. 546-553.

119. Whitby, C.P., D. Fornasiero, and J. Ralston, *Effect of adding anionic surfactant on the stability of Pickering emulsions.* J Colloid Interface Sci, 2009. **329**(1): p. 173-181.

120. Aveyard, R., B.P. Binks, and J.H. Clint, *Emulsions stabilised solely by colloidal particles.* Adv Colloid Interface Sci, 2003. **100-102**: p. 503-546.

121. Prestidge, C.A., T. Barnes, and S. Simovic, *Polymer and particle adsorption at the PDMS droplet-water interface.* Adv Colloid Interface Sci, 2004. **108-109**: p. 105-118.

122. Hunter, T.N., et al., *The role of particles in stabilising foams and emulsions.* Adv Colloid Interface Sci, 2008. **137**(2): p. 57-81.

123. Gonzenbach, U.T., et al., *Ultrastable Particle-Stabilized Foams.* Angew Chem Int Ed, 2006. **45**(21): p. 3526-3530.